공학박사 학위논문

Assessment of Seismic Behavior of Piles in Slope during Liquefaction

액상화 경사지반에 근입된

말뚝의 지진거동 평가

2023년 2월

서울대학교 대학원

건설환경공학부

유 병 수

Assessment of Seismic Behavior of Piles in Slope during Liquefaction

지도 교수 김 성 렬

이 논문을 공학박사 학위논문으로 제출함

2022 년 12월

서울대학교 대학원

건설환경공학부

유 병 수

유병수의 공학박사 학위논문을 인준함

2023 년 1 월

위 원 장 ___정 충 기___ **(인)**

부위원장 ___김 성 렬___ **(인)**

위 원 ___박 준 범___ **(인)**

위 원 ___한 진 태___ **(인)**

위 원 ___박 헌 준___ **(인)**

Abstract

Assessment of Seismic Behavior of Piles in Slope during Liquefaction

Yoo, Byeong-Soo

Department of Civil & Environmental Engineering

The Graduate School

Seoul National University

Liquefaction of ground due to seismic load can induce severe damage in the horizontal and vertical stability of pile foundations. The liquefaction-induced lateral displacement causes bending failure of the piles. Furthermore, development and dissipation of excess pore pressure results in the buckling of the pile shafts and settlement of the pile due to negative skin friction, respectively. In order to prevent foundation damage due to liquefaction, it is necessary to understand the behavior of the pile foundation in liquefied ground.

Previous research on piles in liquefied ground has mainly focused on levelled ground or infinite slope conditions. However, it is common that pile foundations of waterfront structures are founded in a finite slope with relatively high inclination angles. The behavior of piles in liquefied finite slopes depends on various factors such as the slope length, height, and horizontal distance of the pile from the slope toe, unlike those in liquefied infinite slopes. Furthermore, piles in liquefied finite slopes are subjected to complex loads including static dead load, dynamic inertial load, liquefaction-induced lateral load, and negative skin friction due to post-liquefaction settlement. Therefore, research on the

behavior of piles in liquefied finite slopes is necessary.

In this dissertation, a series of centrifuge tests were performed by simulating a pile-supported wharf in Pohang New Port, Korea. The model structures were composed of mass decks supported by single and group piles. The model grounds were constructed with the slopes of 15° and 27° using saturated silica sand. The test model was subjected to ramped and constant cyclic loading with the maximum acceleration of 0.2 g and 0.1 g at the container base, respectively.

In this experiment, pure water and hydroxypropyl methyl cellulose (HPMC) solution were examined as the pore fluid material, since the drainage condition can be affected by the fluid viscosity during dynamic centrifuge tests. When pure water was used as the pore fluid material, the development of excess pore pressure was interrupted by the rapid drainage of the pore fluid. In addition, different time-dependent structural behaviors were obtained, depending on the type of the pore fluid. It was shown that structures with pore water recovered from deformation after the end of the shaking, whereas those with viscous pore fluid experienced significant permanent deformations.

Variation in the axial load distribution of the piles was monitored before and after shaking. During the centrifuge spinning, the obtained drag load due to the negative skin friction agreed with the value calculated with the beta method for shaft resistance. After shaking, it was found that the liquefaction caused a loss of spin-induced drag load, while the dissipation of excess pore pressure resulted in reconsolidation settlement, leading to large drag loads acting on the pile. In addition, the negative skin friction was found to be larger than the liquefied residual strength that is recommended in the current design codes used in practice. As a result, it is seen that the consideration of the strength reduction is not necessary for the calculation of the negative skin friction induced by reconsolidation, since the piles in liquefied ground regain skin friction after the dissipation of excess pore pressure.

In this study, two different numerical modeling methods for liquefied soils

were used to simulate the results of centrifuge model tests. The first method, which converts the liquefied soil into a static linear distributed load, was adopted to evaluate the bending moment of piles. The linear relationship between the liquefied soil pressure and total overburden stress was expressed with an empirical gradient factor. The factor was calibrated for the single piles based on the test results, and was used to assess the effect of the experimental test conditions on the liquefied soil pressure. The liquefied soil pressure for the analysis of the group pile behavior was defined based on the conventional empirical factor and calibrated factor from this study. As a result, the use of the calibrated factor showed improved accuracy for predicting the bending moment profile of group piles, compared to the when the conventional factor was used.

In the second modeling method, the numerical model was constructed with rigorous simulation of the liquefied soil, pile, deck, and container to evaluate the seismic behavior of piles in liquefied finite slopes. The modeling of soil–pile interface, which considers the development and dissipation of excess pore pressure adjacent to the pile, was proposed to improve the accuracy of the model. The model was validated with the results of centrifuge experiments. Based on the results of the numerical model, analyses were carried out on the failure mechanism of liquefied finite slopes, and the soil–pile interface which is used to simulate the induced seismic behavior of the piles. By using the established numerical model, the effects of slope inclination and amplitude of the cyclic load on the seismic behavior of the piles in finite slopes were studied.

Keywords: pile; slope; liquefaction; seismic behavior; centrifuge test; numerical simulation; liquefied soil pressure; pile axial load
Student Number: 2018-37864

Contents

List of Tables

List of Figures

Chapter 1. Introduction

1.1 Research Background

South Korea has experienced large earthquakes of historic magnitude, including the Gyeongju earthquake in 2016 and the Pohang earthquake in 2017. In the case of the Pohang earthquake, ground liquefaction and subsequent damages were observed for the first time in Korea (Figure 1-1). As a result of public interest in disaster management, advanced seismic design for the liquefaction phenomena is required.

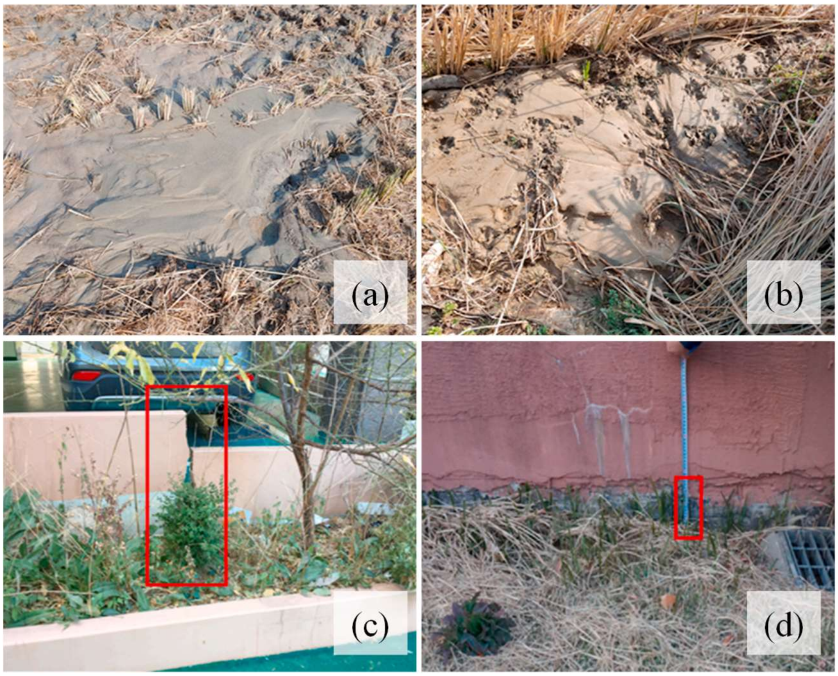

Figure 1-1 Liquefaction occurrence induced by Pohang earthquake: (a) and (b) sand boils, (c) and (d) ground settlement (Kim et al., 2021)

Ground liquefaction indicates the following sequential events (Ishibashi et al., 1977; Kramer, 1996). Loose sand ground has high compressibility due to the void in the ground. In the case of undrained loading, such as an earthquake, pore water instead of soil particles resists the load due to its low compressibility. Excess pore water pressure in the ground results in a loss of soil strength. After the end of undrained loading, the excess pressure dissipates with reconsolidation settlement (Figure 1-2).

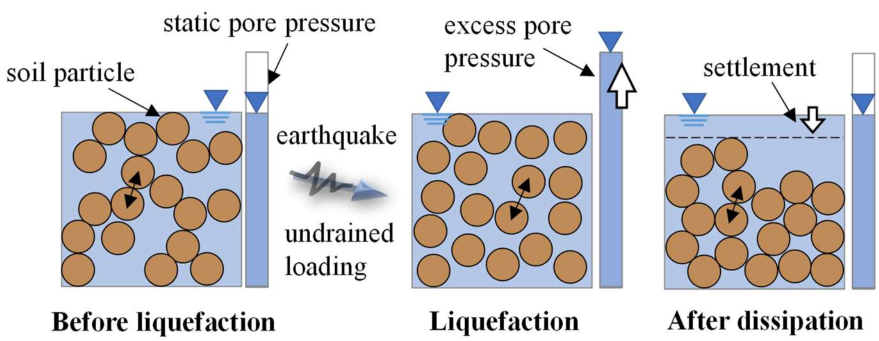

Figure 1-2 Schematic diagram of ground liquefaction

Pile foundation has been severely damaged by the ground liquefaction. The cracks and damage of the piles were located at the boundary of non-liquefied and liquefied soil layers as shown in Figure 1-3 (Kawamura et al., 1985; Yoshida, 1990). In addition, pile foundation supporting waterfront structures is susceptible to the ground liquefaction corresponding lateral soil movement (Berrill et al., 2001; Hamada & O'Rourke, 1992; PIANC, 2001a; Youd, 1993).

Mechanisms of pile damage by the liquefaction have been introduced. These are pile bending failure induced by the lateral soil pressure due to liquefied soil movement (Abdoun & Dobry, 2002; Boulanger et al., 2003), pile buckling failure occurred with high slenderness ratio due to loss of ground confinement (Bhattacharya & Madabhushi, 2008), and pile settlement over serviceability caused by the downdrag due to the post-liquefaction settlement (Verdugo & Peters, 2010; Yen et al., 2011).

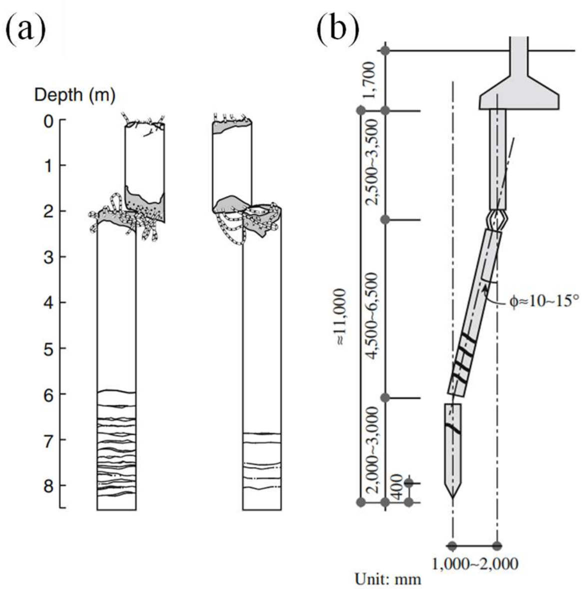

Figure 1-3 Pile damage patterns due to ground liquefaction (Bhattacharya & Madabhushi, 2008)

For the calculation of the lateral soil pressure, equivalent uniform and linear soil pressure have been proposed on the basis of data obtained from case studies and experiments. In the first method, uniform soil pressure was assumed to be a constant value from 10 to 40 kPa (Dobry et al., 2003; He et al., 2009; Tang et al., 2015). In the latter method, the soil pressure was assumed to be proportional to the total stress by an empirical gradient factor ranging from 0.05 to 1.0 (He et al., 2009; JRA, 2012; JSWA, 1997; Su et al., 2016).

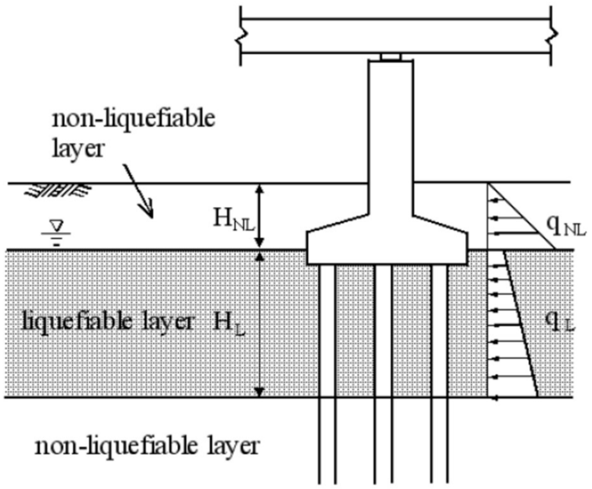

Figure 1-4 Lateral soil pressure due to liquefied soil movement (JRA, 2012)

For the estimation of pile settlement after excess pore pressure dissipation, the magnitude of negative skin friction have been examined with several studies. Boulanger and Brandenberg (2004) modeled the negative skin friction within the liquefied layer as equal to the positive skin friction by multiplying a reverse proportional coefficient by the excess pore pressure ratio as shown in Figure 1-5. Sinha et al. (2022) reported that the drag load within the liquefied layer was equal to the drained interface shear strength. Muhunthan et al. (2017) suggested negative skin friction is assumed to be fully developed along the shaft above the neutral plane after liquefaction.

AASHTO (2020) suggested negative skin friction in the liquefied layer as a residual soil strength. However, Rollins et al. (2018) and Rollins and Hollenbaugh (2015) reported that the drag load in the liquefied layer was only approximately 50% of the positive shaft resistance before the liquefaction occurrence. Similarly, Kevan (2017) and Elvis (2018) agreed with the smaller drag load than the positive shaft resistance by performing tests on various pile types. Furthermore, Fellenius et al. (2020) assumed zero drag load within the liquefied layer (Figure 1-6).

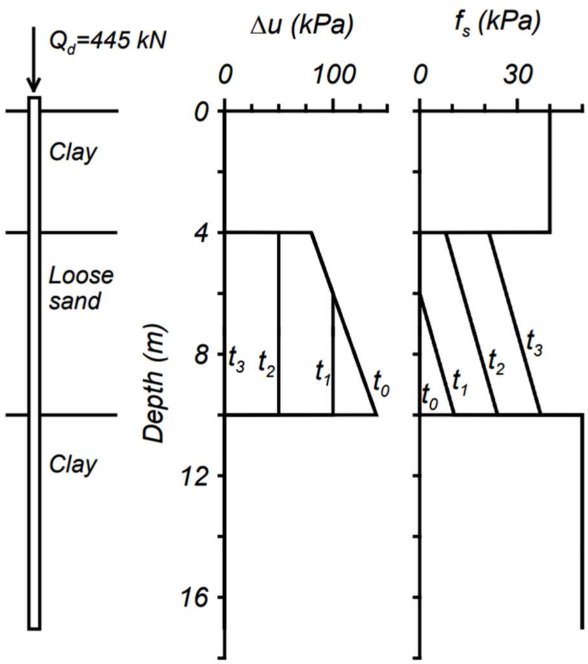

Figure 1-5 Negative skin friction with dissipation of excess pore pressure (Boulanger & Brandenberg, 2004)

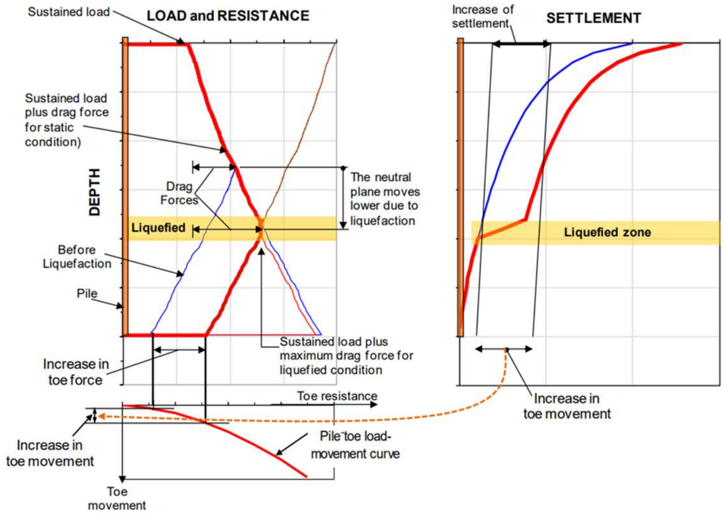

Figure 1-6 Effect of liquefaction below the force-equilibrium neutral-plane (Fellenius et al., 2020)

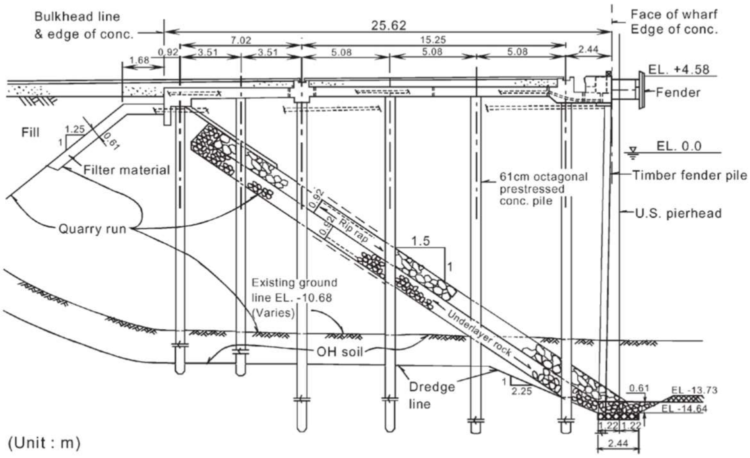

Figure 1-7 Los Angeles Port wharf installed in finite slope (PIANC, 2001a)

The previous studies agreed on the necessity of the liquefaction consideration in seismic designs. However, the wide range of suggested values makes it difficult to select appropriate value for the practical design. Further, liquefaction studies related to lateral soil pressure have been mainly conducted on infinite gentle slope or horizontal ground. The foundation of the waterfront structure is usually embedded in a finite slope with relatively high inclination. The structure has been damaged by liquefaction of finite slope (PIANC, 2001b; Sumer et al., 2007). Case studies on damaged pile-supported wharf by liquefaction summaries in Table 1-1.

Table 1-1 Case histories of pile-supported wharf damaged by liquefaction

Structure	Case	Damage comments	Reference
7th terminal wharf	Port of Oakland, USA	Failure of batter pile head	Benuska (1990) Egan et al. (1992)
APL terminal	Los Angeles Port, USA	Displacement of expansion joint (8 cm) Damage to crane rails	Hall (1995) Iai and Tsuchida (1997)
Takahama wharf	Kobe Port, Japan	Buckling of steel piles at the pile cap and in the embedded location.	Iai (1998)
Sumiyoshihama district	Kobe Port, Japan	buckling of steel piles (lateral deformation: 1.0 m)	Nishizawa et al. (1998)
UM Shipyard	Kocaeli, Turkey	Pier damaged and collapsed below water	Summer et al. (2002)
Klor Alkali	Kocaeli, Turkey	Pier damaged and collapsed below water	Yuksel et al. (2000)

1.2 Objectives

Based on the above discussion, this dissertation aims to investigate the seismic behavior of piles in liquefied slope by conducting a series of centrifuge model tests and numerical analysis. In summary, the main objectives of the present study are as follows:

(1) to investigate the effect of pore fluid viscosity on the ground liquefaction in the centrifuge model test;

(2) to investigate seismic behavior of piles subjected to liquefied slope;

(3) to evaluate the lateral soil pressure on piles induced by the liquefied slope;

(4) to investigate the variation in axial load distribution of piles before and after the liquefaction;

(5) to evaluate the negative skin friction due to the post-liquefaction settlement for seismic design of piles in liquefiable soil.

1.3 Scope of work

A series of centrifugal model tests have been conducted in the aspect of experimental approach. The prototype of the centrifuge test model is a segment of a pile-supported wharf in Pohang New Port, Korea. A concrete slab is supported by rows of steel pipe piles inserted in a finite slope of 27°. The slope consists of two layers of sand overlying the rock layer: loose sand and an underlying dense gravel layer. The piles are socketed into the rock layer.

The structure and ground are modeled in the centrifuge tests as following conditions.

- The abutment, caisson, and rubble mound included in prototype structure are not simulated in centrifuge model to focus on the interaction between the piles and liquefied slope.

- A 2×2 end-bearing aluminum pipe piles are considered to simulate the rows of steel pipe piles socketed in the rock layer with identical flexural stiffness in prototype scale.
- The concrete slab mounted on the pile heads is simulated by a mass block considering the weight of the slab.
- The loose sand layer is extended to the rock layer by replacing the dense gravel layer to maximize the effect of the liquefied slope on the piles.
- Poorly graded silica sand is adopted as a geomaterial to prevent soil segregation during installation of model ground using wet pluviation method.
- The viscous pore fluid is prepared by hydroxypropyl methylcellulose (HPMC) solution considering the scale law for centrifuge tests.
- The sinusoidal base motion is considered for liquefaction of model ground.

Numerical studies have been performed using various programs. LPILE and Group v2019 are adopted to modify a design liquefaction-induced lateral force suitable for the finite slope condition. Fast Lagrangian Analysis of Continua in 2 Dimensions (FLAC2D) is adopted to reproduce conducted centrifuge tests through numerical simulation.

The structure and ground are modeled in the numerical analysis as following conditions.

- Properties of piles are considered in prototype scale.
- For LPILE and Group analysis, Pile foundation and liquefied soil are modeled as a beam-column material and a distributed lateral force along the pile length, respectively.
- For numerical simulation of centrifuge tests, materials (container, soil, pile, deck) and their interfaces has been considered.
- Elastic model with large modulus has been considered for the rigid container and deck on group piles.
- liquefied soil is modelled using PM4Sand v3.2 (Boulanger and Ziotopoulou, 2022) which is a sand plasticity model for earthquake engineering applications.
- Beam-interface is applied to allow the separation between the soil and the container.
- Effect of liquefaction is considered using pile–soil interface spring.

1.4 Organization of dissertation

This dissertation comprises six chapters which are briefly introduced as follows:

In Chapter 1, the background, objective, scope of work, and dissertation structure are presented.

In Chapter 2, previous studies are reviewed to identify research gaps. An appropriate centrifuge model test requires experimental design considering the similitude laws. literature reviews on the effect of viscous pore fluid are conducted. Studies on the proposed lateral load on piles in liquefiable ground are presented. Previous research on pile skin friction in peri- and post-liquefaction is introduced.

In Chapter 3, the planning, preparation, and implementation of dynamic centrifuge model tests are described. The descriptions of the prototype wharf and the centrifuge model are provided. The total process of designing, manufacturing, and applying viscous fluid in consideration of the scale law is described. The detailed installation process of the experiment model, composed of various elements such as ground, structure, and measurements, is presented. The liquefaction occurrence of the model ground is presented.

In Chapter 4, the test results of centrifuge model tests to simulate the seismic behavior of piles embedded in liquefied finite slopes are presented. Lateral pile-deck system response to seismic loading is analysed. The effect of liquefied finite slope is analyzed based on the bending moment of the piles. Variation in axial load distribution is analysed. The effect of development and dissipation of excess pore pressure on skin friction is analysed.

In Chapter 5, utilizing the computational platform to perform various numerical studies based on the data obtained from the experiments in order to obtain and validate additional information. A liquefaction-induced lateral force model suitable for finite slopes is proposed by using experimental data obtained from single piles subjected to liquefaction at different locations within slope. The improved empirical factors are used to assess the applicability of the proposed liquefied soil force model to a group of piles and the group effect. A numerical modeling of the liquefiable finite slope is performed to analyze the ground motion which is not directly observed in the experiment. Soil–pile interface modeling with consideration of liquefaction is proposed. Based on the interface modeling, a series of numerical modeling of the piles in liquefiable finite slope are carried out to simulate the conducted centrifuge model tests in Chapters 3 and 4. Parametric studies are conducted to assess the effects of slope inclinations and amplitude of input motions.

Finally, in Chapter 6, the main conclusion of the present study and recommendations for further research are presented.

Chapter 2. Literature review

2.1 Introduction

The objective of this study is to analyze the seismic behavior of piles in liquefiable ground. In this chapter, previous studies are reviewed to identify research gaps.

In sections 2 and 3, the advantages of centrifuge model tests, which are distinguished from other model experiments, are examined based on dimensional analysis. An appropriate centrifuge model test requires experimental design considering the similitude laws. In particular, considering the viscosity of pore fluid is necessary in simulating liquefaction in the centrifuge model experiment. Thus, literature reviews on the effect of viscous pore fluid are conducted.

In section 4, studies on the proposed lateral load on piles in liquefiable ground are presented. Based on the field reports of ground liquefaction, damage of piles is mainly caused by lateral spread. Therefore, design lateral force inducing bending failure of piles has been proposed for practical design.

In section 5, previous research on pile skin friction in peri- and post-liquefaction is introduced. Development of excess pore pressure weakens confinement of soils to pile shaft. Dissipation of excess pore pressure induces drag loads on pile shaft due to the post-liquefaction settlement. As a result, many experimental and numerical studies have been conducted on ground liquefaction and pile skin friction.

2.2 Centrifuge model test

Experiments are performed using miniatured models to test the behavior of large-scale structures and ground. Proper scale factors should be applied to each variable in order for the model system to accurately simulate the full-scale system. The scaling laws for model testing can be obtained by applying dimensional analysis through Buckingham Π theorem to the momentum conservation equation (Konkol, 2014).

$$div(\sigma) + \rho \cdot \left(g - \frac{\partial^2 u}{\partial t^2}\right) = 0 \qquad (2\text{-}1)$$

$$f\left(\frac{\sigma}{x \cdot g \cdot \rho}, \frac{u}{x}, \frac{g \cdot t^2}{x}\right) = 0 \qquad (2\text{-}2)$$

where, σ: stress [$kgm^{-1}s^{-2}$], x: position [m], g: gravitational acceleration [ms^{-2}], ρ: density [kgm^{-3}], u:displacement [m], t: time [s].

In typical model experiments, a reduced model structure, where the length of the original structure is reduced to 1/n, is used to conduct experiments under gravitational acceleration of 1g. Under these conditions, the scale factors for the stress and the strain are different from each other.

$$\sigma^* = x^* \cdot g^* \cdot \rho^* = \frac{1}{n} \cdot 1 \cdot 1 = \frac{1}{n} \qquad (2\text{-}3)$$

$$u^* = \frac{1}{n} \qquad (2\text{-}4)$$

$$\epsilon^* = \frac{\Delta u^*}{\Delta x^*} = 1 \qquad (2\text{-}5)$$

where superscript $*$ indicates scale factor.

To solve this problem, it is important to accurately simulate the stress–strain behavior of the prototype system in model system, so the modulus of the model system should be adjusted to 1/n times that of the prototype. However, it is very difficult to adjust the modulus of the ground, so in the model test applying large scale factor, the stress-strain behavior of the model ground can differ significantly from the prototype.

$$E^* = \frac{\sigma^*}{\epsilon^*} = \frac{1/n}{1} = 1/n \qquad (2\text{-}6)$$

However, in a centrifuge model test, the model system is tested under the condition of applying a centrifugal acceleration ng to the model system, so the scale factors for the stress and the strain are equal to one. Therefore, it can be applied to ground structures with large scale factors such as pile foundation.

$$\sigma^* = x^* \cdot g^* \cdot \rho^* = \frac{1}{n} \cdot n \cdot 1 = 1 \qquad (2\text{-}7)$$

2.3 Pore fluid viscosity in centrifuge test

A centrifuge model test is one of the most widely used experimental techniques in geotechnical engineering since it is able to simulate ground confinement in deep depth, which is an important factor in determining soil behavior. For a successful centrifugal model experiment, the properties and dimensions of the scale-down model structure and ground must be appropriately adjusted as shown in Table 2-1.

Table 2-1 Scale factors adopted from Madabhushi (2017)

Parameter	Model	Prototype	Units
Length	1	n	m
Mass	1	n^3	$N \cdot s^2 m^{-1}$
Flexural stiffness (*EI*)	1	n^4	$N \cdot m^2$
Compressive stiffness (*EA*)	1	n^2	N
Displacement	1	n	m
Acceleration	1	n^{-1}	ms^{-2}
Strain	1	1	-
Pressure	1	1	Nm^{-2}

For the simulation of ground liquefaction in centrifuge test, variation of pore pressure in saturated model ground during shaking should be considered. Thus, it is important to simulate the consolidation phenomenon that controls changes in pore pressure. The scale factor of the consolidation time is described based on the dimensionless time factor given as a solution to the one-dimensional consolidation equation.

$$T_v = C_{v,m}\frac{t_m}{d_m^2} = C_{v,p}\frac{t_p}{d_p^2} \quad (2\text{-}8)$$

$$t_m = \frac{C_{v,p}}{C_{v,m}} \times \frac{d_m^2}{d_p^2} = \frac{C_{v,p}}{C_{v,m}} \times \frac{d_p^2/n^2}{d_p^2} \times t_p = \frac{C_{v,p}}{C_{v,m}} \times \frac{t_p}{n^2} \quad (2\text{-}9)$$

where, T_v: dimensionless time factor for consolidation, C_v: consolidation coefficient, d: drainage distance, t: time, suffix m and p indicate model and prototype, respectively.

However, this value is much larger than that of the dynamic time. As a result, the consolidation time in the model is n^2 times faster than that in the prototype, while the dynamic time is n times faster. Therefore, it is necessary to delay the consolidation time by adjusting the grain size distribution of the ground material or the viscosity of the pore fluid.

$$t_m = \sqrt{\frac{L_m}{A_m}} = \sqrt{\frac{L_p/n}{A_p \times n}} = \frac{t_p}{n} \tag{2-10}$$

$$C_v = \frac{k}{\gamma_f m_v} = \frac{\kappa_s}{m_v \mu} \tag{2-11}$$

where, L: length, A: acceleration, k: permeability, γ_f: fluid density, m_v: coefficient of volume compressibility, κ_s: intrinsic permeability of soil, and μ: dynamic viscosity of fluid.

Adamidis and Madabhushi (2015) recommended that it is more appropriate to adjust the consolidation time through fluid viscosity rather than grain size distribution in order not to affect the constitutive behavior of the ground. Dewoolkar et al. (1999) confirmed that the Hydroxypropyl methylcellulose (HPMC) solution did not affect the ground strength by conducting triaxial test, while the permeability properly increased using HPMC solution by performing permeability test (Figure 2-1). In addition, Adamidis and Madabhushi (2015) showed that the adjusted pore fluid viscosity using HPMC solution is not affected by shear rate during earthquake motion. Shearing rate during an earthquake is estimated using one-dimensional wave propagation.

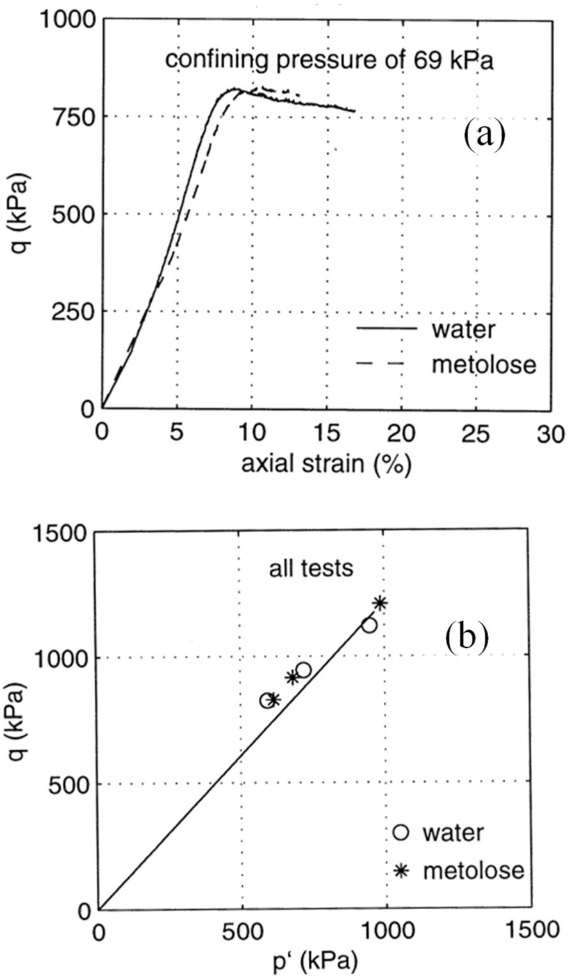

Figure 2-1 Comparison of triaxial test results with water and HPMC solution as pore fluid (Dewoolkar et al., 1999)

Liu and Dobry (1997) performed a series of centrifugal model tests using water and viscous fluid as pore fluid on a circular foundation overlying saturated base ground. Experimental results showed that different behaviors in both development and dissipation of excess pore pressure due to the pore fluid viscosity. In addition, it was found that the result with viscous pore fluid reflected delayed foundation failures observed in the field. Dewoolkar et al. (1999) performed a centrifugal model experiment on the saturated ground with water and viscous fluid. The model was excited by a strong sinusoidal motion with a maximum acceleration of 15 g. The experimental results showed that the development of excess pore pressure was restricted in the ground saturated with viscous fluid, and subsequent ground settlement after the dissipation was also relatively small (Figure 2-2).

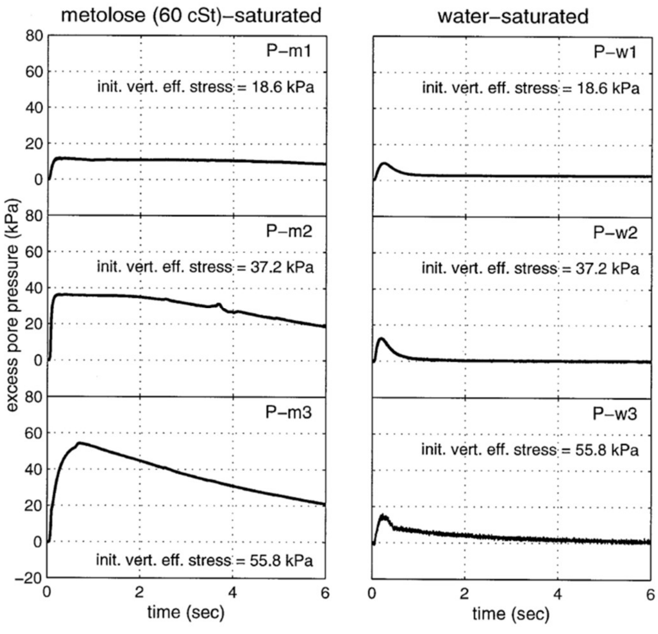

Figure 2-2 Comparison of excess pore pressure development with water and HPMC solution as pore fluid (Dewoolkar et al., 1999)

González et al. (2009) analyze pile behavior subjected to lateral spread of liquefied ground with water and viscous fluid as a pore fluid. The experimental results showed that there was no significant difference in the occurrence of liquefaction and the horizontal displacement of the ground. However, the pile bending moment and the pile head displacement was considerably greater with viscous pore fluid than that with water pore fluid (Figure 2-3). On the other hand, Wilson (1998) performed a series of centrifuge experiments on pile–mass system subjected to lateral spread of liquefied ground. It was reported that viscous pore fluid had minor effects in the pile bending moment and ground acceleration except for the dissipation time (Figure 2-4).

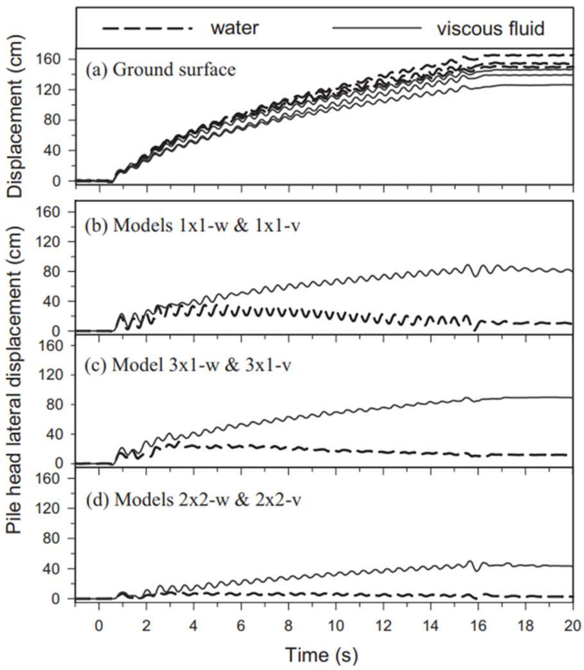

Figure 2-3 Comparison of pile head displacements with water and HPMC solution as pore fluid (González et al., 2009)

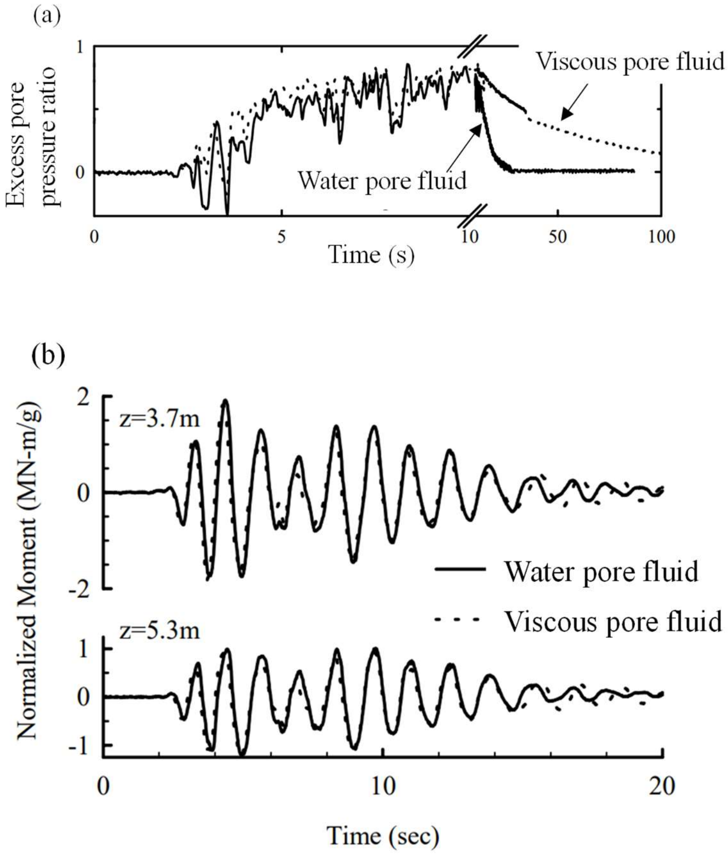

Figure 2-4 Comparison of (a) excess pore pressure ratio and (b) normalized bending moment with water and viscous fluid as pore fluid (Wilson, 1998)

2.4 Liquefaction-induced lateral force

Bending failure is the most common failure mechanism deduced by damage reports of pile foundations subjected to lateral soil movement due to liquefaction. Two different design concepts are suggested. One is the direct application of the ultimate design lateral force from the ground to the pile. The other is the application of the lateral ground displacement to the soil–pile spring.

Thus, several methods for determining the design lateral force (Dobry et al., 2003; JRA, 2012; JSWA, 1997), lateral ground displacement (Brandenberg et al., 2007; Tokimatsu & Asaka, 1998; Youd, 2018), and liquefied soil–pile spring (AIJ, 2001; Brandenberg et al., 2005; Dash et al., 2017; Liu & Dobry, 1995) have been proposed.

The lateral force method is a conservative method since the lateral pile stability is evaluated by applying the ultimate design load direct to the pile. In terms of the lateral force method, JRA (2012) and Dobry et al. (2003) are considered pioneering studies. JRA (2012) and Dobry et al. (2003) proposed a linear soil pressure proportional to the total stress and an equivalent uniform soil pressure, respectively.

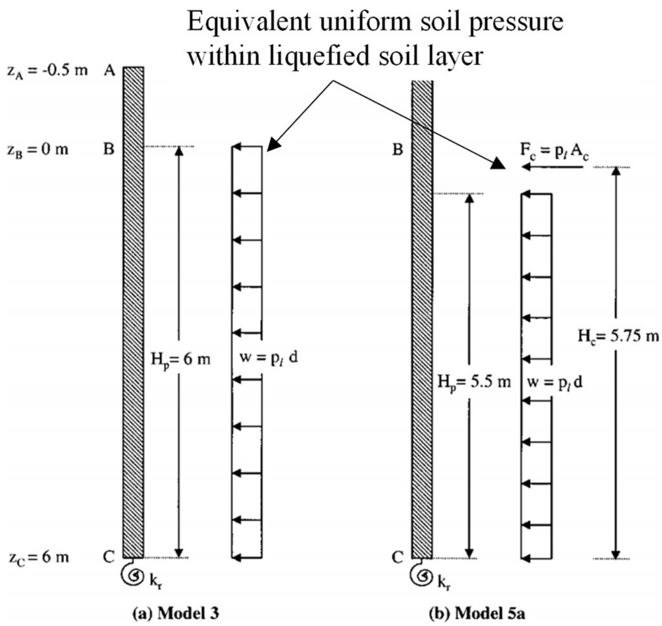

Figure 2-5 Free body diagrams for limit equilibrium evaluation (Dobry et al., 2003)

Dobry et al. (2003) suggested approximately 10 kPa of equivalent uniform soil pressure within liquefied layer using centrifuge model tests on piles in liquefied gentle slope (Figure 2-5). The equivalent uniform soil pressure was back-calculated using free body diagrams with maximum bending moment. JRA (2012) proposed the lateral soil pressure acting on the pile within the liquefied layer as proportional to the total stress. This model was based on the back-calculation of reported field cases during the 1995 Kobe Earthquake. Consequently, the lateral force per unit length of a single pile based on the equivalent uniform and linear soil pressure can be calculated as follows.

$$P_{\mathrm{US}} = \alpha \times D \qquad (2\text{-}12)$$

$$P_{\mathrm{LS}} = C_{\mathrm{L}} \times \sigma_v \times D \qquad (2\text{-}13)$$

where, P_{US} and P_{LS}: lateral force per unit pile length based on uniform and linear soil pressure, respectively, α: equivalent uniform soil pressure, D: pile diameter, C_{L}: empirical gradient factor, σ_v: total stress at considering depth.

Thereafter, analyses on the pile foundation subjected to the liquefied soil movement have been conducted. He et al. (2009) performed large shake table test with different thickness of liquefied soil layer (Figure 2-6). The estimated uniform soil pressure varied greatly according to the thickness of the liquefied layer. However, the empirical factor for the linear distribution was relatively constant. Based on these results, an empirical factor of 1.0 was proposed, which is the hydro-static pressure of a liquefied soil.

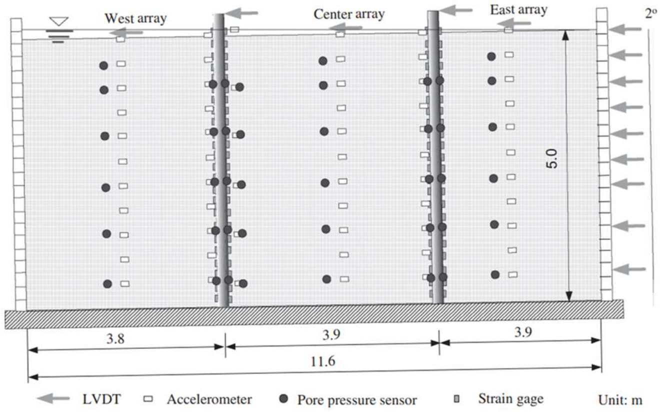

Figure 2-6 Large shaking table test conducted by He et al. (2009)

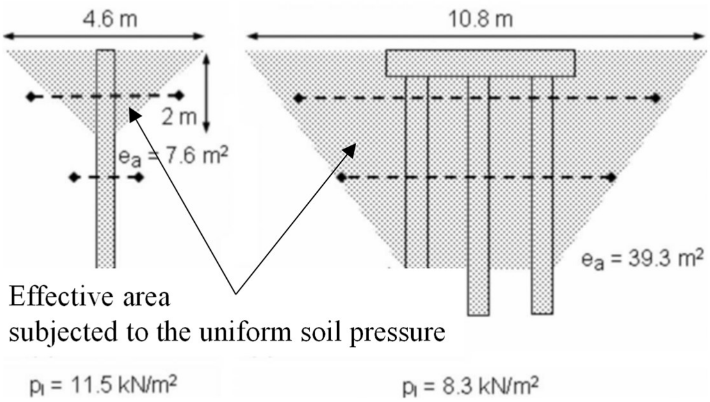

Figure 2-7 Effective area suggested by González et al. (2009)

González et al. (2009) performed centrifuge tests on single and group piles in liquefied gentle slope. The experimental soil pressure estimated using measured bending moment was consistent with the linear distribution of JRA (2012) in general. However, it was found that a significantly large pressure concentrated near the ground surface. Based on these concentration with negative pore pressure near ground surface, González et al. (2009) suggested effective area adjacent to the pile subjected to uniform soil pressure (Figure 2-7).

The design liquefied soil pressures were calibrated according to the experimental results of each study without a consensus. The calibrated range of the uniform soil pressure and the empirical factor was 5-40 kPa and 0.12-1.0, respectively. The calibrated values of each experiment are summarized in Table 2-2.

Table 2-2 Calibrated liquefied soil pressure

Research	Uniform pressure, kPa	Empirical factor	Data
Haigh (2002)	16.0	-	Centrifuge
Dobry et al. (2003)	10.3	-	Centrifuge
Gonzalez et al. (2009)	8.3, 11.5	-	Centrifuge
He et al. (2009)	9.0 - 40.0	1.00 - 1.23	Shaking Table
JRA (2012)	-	0.30	Field report
Tang et al. (2015)	19.5	-	Shaking Table
Su et al. (2016)	5.0	0.70	Shaking Table
Li et al. (2021)	-	0.12 - 0.24	Centrifuge

Furthermore, JRA (2012) considered the lateral force on the individual piles of the group to be distinct from the force on the single pile by applying a multiple ratio of the width of the group to the number of piles.

$$P_{\mathrm{LG}} = C_{\mathrm{L}} \times \sigma_v \times W/N \qquad (2\text{-}14)$$

where, P_{LG}: lateral force on the individual piles in group per unit length, W: the width of the pile group, N: the number of piles in group.

2.5 Pile skin friction in liquefied soil

During seismic loading, ground liquefaction causes loss of ground strength (Boulanger & Idriss, 2015; Zeghal et al., 1999).

During liquefaction, loss of ground confinement on the pile shaft increases the free length of the pile, leading to the risk of buckling failure (Bhattacharya & Madabhushi, 2008) (Figure 2-9). Following the excess pore pressure dissipation, the negative skin friction increases the load on pile toe beyond the pile head load (Sinha et al., 2022).

After the end of shaking, post-liquefaction settlement occurs due to the dissipation of excess pore pressure (Adamidis & Madabhushi, 2016; Basu et al., 2022; Guan et al., 2022). Thus, the effect of ground liquefaction on axial pile stability should be considered separately during and after the end of shaking.

Field blast liquefaction test, centrifugal model experiments and analytical studies were performed to analyze the pile behavior subjected to the dynamic liquefaction (Hussein & El Naggar, 2021; Ishimwe et al., 2018; Knappett & Madabhushi, 2008; Lusvardi, 2020; Xu et al., 2021).

Previous studies have commonly pointed out the reduction of shaft friction during shaking and the drag load after shaking. However, each researcher's details on each topic were different.

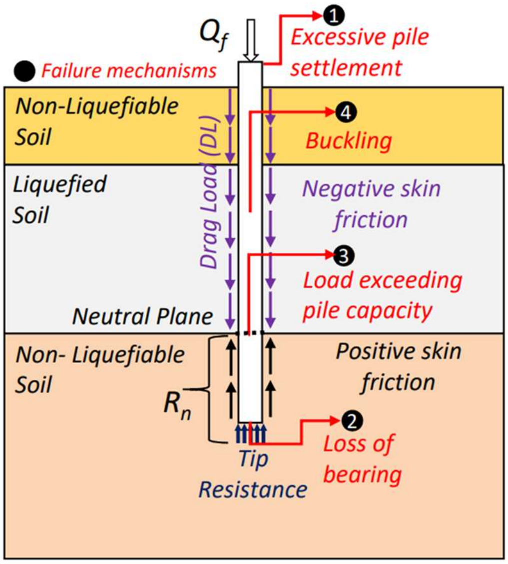

Figure 2-8 Axially loaded pile in liquefiable soil (Ziotopoulou and Wilson, 2018)

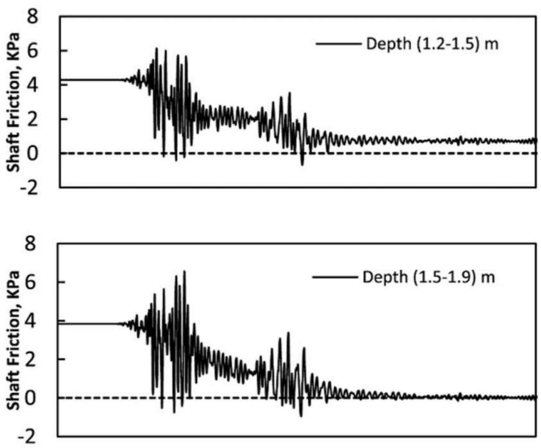

Figure 2-9 Loss of pile shaft resistance due to liquefaction (Hussein & El Naggar, 2021)

Rollins et al. (2018) reported the complete loss of positive shaft resistance in the liquefied layer by performing a field blast liquefaction test. Sinha et al. (2022) showed that the accumulated drag load during the spinning process for the centrifuge test was diminished by full liquefaction. The positive skin friction was not observed even the piles suffered significant settlement during shaking. However, Stringer and Madabhushi (2013) found that, despite the complete liquefaction, the positive shaft resistance was still recorded based on the dynamic centrifuge test (Figure 2-10). It was found that the shearing between the pile and soil due to the liquefied soil lateral movement resulted in the apparent shaft friction during full liquefaction. Reflecting on experimental results, ASCE (2014) recommended suitably reduced skin friction for the liquefiable layer, even if the layer does not reach full liquefaction.

The negative skin friction is caused by the relative settlement of the adjacent soil pulling the pile downward. Fellenius (2017) stated that the ultimate skin friction between the ground and the pile is independent of the direction. Thus, the negative skin friction can be calculated based on the interface shear strength between the ground and the pile as follows:

$$f_s = K\sigma_v' \tan\delta \qquad (2\text{-}15)$$

$$f_s = \beta\sigma_v' \qquad (2\text{-}16)$$

where f_s: the ultimate skin friction (=negative skin friction), K: the coefficient of lateral earth pressure, σ_v': the effective overburden stress, δ: the mobilized soil–pile interface friction angle, and β: the combined skin friction coefficient.

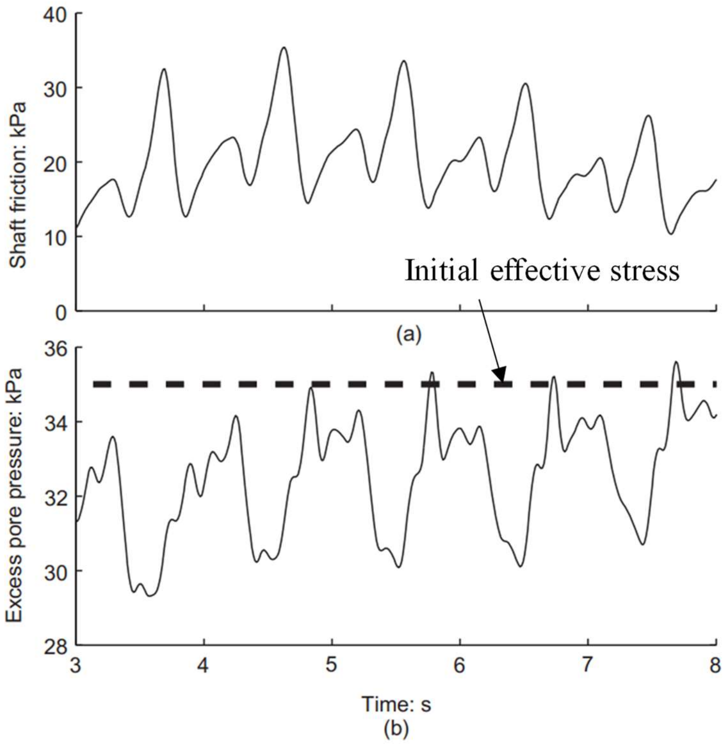

Figure 2-10 Residual shaft resistance during liquefaction (Stringer & Madabhushi, 2013)

δ can be considered as the soil friction angle ϕ for the piles with rough surfaces (Frost & DeJong, 2005). Fleming et al. (2008) suggested that the values of K for the static bored pile in sand and silt were 0.9 and 0.6, respectively, which were larger than the coefficient of lateral earth pressure at rest. In particular, Sinha et al. (2022) proposed $K = 1$ and $\delta = \phi$ in the analysis of liquefaction-induced downdrag. However, K is difficult to be determined because it depends on various factors such as the friction angle and the stress increment caused by superstructure (Kulhawy, 1991; Meyerhof & Adams, 1968).

Instead of using K and δ, the skin friction can be expressed proportionally to the effective overburden stress using a coefficient β. The β-coefficient varies with factors such as soil type, friction angle, relative density, pile surface roughness, and effective overburden stress (Fellenius, 2017; Fioravante, 2002; Loukidis & Salgado, 2008). The β-coefficient for the cohesionless soil was proposed based on the various case histories (Clausen et al., 2005; Fellenius, 2017; Rollins et al., 2005). Based on these works, CFEM (2006) suggested the β-coefficient of drilled piles with soil type for a practical design purpose in Table 2-3.

Table 2-3 beta-coefficient of bored piles from CFEM (2006)

Soil type	β
Silt	0.2-0.3
Loose sand	0.2-0.4
Medium sand	0.3-0.5
Dense sand	0.4-0.5
Gravel	0.4-0.7

The magnitude of drag load after liquefaction varies with the studies. Boulanger and Brandenberg (2004) modeled the negative skin friction within the liquefied layer as equal to the positive skin friction by multiplying a reverse proportional coefficient by the excess pore pressure ratio. Sinha et al. (2022)

reported that the drag load within the liquefied layer was equal to the drained interface shear strength (Figure 2-11).

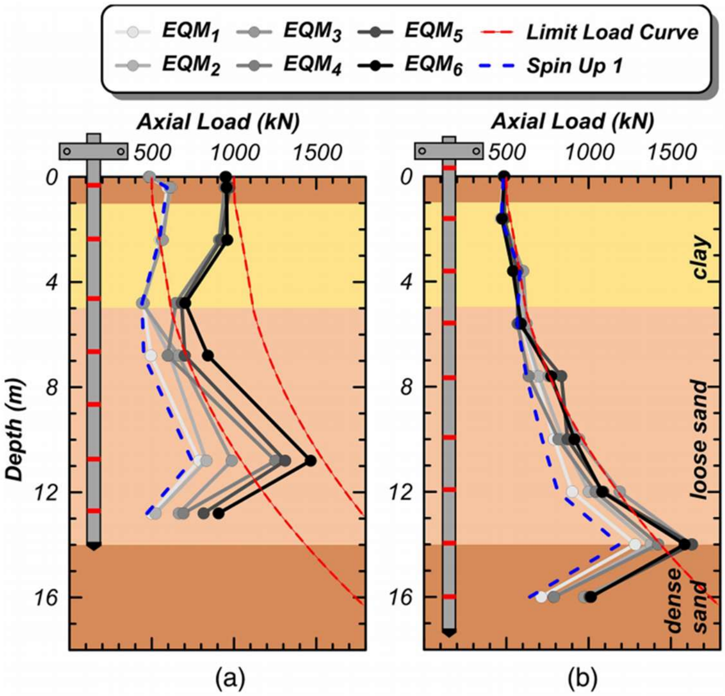

Figure 2-11 Drag load induced by post-liquefaction settlement (Sinha et al., 2022)

However, Rollins et al. (2018) and Rollins and Hollenbaugh (2015) reported that the drag load in the liquefied layer was only approximately 50% of the positive shaft resistance before the liquefaction occurrence (Figure 2-12). Similarly, Kevan (2017) and Elvis (2018) agreed with the smaller drag load than the positive shaft resistance by performing tests on various pile types. Based on the field test results, AASHTO (2020) recommended negative skin friction in the liquefied layer as a residual soil strength. Furthermore, Fellenius et al. (2020) assumed zero drag load within the liquefied layer.

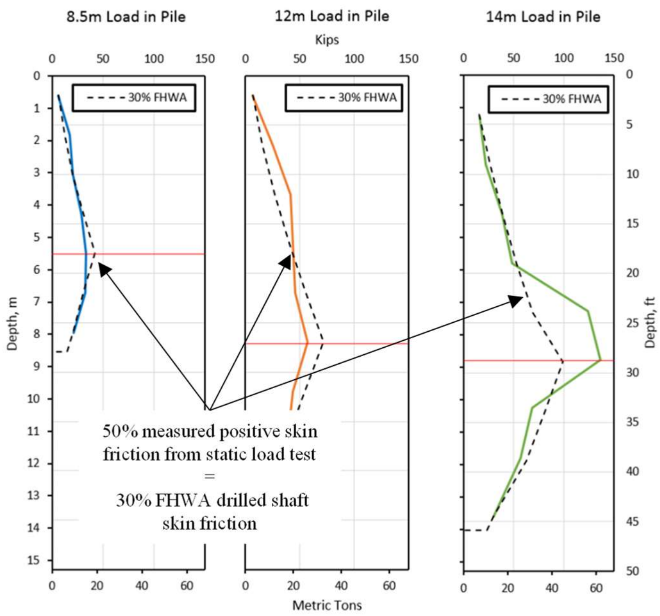

Figure 2-12 Drag load from blast liquefaction test (Rollins & Hollenbaugh, 2015)

2.6 Summary and research gap

As the result of earthquakes in recent decades, ground liquefaction has caused substantial damage to pile-supported structures, which has led to an increased need for research. Several studies have been conducted to investigate the seismic behavior of pile foundations in liquefied ground using experimental, analytical, and numerical approaches. Primary results show that pile bending moment induced by liquefied soil pressure and drag load due to post-liquefaction settlement are essential for research and practical designs.

Liquefaction studies have been mainly conducted on infinite gentle slope. However, many foundations of the waterfront structure are embedded in a finite slope with relatively high inclination. Due to the slope failure associated with the liquefaction, the lateral soil pressure on piles varies depending on the slope geometry. Furthermore, the piles in the liquefied slope are exposed to complex load combinations including static dead load, dynamic inertial load, drag load caused by reconsolidation settlement, and kinematic load caused by horizontal displacement of the ground.

For seismic pile design in liquefied slopes, it is crucial to have an accurate estimate of liquefied soil pressure and post-liquefaction drag load. However, current studies on this issue cannot sufficiently ensure the good performance of the pile foundation subjected to the liquefaction. The lack of knowledge and research raises motivation for further investigations, especially within the scope of the research work presented in this dissertation, as follows.

- Effect of liquefied slope on the overall seismic behavior of pile-supported structures
- Evaluation of liquefied soil pressure considering ground geometry, pile location, input acceleration
- Effect of pile grouping on liquefied soil pressure enhancing lateral stability against pile bending failure
- Effect of liquefaction on variation in axial load distribution of end-bearing piles
- Evaluation of ultimate drag load induced by post-liquefaction settlement

Chapter 3. Dynamic centrifuge test

3.1 Introduction

This chapter describes the planning, preparation, and implementation of dynamic centrifuge model tests performed to analyze the seismic behavior of piles in liquefied finite slope.

In section 2, the descriptions of the prototype wharf and the centrifuge model are provided. The total process of designing, manufacturing, and applying viscous fluid in consideration of the scale law is described. The detailed installation process of the experiment model, composed of various elements such as ground, structure, and measurements, is presented. The relative density and saturation level of the prepared model ground are discussed. The total of four experimental cases are introduced.

In section 3, the liquefaction occurrence of the model ground is presented. The model ground should be fully liquefied to analysis of the piles in liquefied slope. Therefore, the liquefaction of the ground is confirmed through the analysis of the excess pore pressure measured in each experimental case. The effects of the viscosity of the pore fluid and the input amplitude on the liquefaction of the ground are also analyzed.

3.2 Centrifuge model

3.2.1 Equipment

Centrifuge tests were conducted at the Korea Advanced Institute and Science Technology using beam-type geotechnical centrifuge equipment with a 5 m radius. The maximum capacity of the centrifuge machine is roughly 240 g-t. The seismic loading was carried out on the container base using a self-balanced biaxial shaking table. The shaking table has operation limits of maximum shaking acceleration of 20 g and payload of 700 kg under a centrifugal acceleration of 100 g. Data acquisition system have 64 strain gauge channels, 32 LVDT channels, and 32 accelerometer channels with 1 kHz dynamic sample rate.

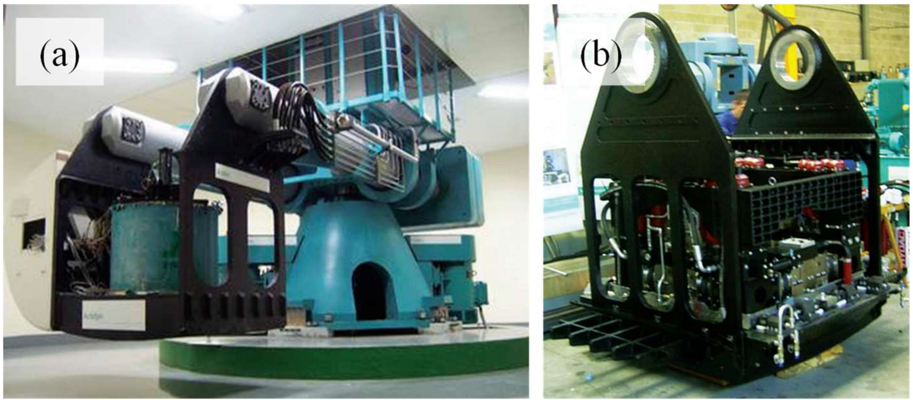

Figure 3-1 Centrifuge facilities at Korea Advanced Institute of Science and Technology: (a) centrifuge machine, (b) biaxial shaking table (KOCED, 2016)

The test model was built in a rigid container with internal dimensions of 490 mm × 490 mm × 590 mm covered by natural cork materials to minimize the boundary effect (Figure 3-2). Gibson et al. (1981) found that cork has a large energy absorption capacity because of its distinctive cellular structure.

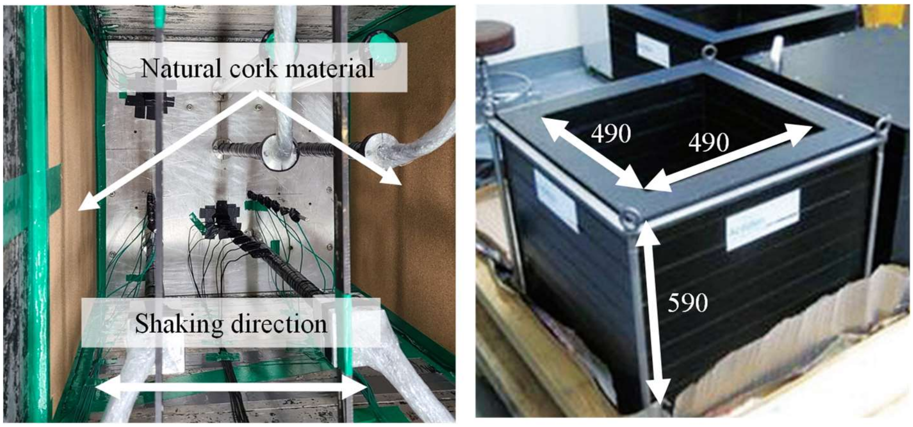

Figure 3-2 Rigid soil container covered with natural cork

3.2.2 Model configuration

The prototype of this experimental model was a pile-supported wharf in Pohang New Port that is a deck mass supported by numerous piles as shown in Figure 3-3.

A model structure supported by 2 × 2 group piles was designed to simulate a segment of the prototype structure. The concrete slab mounted on the pile heads is simulated by a mass block considering the weight and dimension. The abutment, caisson, and rubble mound included in prototype structure are not simulated in centrifuge model to focus on the interaction between the piles and liquefied slope. End-bearing piles are considered to simulate the prototype pile socketed in the rock layer.

A model ground considered a finite slope of 27°, which simulates prototype ground geometry. The prototype dense sandy gravel layer is replaced with a loose sand layer to maximize the effect of the liquefied slope on the piles. Poorly graded silica sand is adopted as a geomaterial to prevent particle size segregation during model ground installation by wet pluviation method.

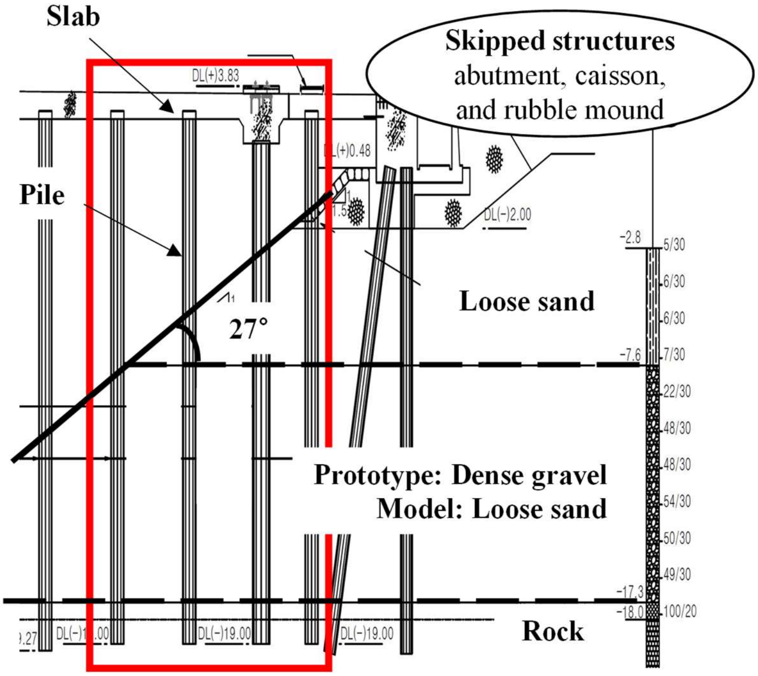

Figure 3-3 Prototype pile-supported wharf in Pohang New Port, Korea

Figure 3-6 shows three types of centrifuge model adopted in this study. Model 1 was a single pile and a 2 × 2 pile group installed in a finite 27° slope with water as a pore fluid. Viscous fluid was applied to Model 2 instead of water with an additional single pile. Slope inclination of 15° was adopted to Model 3. Two additional piles were included. The first was located approximately in the middle of the group piles to investigate the group effect. The other was installed near the slope crest to consider the slope effect.

A length scale factor of approximately 34 was applied to Model 1, and that of 46 was considered for Models 2 and 3. All data were presented in prototype scale unless stated otherwise. Note that different scale factors were adopted to simulate identical prototype structures considering different model pile dimensions.

Table 3-1 and Table 3-2 present the dimensions of model piles and decks determined in accordance with the scaling law of Madabhushi (2017). An aluminum pipe was selected to simulate the prototype steel pipe pile. The dimension of the model pile was determined on the basis of the scale of flexural stiffness to adequately simulate the pile’s response to the horizontal load. The model pile of Model 1 had a diameter of 0.85 m and that of Models 2 and 3 was 0.92 m in the pile diameter.

The single and group piles were instrumented with a number of pairs of strain gauges to obtain the bending moment and axial load. The Young’s modulus of the instrumented piles was calibrated from a pile bending test under the cantilever condition (Figure 3-4).

The dimension of the model deck on the pile group was determined on the basis of the weight of the superstructure. The deck on the single pile was designed as one-fourth of that mounted on the group.

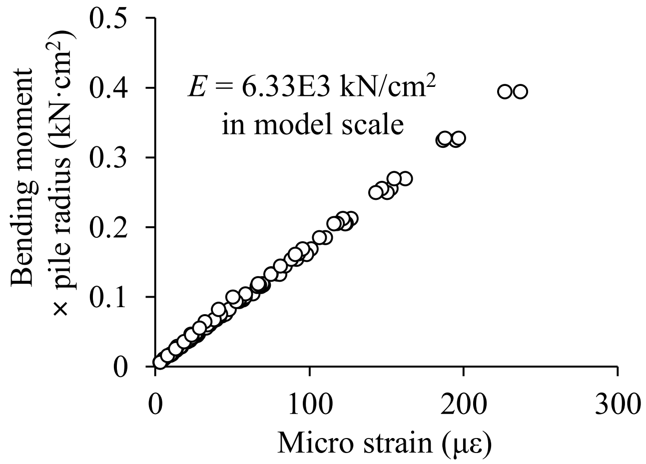

Figure 3-4 Calibration of Young's modulus

Table 3-1 Pile properties (in prototype scale)

Model	Diameter (m)	Thickness (m)	Total length (m)	Flexural stiffness (kN·m2)	Compressional stiffness (kN)
1	0.85	0.07	18.0	8.31E5	-
2 & 3	0.92	0.05	20.0	7.66E5	7.79E6

Table 3-2 Deck properties (in prototype scale)

Foundation type	Width (m)	Length (m)	Thickness (m)
Single pile (Model 1)	2.4	2.4	2.3
Single pile (Models 2 & 3)	2.3	2.3	2.7
2 × 2 pile group (Model 1)	7.1	7.1	1.0
2 × 2 pile group (Models 2 & 3)	7.3	7.3	1.0

A finite slope with toe and crest was prepared using saturated silica sand whose physical properties are presented in Table 3-3 and Table 3-4, Figure 3-5. The model material was poorly graded sand, which had maximum and minimum dry unit weights of 16.1 kN/m^3 and 12.2 kN/m^3, respectively.

Properties of the model ground were determined by performing a preliminary ground installation identical to the main centrifuge tests. Aluminum cans were recovered in the model ground of the preliminary ground preparation and subsequently used to extract soil for oven drying analysis. The saturated unit weight and relative density of the model ground were approximately 17.2 kN/m^3 and 26%, respectively.

Table 3-3 Physical properties of silica sand (Kim et al., 2016)

Properties	Values
Specific gravity	2.65
Maximum dry unit weight (kN/m^3)	16.1
Minimum dry unit weight (kN/m^3)	12.2
Soil classification (USCS)	SP

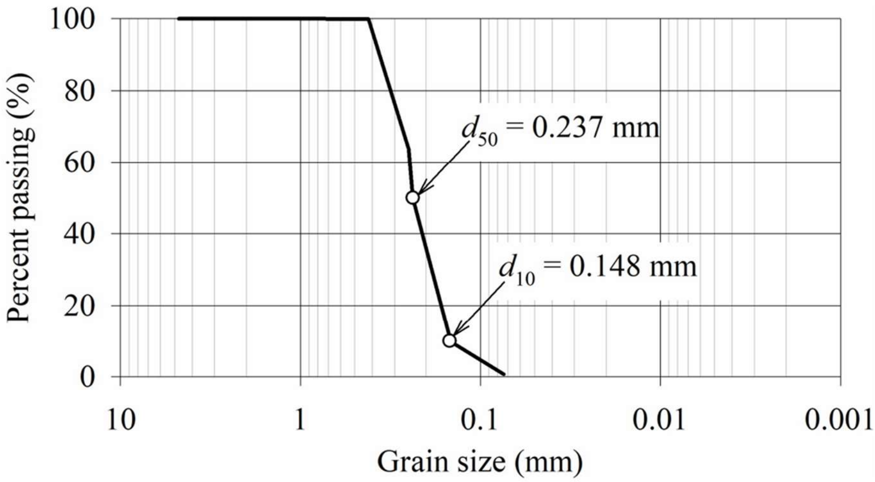

Figure 3-5 Grain size distribution curve of silica sand (Tran, 2021)

Table 3-4 Mechanical properties of silica sand (Kim et al., 2016)

Relative density (%)	Effective confining pressure (kPa)	Peak friction angle (°)	Critical friction angle (°)
48	100	39.7	
44	200	38.0	
47	400	37.9	
59	600	36.8	
64	50	43.2	
69	100	43.9	36.6
67	200	41.8	
66	400	40.1	
83	100	45.2	
78	200	43.1	
84	400	42.8	

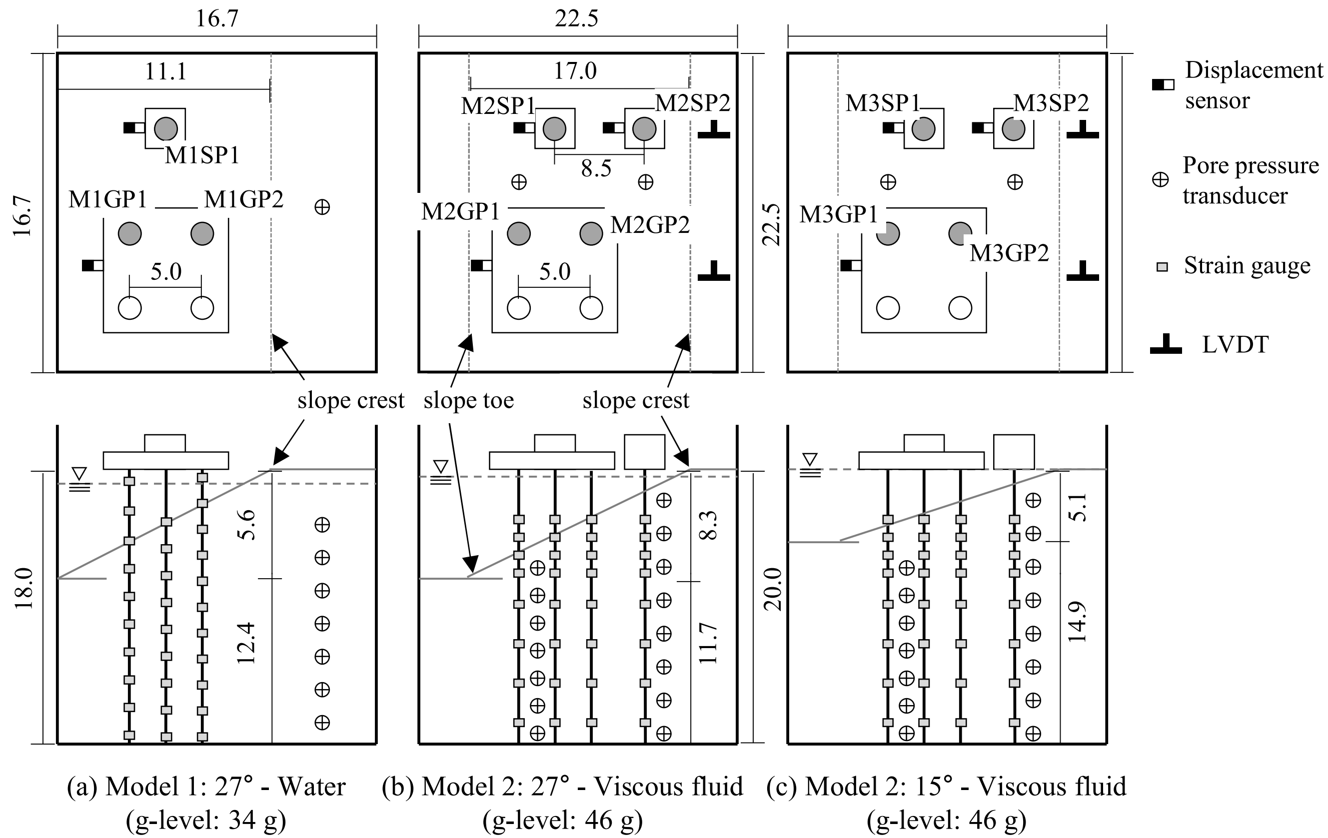

Figure 3-6 Layouts of dynamic centrifuge tests

3.2.3 Viscous fluid preparation

For the simulation of ground liquefaction in centrifuge test, variation of pore pressure in saturated model ground during shaking should be considered. However, an inconsistency exists in the scaling of time between dynamic and diffusion phenomena. The consolidation time in the model is n^2 times faster than that in the prototype, while the dynamic time is n times faster. Thus, it is necessary to delay the consolidation time by adjusting the grain size distribution of the ground material or the viscosity of the pore fluid.

This inconsistency was solved by increasing pore fluid viscosity in this study. hydroxypropyl methylcellulose (HPMC) solution was adopted as a pore fluid. The HPMC solution has been applied as a pore fluid in many previous studies simulating the liquefaction phenomenon (Chian & Madabhushi, 2010; Li et al., 2021; Saha et al., 2020; Sawamura et al., 2021).

In order to prepare HPMC solution, the hot-cold method is used, which dissolves the powder in hot water over 90 °C and then lowers the temperature of the solution (Figure 3-7). The detailed process of hot-cold method is as follows:

1. The water should be at least 90°C for about half of the required amount in a vessel. Gradually add HPMC powder while stirring.
2. HPMC powder initially floats on the surface of the hot water, but gradually disperses to form a uniform slurry. Make sure that all particles are thoroughly soaked in the hot water by stirring and dispersing.
3. Add the rest of water as cold or ice water while stirring. For sufficient hydration, the temperature of mixture should be less than 40 °C.

4. Cool the resultant mixture while stirring until it becomes transparent.

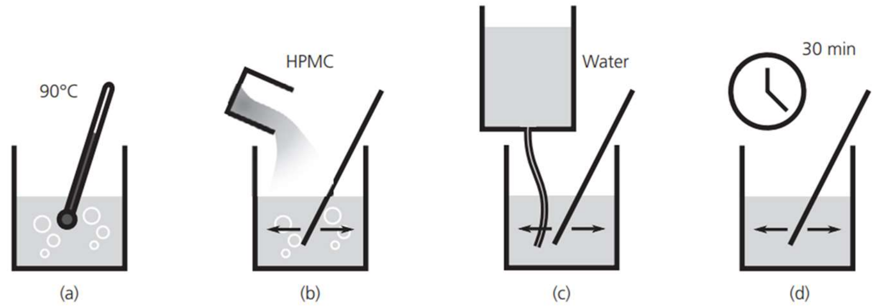

Figure 3-7 Hot-cold method for preparation of HPMC solution (Adamidis & Madabhushi, 2015)

Figure 3-8 Preparation of HPMC solution

A large amount of bubble was generated during the HPMC solution production process. however, clear fluid was obtained after stabilization time of approximately 6 h. The fluid was stored in airtight containers. It was confirmed that the viscosity of the fluid at laboratory temperature of 15 - 16 ℃ has approximately 46 times that of water. Thereafter, the soil-fluid slurry had been immersed with the pore fluid for over 24 h before pluviation.

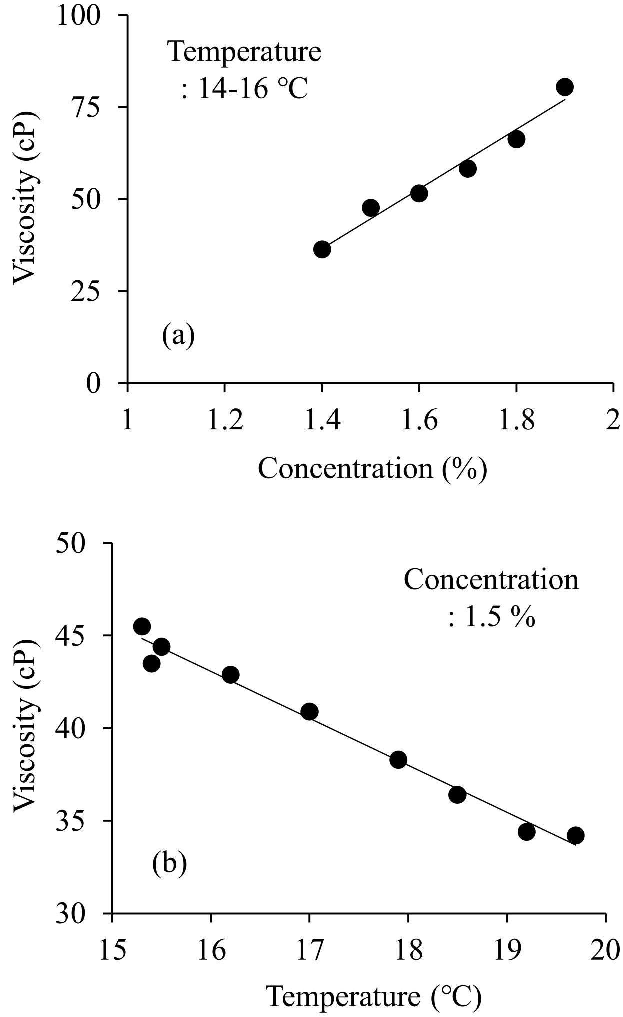

Figure 3-9 Viscosity of HPMC solution depending on (a) concentration of HPMC solution and (b) fluid temperature

Figure 3-10 Saturation of soil–fluid slurry

3.2.4 Model installation

The experimental model was constructed as follows. First, the thin steel bar with pore pressure transducers and model piles with strain gauges were fixed on the container base.

Second, the model ground was prepared in sequence using different preparation methods. The ground below the slope toe was constructed with using the wet pluviation method, raining the saturated silica sand on the fluid-filled soil container through a sieve (Bradshaw & Baxter, 2007).

The model soil had been immersed with the pore fluid for over 24 h before pluviation. Thereafter, the ground above the slope toe was manually formed using the slurry deposition method, depositing the saturated silica slurry in advance according to the slope level marked on the wall (Kuerbis & Vaid, 1988). Fluid level was set slightly higher than the ground level to maintain saturation.

Finally, decks were rigidly connected to the pile heads, and laser sensors were installed to record deck displacement.

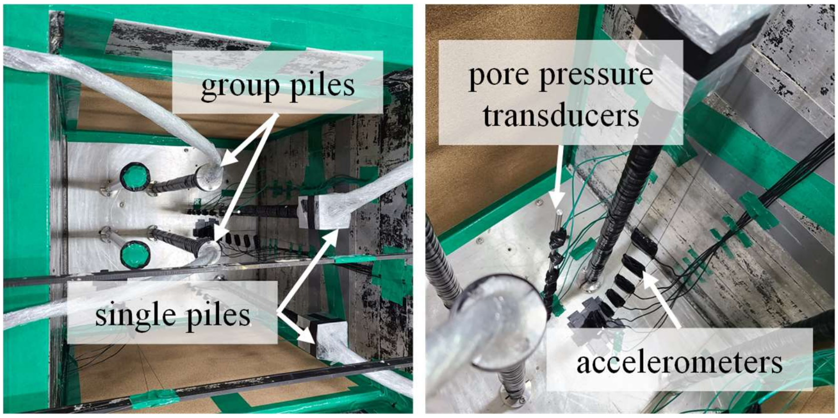

Figure 3-11 Model installation before wet pluviation

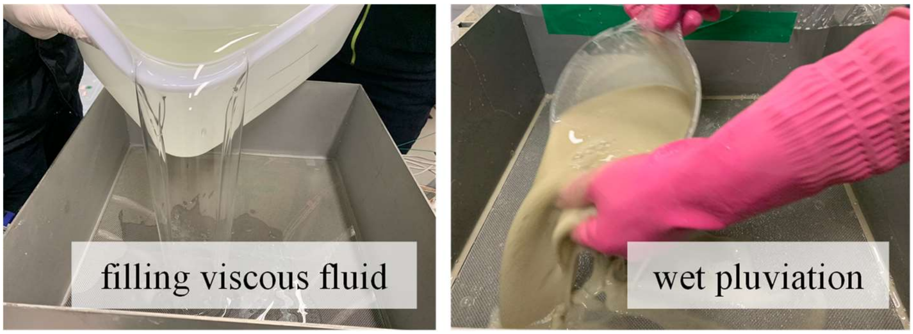

Figure 3-12 Wet pluviation for model ground below slope toe

Figure 3-13 Model ground above slope toe with slurry deposition method after preliminary ground preparation. Note that photos were taken after lowing fluid level for better visibility.

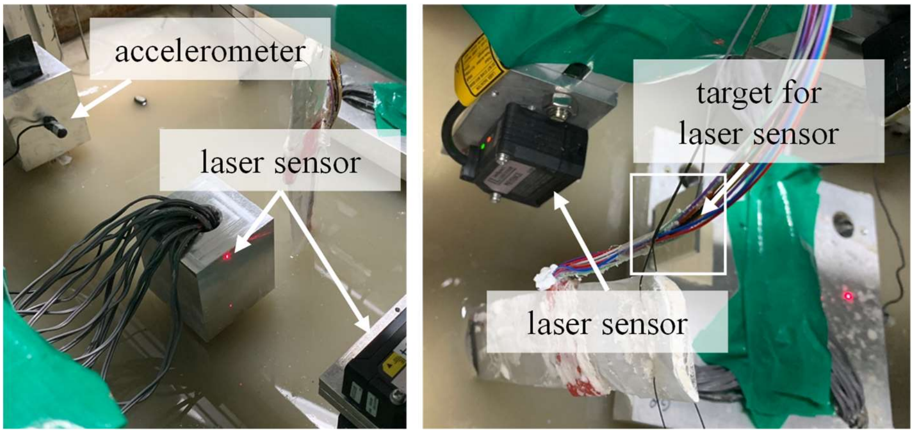

Figure 3-14 Measurements for deck connected to pile head

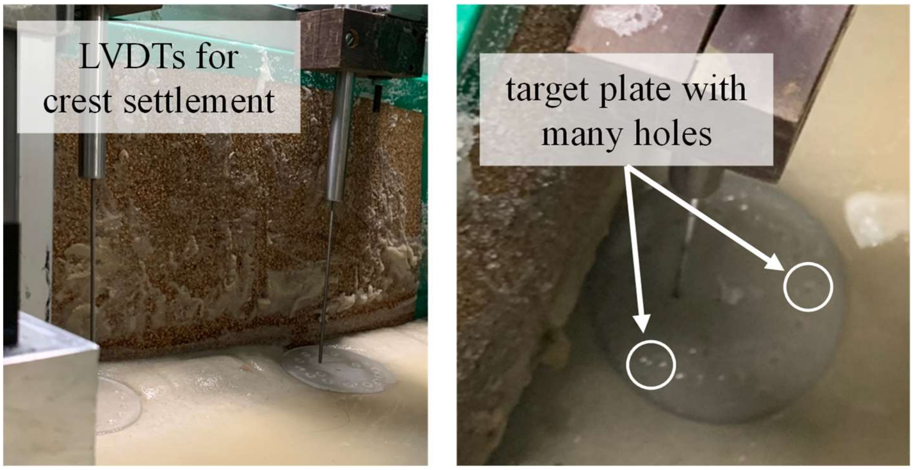

Figure 3-15 LVDTs for crest settlement measure

3.2.5 Discussion on the test model

- Loose density (26%)

The model ground showed loose density because it was prepared using wet pluviation method. The wet pluviation method constructs the model ground by dropping the saturated sand particles into a fluid-filled soil container. Each particle passing through the sieve falls vertically through the fluid and is deposited at the ground surface layer by layer (Vaid & Negussey, 1988). The prepared ground has a substantially loose initial density because the particles are subjected to the drag force of the fluid.

Vaid and Negussey (1988) reported that the initial relative density of specimens made by wet pluviation of Ottawa sand were 28-30%. Ha et al. (2011) reported initial relative density of 20-30% in 1g shaking test using various sands (Jumunjin, Yeongjong, Incheon, and Hangang) in Korea.

One disadvantage of this method is that the initial density cannot be controlled during model ground preparation. Preparing the ground with desirable relative density is possible by applying additional compaction after wet pluviation (Varghese & Madhavi Latha, 2014). However, additional compaction was disregarded in this study due to the maintenance of the slope condition. Therefore, the relative density of the model ground in this study was 26%, which is the initial relative density followed by the wet pluviation method.

- Saturation

In this study, the degree of saturation of the model ground was not directly confirmed. However, several methods were applied to saturate the model ground.

First, the void air was removed by using boiled water during the production of viscous fluid. The fluid-soil slurry was kept in a sealed box to prevent the ingress of external air. The slurry was pluviated into the soil container filled with viscous fluid to minimize contact with air.

Additionally, previous studies have reported that the wet pluviation method has advantages for soil saturation. Vaid and Negussey (1984) and Kuerbis and

Vaid (1988) suggested that the wet pluviation method using de-aired water ensure saturation of soil specimen in laboratory. Furthermore, Huang et al. (2019) reported that the full saturation of the model ground prepared by wet pluviation method in centrifuge test.

- Buckling instability of model pile

In this study, in order to ensure bending failure of the model piles, buckling instability of the model piles was examined based on the slenderness ratio and Euler's buckling load.

The slenderness ratio is defined as a ratio of effective length and minimum radius of gyration. The effective length of single pile, which is vulnerable to be slender pile, was determined to be 2 times of unsupported length of the pile (Bhattacharya & Madabhushi, 2008). The minimum radius of gyration was calculated using the outer and inner diameters of the aluminum pipe pile used in this study. The calculated slenderness ratio was 129 and classified as a 'slender column'.

$$(slenderness\ ratio) = \frac{L_{\mathrm{eff}}}{r_{\mathrm{min}}} = 129 \qquad (3\text{-}1)$$

$$r_{\mathrm{min}} = \sqrt{\frac{I}{A}} = \sqrt{\frac{0.0119}{0.1237}} = 0.31\ m \qquad (3\text{-}2)$$

$$L_{\mathrm{eff}} = 2 \times L_0 = 40\ m \qquad (3\text{-}3)$$

where, I: second moment area [m4], A: cross-sectional area [m2], L_0: unsupported length (pile length in liquefied soil) [m]

Table 3-5 Various cases of effective length of piles in liquefiable soils (Bhattacharya and Madabhushi, 2008)

Case	Boundary condition of top and bottom of the liquefied layer		Effective length
	Top	Bottom	
1	Fixed (θ = 0, δ = 0)	Fixed (θ = 0, δ = 0)	0.5×L0
2	θ = 0, δ ≠ 0	Pinned (θ ≠ 0, δ = 0)	2×L0
3	θ = 0, δ ≠ 0	Fixed (θ = 0, δ = 0)	L0
4	Pinned (θ ≠ 0, δ = 0)	Fixed (θ = 0, δ = 0)	0.7×L0
5	Pinned (θ ≠ 0, δ = 0)	Pinned (θ ≠ 0, δ = 0)	0.5L0
6	Free (θ ≠ 0, δ ≠ 0)	Fixed (θ = 0, δ = 0)	2×L0

* θ: rotation angle, δ: displacement

Euler's buckling load of the pile was calculated based on the flexural stiffness and the effective length. The buckling load can amplify lateral deflection of the pile. The buckling amplification factor in this study was only 1.09.

$$P_{cr} = \frac{\pi^2}{L_{\text{eff}}^2} EI = \frac{\pi^2}{4L_0^2} EI = 4637\ kN \quad (3\text{-}4)$$

$$\frac{P}{P_{cr}} = \frac{372}{4637} = 0.08 \quad (3\text{-}5)$$

$$\frac{\delta}{\delta_0} = \frac{1}{1-\frac{P}{P_{cr}}} = 1.09 \quad (3\text{-}6)$$

where, P: pile axial load, δ: lateral deflection of pile in the presence of load P, δ_0: lateral deflection of pile in the absence of load P

3.2.6 Test program

The test model was spun up to the target centrifuge acceleration after the model installation. Thereafter, sinusoidal waves with a frequency of 1.5 Hz were applied at the container base. Figure 3- shows two types of input motions used in centrifuge model tests. The motion with maximum acceleration of 0.1 g was designed to have a longer duration for the occurrence of liquefaction in model ground.

Thus, a total of four cases were conducted with the combination of ground models and maximum accelerations: Model 1 with ramped 0.2 g (Case 1), Model 2 with ramped 0.2 g (Case 2), Model 2 with constant 0.1 g (Case 3), and Model 3 with ramped 0.2 g (Case 4), summarized in Table 3-6. In this study, the model ground was re-constructed in every case without sequential seismic loading. A collapse of the slope was anticipated with the occurrence of liquefaction.

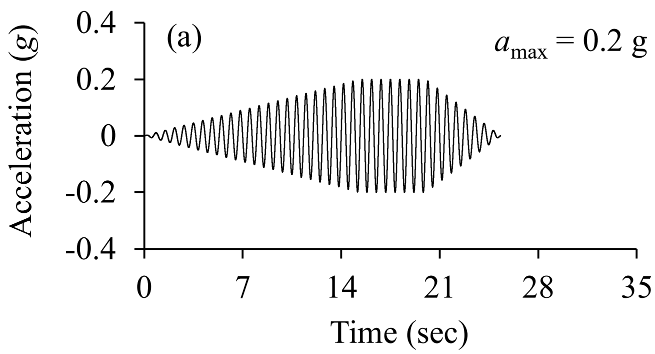

Figure 3-16 Input base motions: (a) ramped motion with 0.2 g and (b) constant motion with 0.1 g

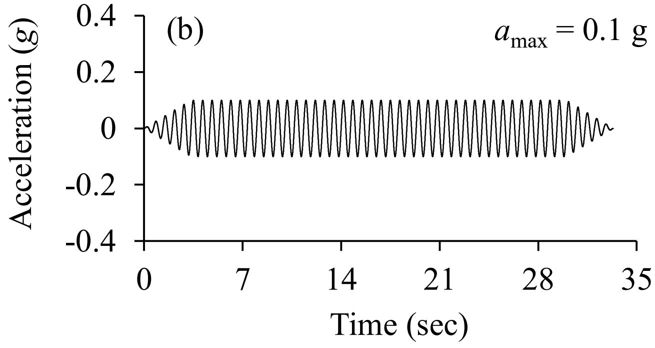

Figure 3-(continued) Input base motions: (a) ramped motion with 0.2 g and (b) constant motion with 0.1 g

Table 3-6 Test program

Case No.	Model ground	Input motion
1	Model 1: 27° slope with water	Ramped 0.2 g
2	Model 2: 27° slope with viscous fluid	Ramped 0.2 g
3	Model 2: 27° slope with viscous fluid	Constant 0.1 g
4	Model 3: 15° slope with viscous fluid	Ramped 0.2 g

3.3 Liquefaction of model ground

3.3.1 Effect of viscous fluid

The liquefaction of the ground can be observed by the excess pore water pressure in the ground. Figure 3-17 shows time histories of excess pore pressure near bottom of the container. It was confirmed that excess pore pressure was developed in every case. In Cases 2 and 4, where ramped 0.2 g motion was applied, the excess pore pressure rapidly increased and reached initial effective stress within the motion. However, the maximum excess pore pressure in Cases 1 and 3 was smaller than the initial effective stresses. The excess pore pressure in Case 1, using water as a pore fluid, started to decrease before the end of seismic loading. The constant 0.1 g motion failed to liquefy the model ground as quickly as the ramped 0.2 g motion, but it kept accumulating excess pore pressure until the end of seismic loading.

Figure 3-18 shows the time history of increase in excess pore water pressure by depth. The cyclic amplitude of pore pressure was filtered out for better visibility. In Cases 3 and 4, the viscous fluid increased the consolidation time resulting in a complete undrained loading condition. As a result, the rate of excess pore pressure increment was constant regardless of the depth. However, in Case 1, the development of excess pore pressure was restrained at the shallower depth due to the fast drainage condition.

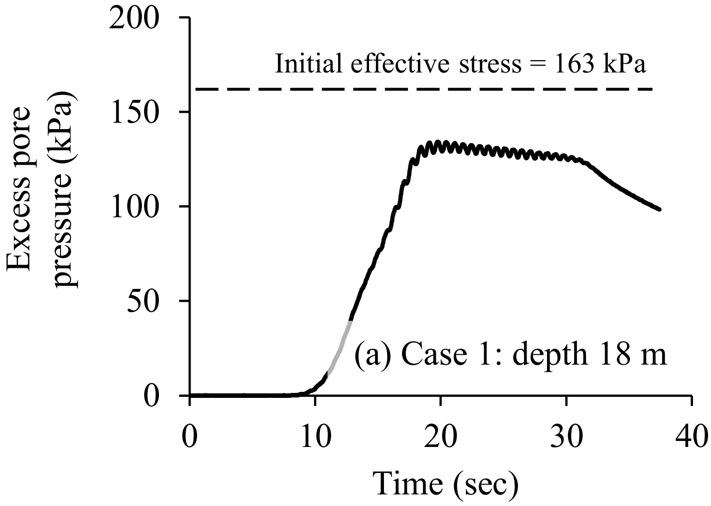

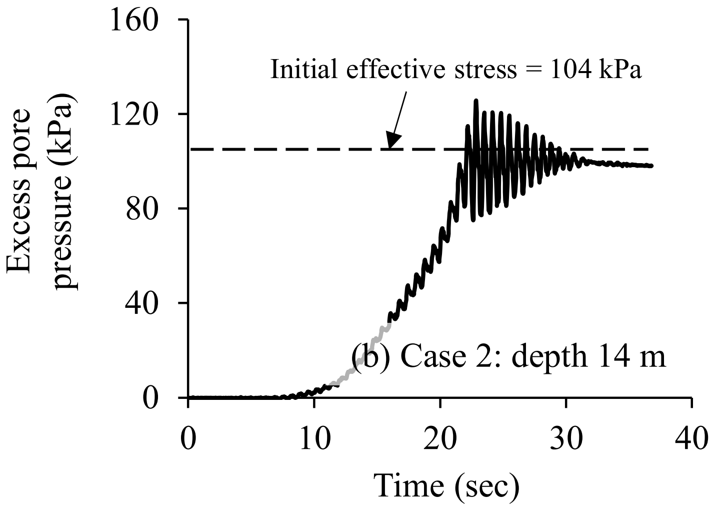

Figure 3-17 Time histories of excess pore pressure near bottom of the container

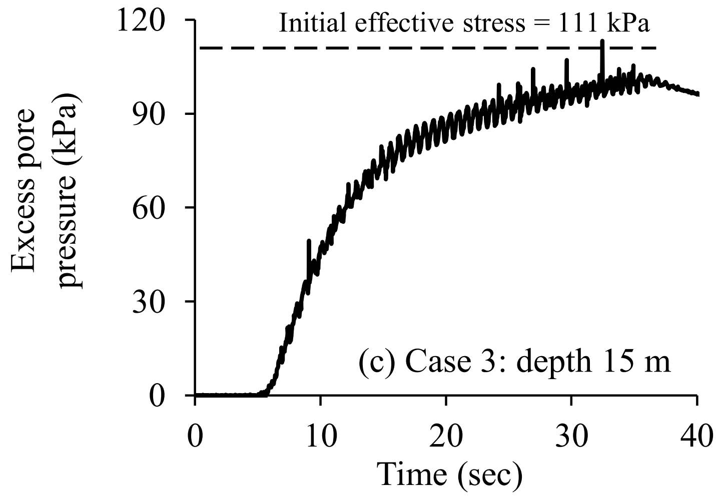

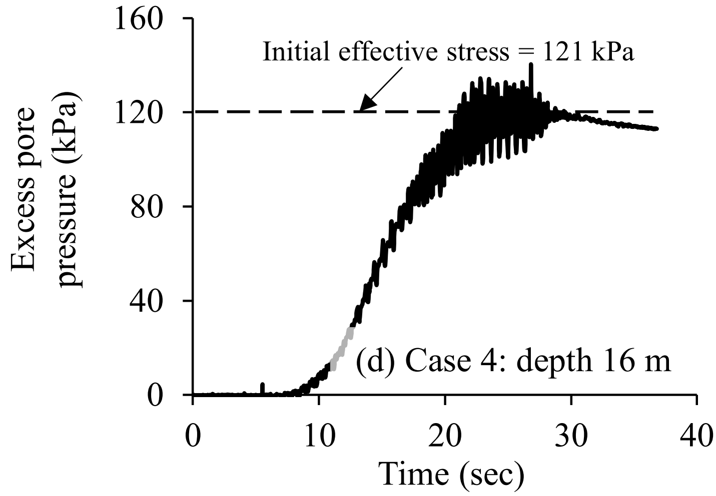

Figure 3-(continued) Time histories of excess pore pressure near bottom of the container

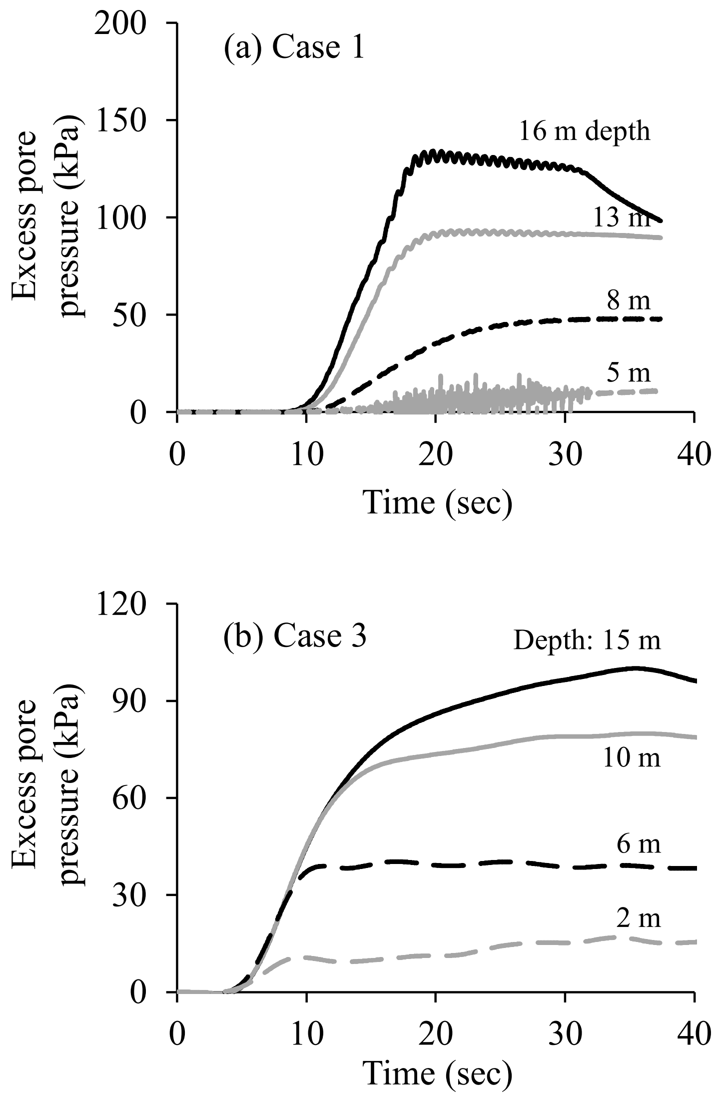

Figure 3-18 development of excess pore pressure at various depths

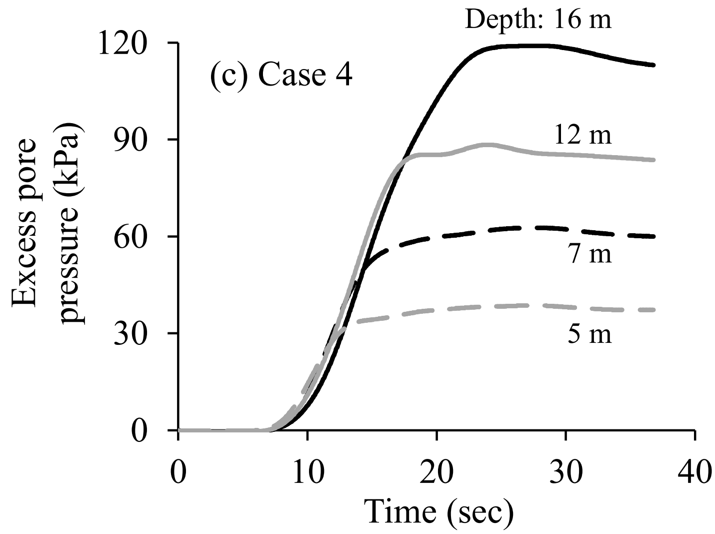

Figure 3-(continued) development of excess pore pressure at various depths

Figure 3-19 shows the profiles of excess pore pressure at various times. In Cases 3 and 4, the model ground was liquefied sequentially from shallow to deep. However, in Case 1, the smaller increase in excess pore pressure was at the shallower depth. As a result, complete liquefaction could not be achieved at any depths. The suppressed increment of excess pore pressure implied that the model ground with water pore fluid in the dynamic centrifuge test was not in undrained condition under seismic loading.

After the end of shaking, the excess pore pressure was dissipated toward ground surface (Figure 3-20). The reconsolidation of liquefied ground in Case 1 was almost finished before approximately 150 s. However, it was still in process after 450 s in Cases 2, 3, and 4 using viscous pore fluid.

Several pore pressure transducers malfunctioned owing to the wrong direction provided in Case 2. The transducer near the bottom and the other transducers were installed in the horizontal direction and vertical directions, respectively. Transducers set in the vertical direction failed to measure owing to the interference of soil particles and centrifugal acceleration. The measured pore pressure near the bottom in Case 2 is shown in Figure 3-17. In the Cases with viscous pore fluid, ground liquefaction started from the shallow depth and gradually spread to the deep depth. Thus, the occurrence of liquefaction in the deepest depth infers that the model ground was liquefied in full depths in Case 2 as well.

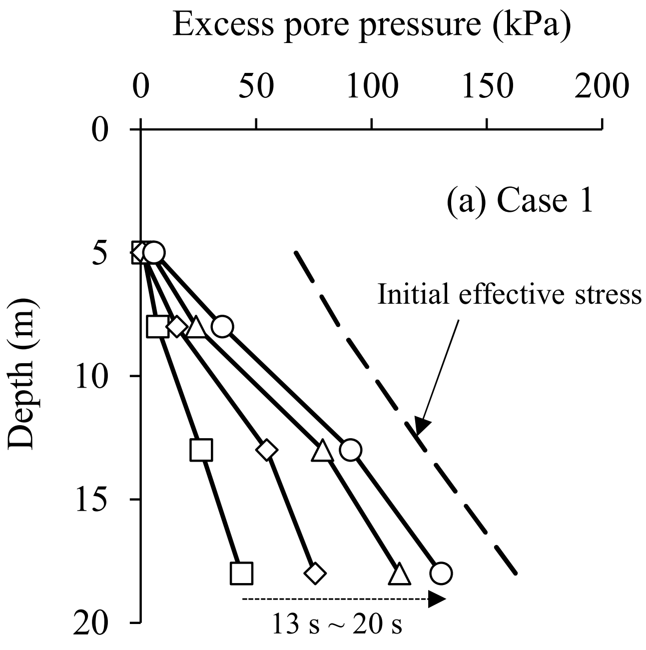

Figure 3-19 Development of excess pore pressure at various depths

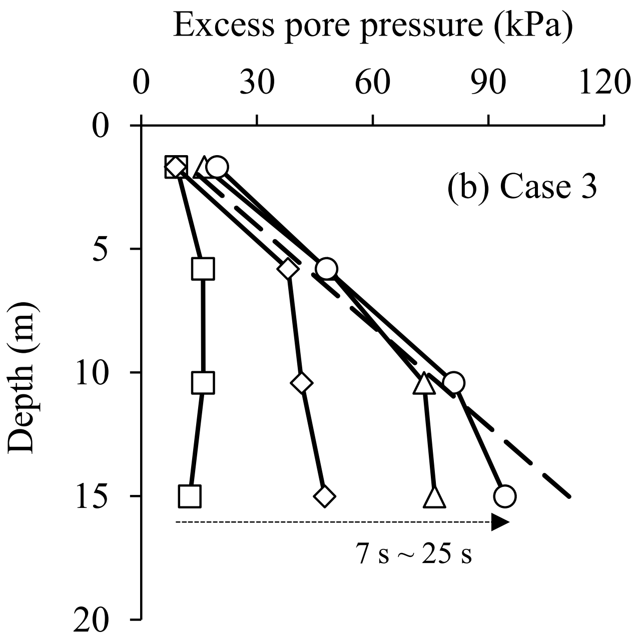

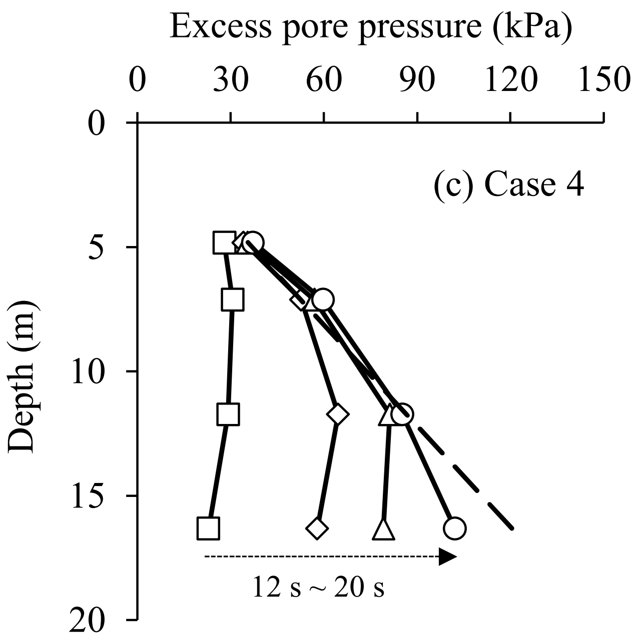

Figure 3-(continued) Development of excess pore pressure at various depths

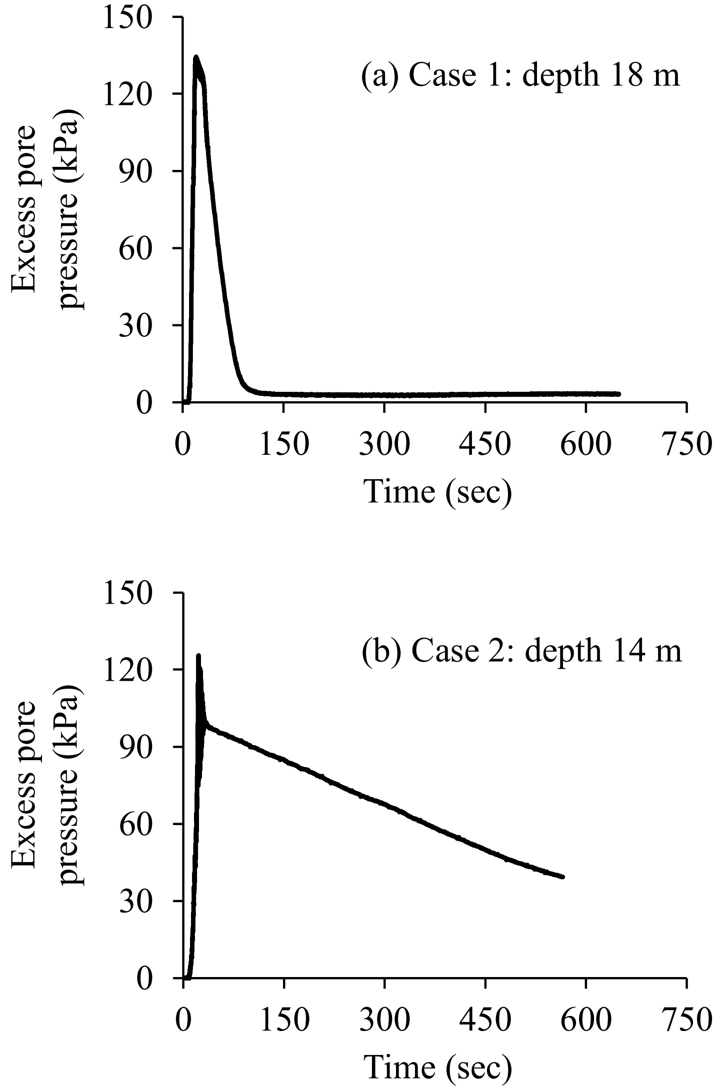

Figure 3-20 Time histories of excess pore pressure dissipation

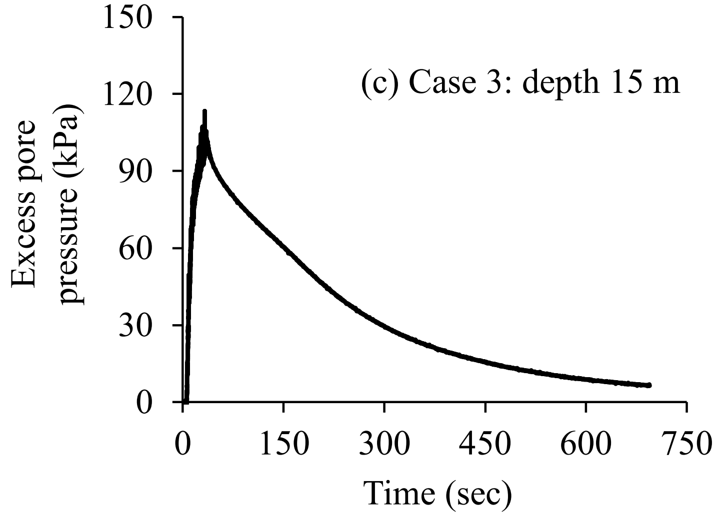

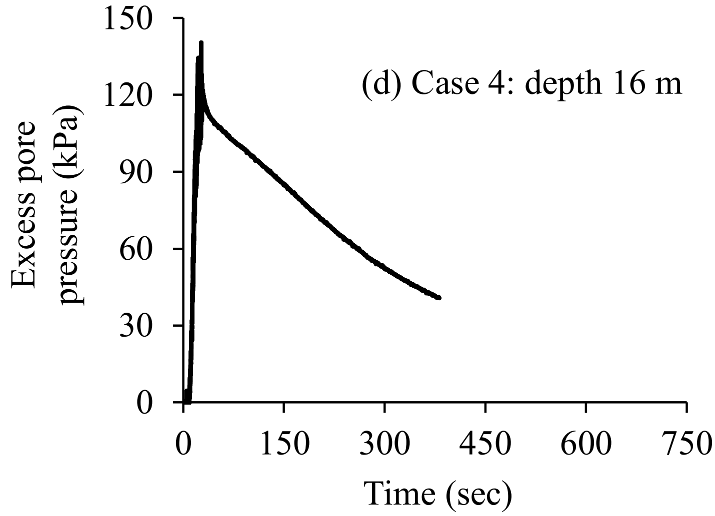

Figure 3-(continued) Time histories of excess pore pressure dissipation

3.3.2 Effect of type of input motion

In this study, ramped 0.2g and constant 0.1g sinusoidal waves were applied to analyze the effect of input motions on the development of excess pore pressure in the model ground. The time histories of the excess pore pressure and the input acceleration were analyzed.

Figure 3-21 and Figure 3-22 show excess pore pressure response to input acceleration in Cases 2 and 3, respectively. It was found that acceleration peaks below 0.04g did not generate excess pore pressure.

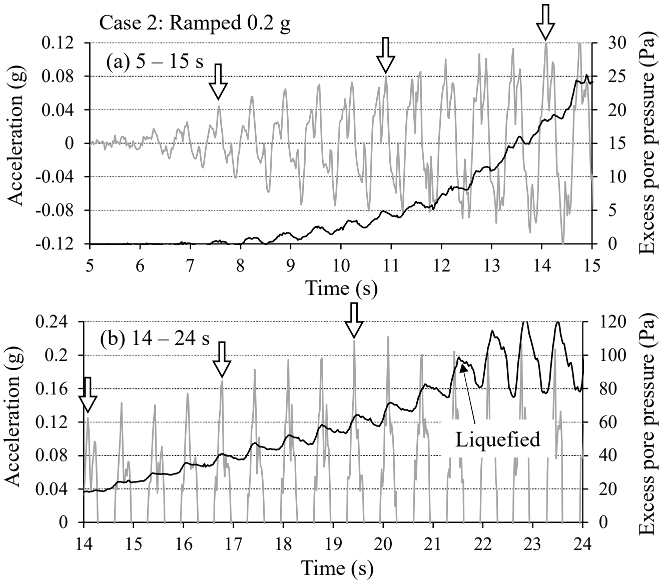

Figure 3-21 Excess pore pressure response to input acceleration in Case 2

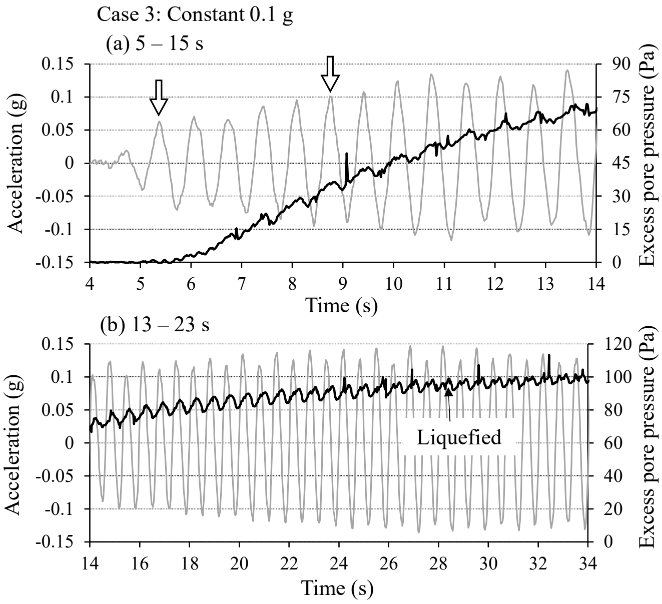

Figure 3-22 Excess pore pressure response to input acceleration in Case 3

The increase in the excess pore pressure ratio per cycle according to the peak amplitude is shown in Figure 3-23. In Case 2, the excess pore pressure ratio increased linearly with the increase in peak amplitude. On the other hand, in Case 3, the excess pore pressure ratio showed a bi-linear increase trend, with a rapid increase initially followed by a sudden decrease in the increase rate.

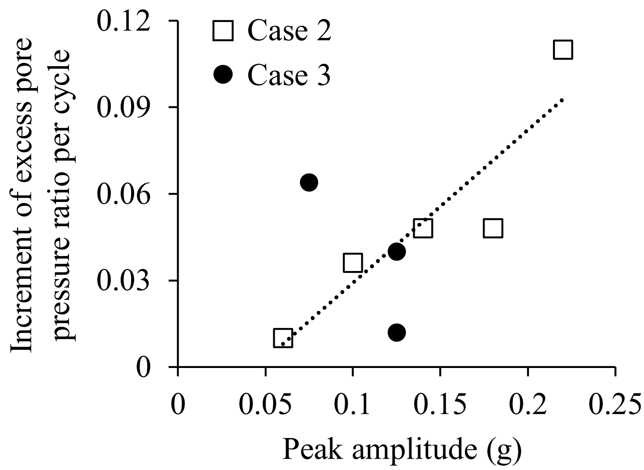

Figure 3-23 Increment of excess pore pressure ratio per cycle corresponding to peak amplitude

3.4 Summary

This chapter described the planning, preparation, and implementation of dynamic centrifuge model tests performed to analyze the seismic behavior of piles in liquefied finite slope.

The main conclusions can be summarized as follows.

(1) A total of three centrifuge models were designed considering slope inclination (27° and 15°) and pore fluid viscosity (water and HPMC solution). The test models were shaken with two types of input motions (ramped 0.2 g motion and constant 0.1 g motion).

(2) The model slope was successfully constructed using the wet pluviation and slurry deposition method. The relative density of the model ground was 26%, which density is sufficiently vulnerable to liquefaction due to the wet pluviation method. The saturation level of the model ground could not be

confirmed through separate tests to preserve the initial slope. However, there were no problems in observing the liquefaction phenomenon.

(3) In order to ensure bending failure of the model piles, buckling instability of the model piles was examined based on the slenderness ratio and Euler's buckling load. The single piles vulnerable to buckling failure were classified as "slender column" which has a high possibility of buckling instability. However, the pile was determined to be safe against buckling instability because the pile axial load was considerably smaller than the Euler's buckling load. The buckling amplification factor was only 1.09.

(4) The viscosity of the pore fluid influenced both the development and dissipation of excess pore pressure. The model soil saturated with pure water failed to meet the undrained condition to dynamic loads under centrifugal acceleration due to low viscosity. As a result, the increase in excess pore pressure was smaller near the ground surface. On the other hand, the model soil saturated with appropriate viscous pore fluid showed a constant increase in excess pore pressure regardless of depth. Therefore, pure water is not suitable for simulating ground liquefaction in centrifuge model test.

(5) The acceleration peaks smaller than 0.04g did not generated excess pore pressure in all Cases.

Chapter 4. Seismic response of piles in liquefied slope

4.1 Introduction

In previous experiments, the model ground was mostly composed of horizontal ground or infinite slope less than 5°. However, many waterfront structures are installed on finite slopes with relatively high inclinations. Therefore, in this study, centrifuge model tests are conducted to simulate the seismic behavior of piles embedded in liquefied finite slopes.

In section 2, lateral pile-deck system response to seismic loading is analysed based on experimental results. The structure responses are decomposed into that to inertial forces and that to liquefied soil forces based on the frequency characteristics. The effect of liquefied finite slope is analyzed based on the bending moment of the piles.

In section 3, variation in axial load distribution is analysed based on the experimental results. The axial load distribution is monitored before, during, and after liquefaction. The skin friction is back-calculated using the measured axial load distribution. In order to evaluate appropriate skin friction from axial load distribution, the residual load, which is the distributed axial load along the pile shaft before shaking, is considered. The effect of development and dissipation of excess pore pressure on skin friction is analysed.

4.2 Lateral pile–deck system response

4.2.1 Deck response

The lateral deck displacement provides an overview of the dynamic response of the pile–deck system given that most of the mass in the system is concentrated on the deck. The liquefied slope failure pushed the deck in the downslope direction while shaking. However, viscosity of pore fluid affected the time dependent behavior of the deck.

Figure 4-1 presents the time histories of lateral displacement of the decks. The deck displacement in Case 1 showed a peak while the base motion was applied, whereas it gradually increased as the base motion was applied and remained after the motion ended in Cases 2, 3, and 4.

The difference in time-dependent deck behavior according to different types of pore fluid was stated in previous studies. In centrifuge test with water pore fluid, Abdoun and Dobry (2002) discovered that the pile head displacement reached a maximum and then decreased. Li et al. (2021) showed the permanent deck displacement in the test using the viscous pore fluid.

González et al. (2009) tried to explain this difference based on the negative excess pore pressure near piles. Negative excess pore pressure was not observed near the ground surface in this study. However, monotonic accumulation of deck displacement could be responsible for the delayed girder failures observed in the field. Hamada and O’Rourke (1992) reported that the girders of Showa bridge began to fall somewhat later after the earthquake motion had ceased based on reliable eyewitnesses.

Figure 4-10 shows lateral deck displacement after the end of shaking. The piles recovered their original position due to the elasticity in Case 1. However, in Cases 2, 3, and 4, the deck displacement was maintained after the end of the shaking. This implies that the piles were pushed by liquefied lateral force during shaking and held by ground confinement in post-liquefaction.

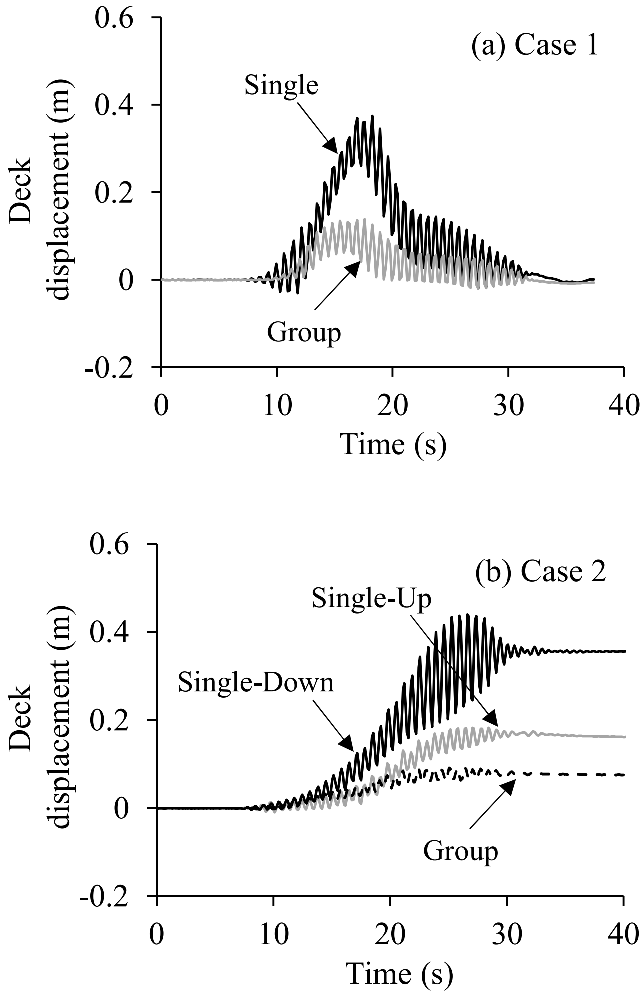

Figure 4-1 Lateral deck displacement during shaking

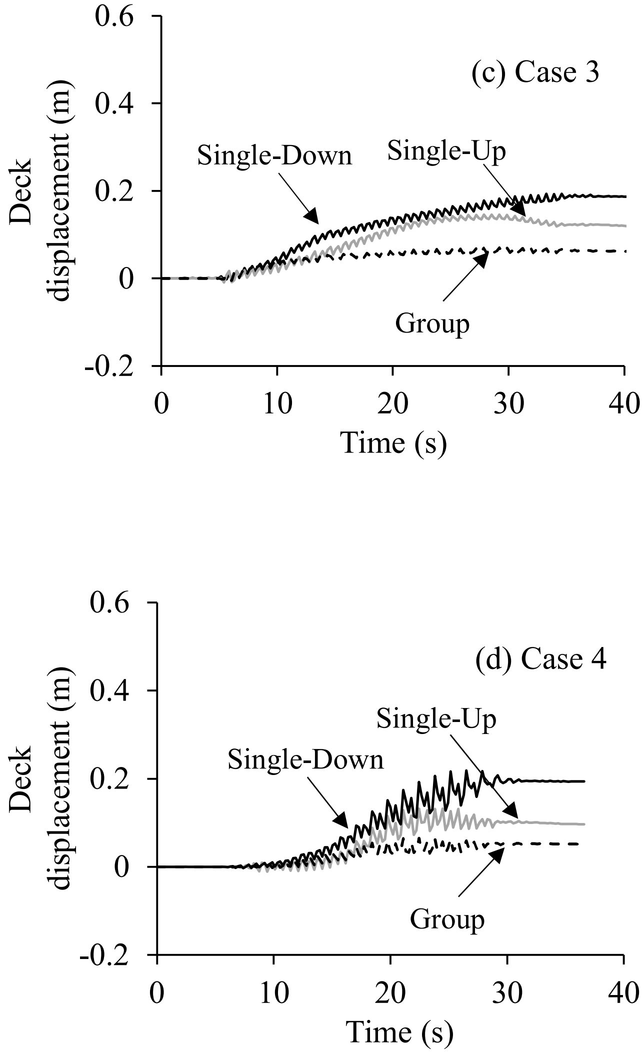

Figure 4-(continued) Lateral deck displacement during shaking

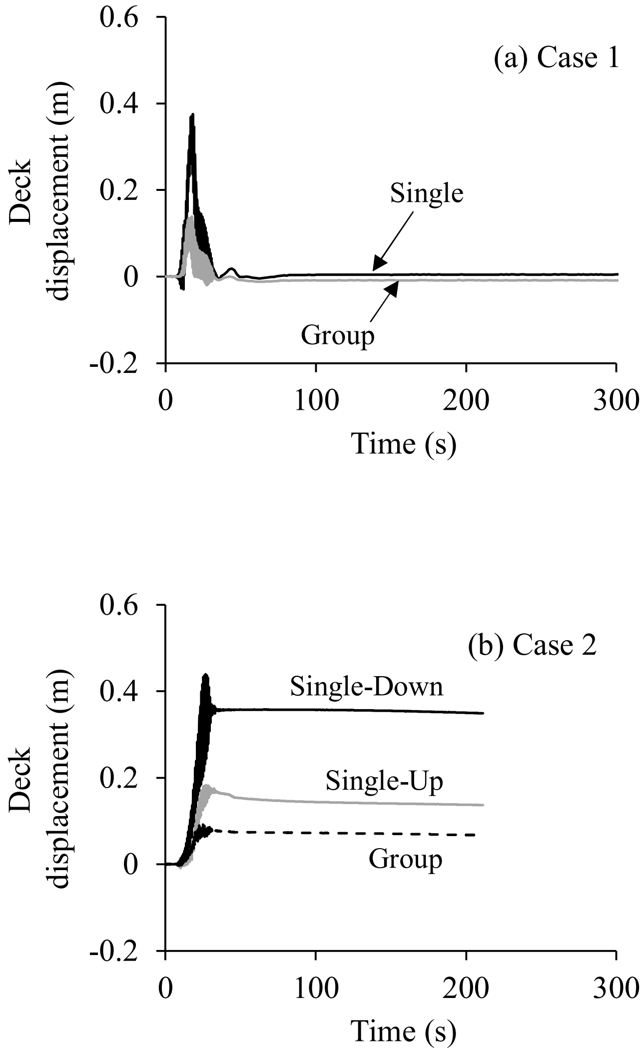

Figure 4-2 Lateral deck displacement after the end of shaking

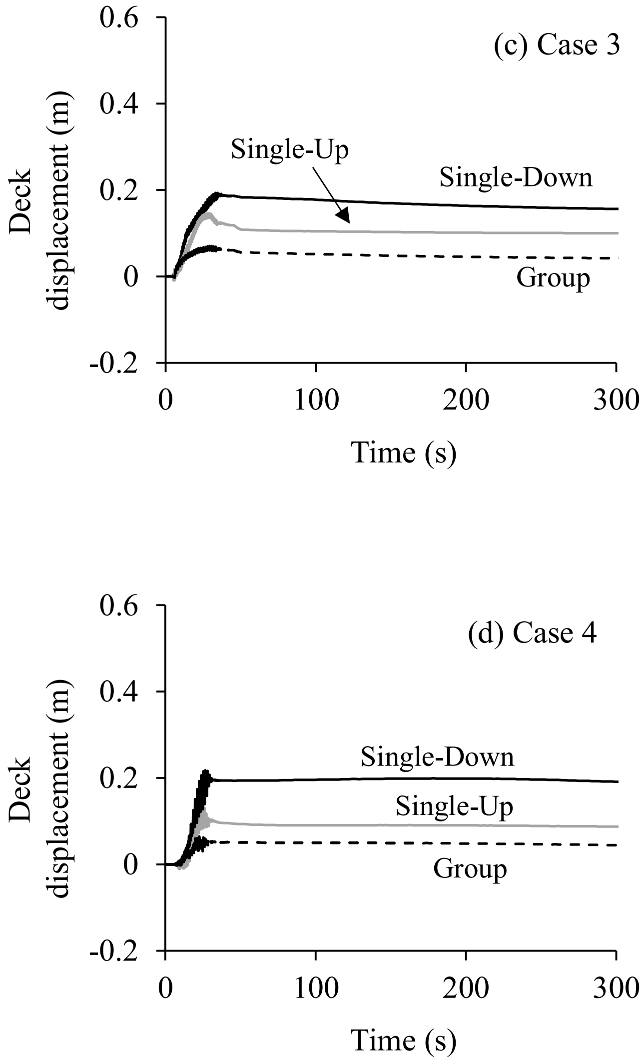

Figure 4-(continued) Lateral deck displacement after the end of shaking

4.2.2 Pile response

Lateral displacement of liquefied ground pushed the pile to the downslope resulting in a large bending moment below the ground surface. The pile bending moment was calculated using bending strain with calibrated flexural stiffness.

The time history of the bending moment at each depth can be divided into a cyclic and monotonic component. The shear forces can be classified according to the rate of the responses when the pile is in the elastic range. Figure 4-3 shows the time history of the cyclic and monotonic bending moment on Single-Down piles in Cases 2, 3, and 4 at various depths. The dominant shear forces were different along the pile length. The mass inertia and the liquefied soil force were dominant at the pile head and the pile toe, respectively. The magnitude of the monotonic bending moment was significantly larger than the cyclic bending moment.

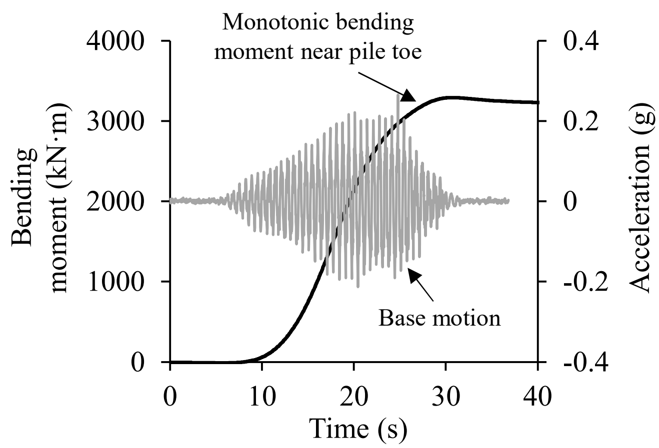

Figure 4-3 Increase of monotonic bending moment with base motion in Case 2

Moreover, the monotonic bending moment near the pile toe kept increasing until the shaking ended. Given that the acceleration decreased after 25 s in Case 2, the increment of bending moment was due to the liquefied slope. Thus, the stability of a pile foundation on a finite slope susceptible to liquefaction is considerably affected by the liquefied soil force rather than an inertia force.

The location of maximum bending moment was significantly affected by the liquefaction. Figure 4-5 shows the bending moment distribution of a Single-Down at different times. r_u denotes a ratio of excess pore pressure to initial effective stress. The location of the maximum bending moment gradually moved toward the pile toe as r_u increased. However, the maximum bending moment in non-liquefied ground occurs near the ground surface to resist pile deformation (Lim & Jeong, 2018). Thus, the down drift of the resisting point was due to liquefaction.

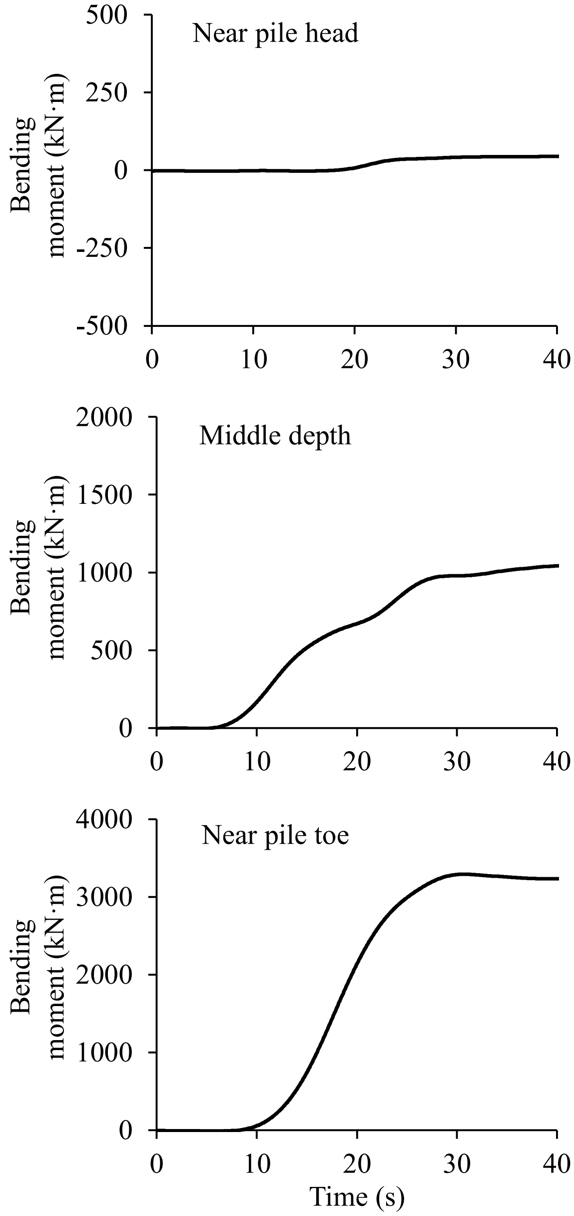

(a) Monotonic bending moment

Figure 4-4 Time histories of monotonic and cyclic bending moment in Case 2

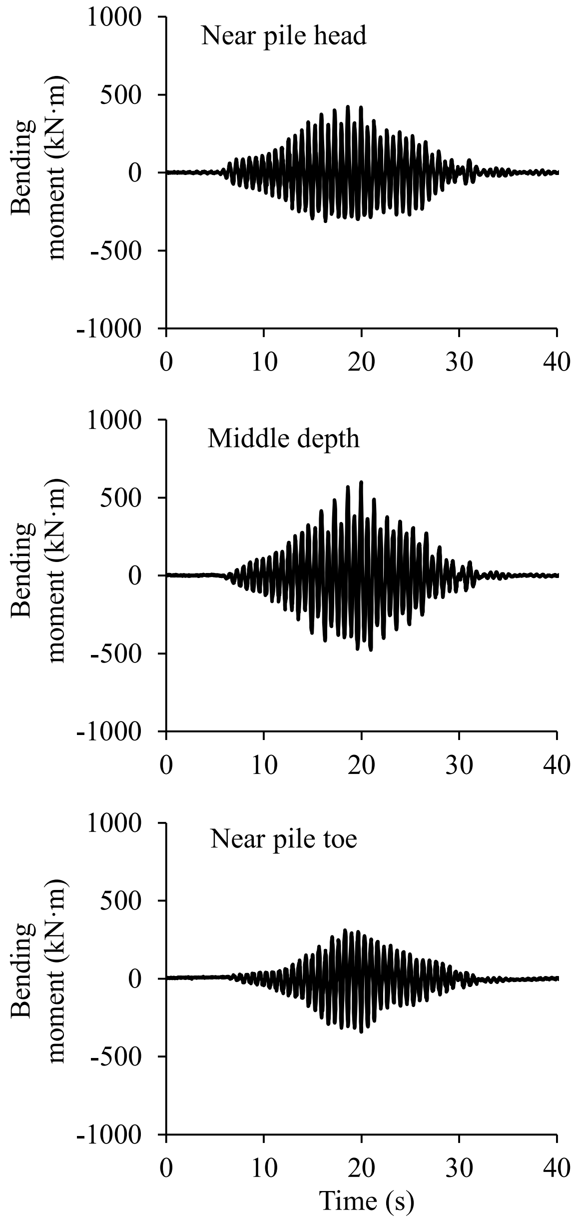

(b) Cyclic bending moment

Figure 4-(continued) Time histories of monotonic and cyclic bending moment in Case 2

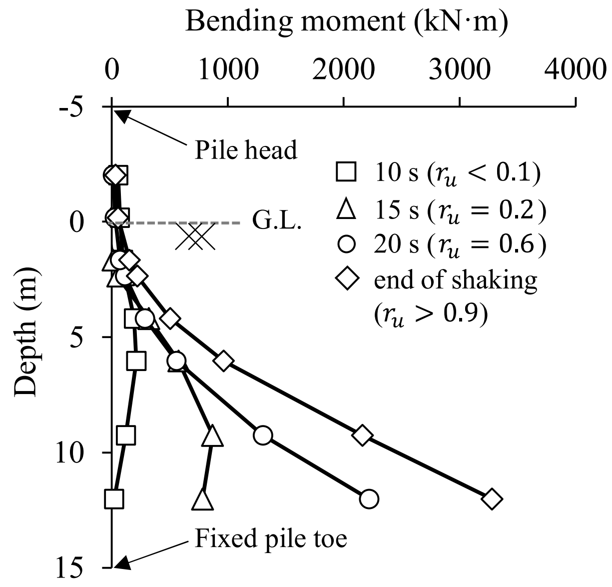

Figure 4-5 Bending moment distribution at various times in Case 2

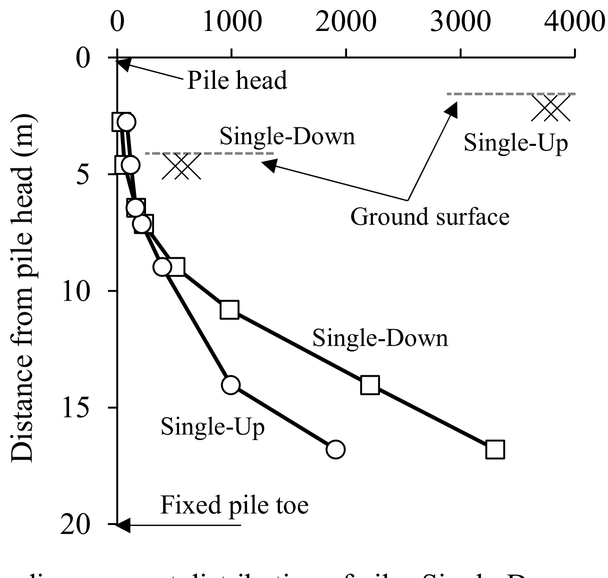

Figure 4-6 Bending moment distribution of piles Single-Down and Single-Up in Case 2

The bending moment of Single-Down was much larger than that of Single-Up. The relative pile location within slope was not considered by conventional lateral force methods since the experiments had been mainly performed on the infinite slope geometry. Considering the suggestion for liquefied soil pressure, the bending moment of Single-Up would be larger than that of Single-Down due to the greater thickness of liquefiable layer near Single-Up. This greater pile bending moment near slope toe was already reported by Li et al. (2021) with centrifuge test on group piles in a finite slope. Thus, it was found that the effect of relative pile location needs to be considered in practical design.

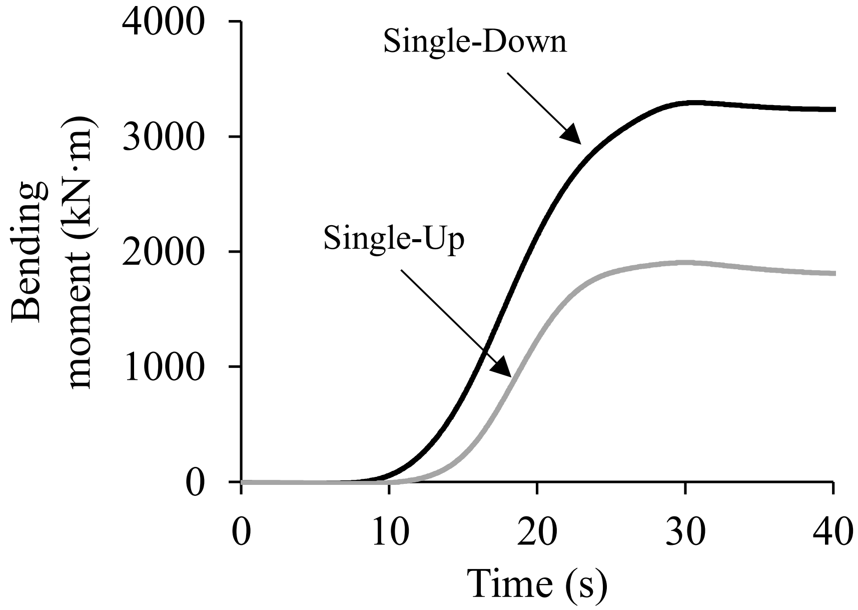

Figure 4-7 Time histories of bending moment near pile toe of piles Single-Down and Single-Up in Case 2

A rigid connection of the deck and pile heads in groups made the difference between group and single piles. Piles Group-Up and Group-Down showed negative bending moment owing to the rotational constraint of the rigid deck–head connection. Meanwhile, the single pile experienced a large maximum bending moment near the pile toe only. In addition, the bending moment difference between piles Group-Up and Group-Down was considerably smaller than that between piles Single-Up and Single-Down. The bending moment of the group piles after the end of shaking were approximately 40% and 70% of those of piles Single-Down and Single-Up, respectively. Thus, pile grouping may increase the stability of the pile against liquefaction-induced soil pressure by distributing the concentrated bending moment from the pile toe to head and that of the pile from upslope to downslope. Lastly, rotational constraint on the group piles caused a bending moment near the pile head, which was approximately 60% of that near the pile toe. This result indicated a risk of damage to the pile–deck connection.

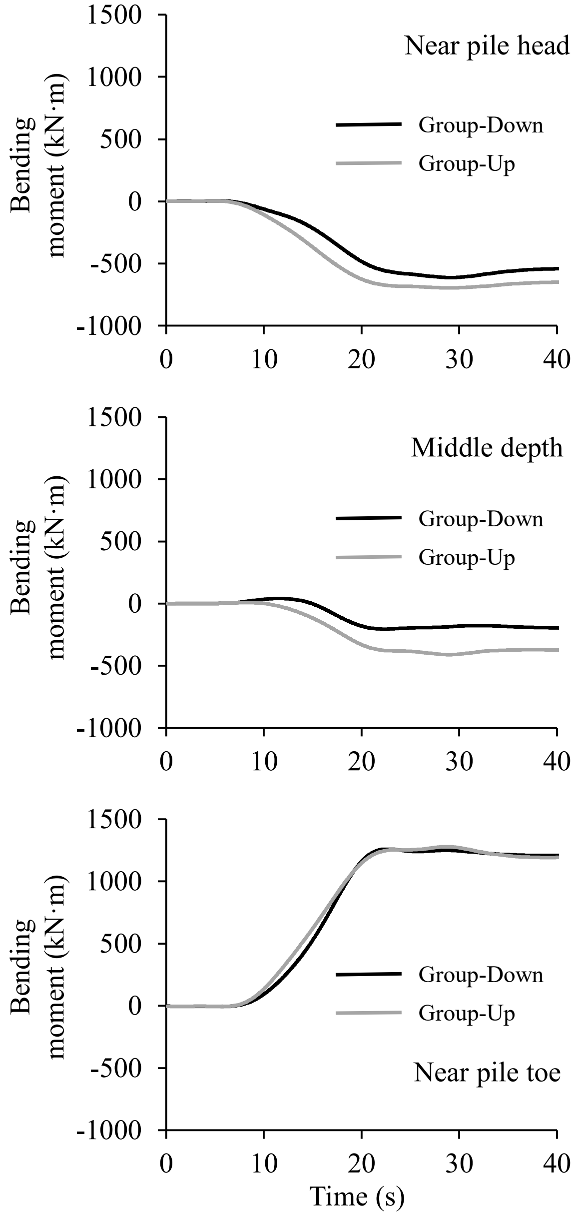

(a) Monotonic bending moment

Figure 4-8 Time histories of monotonic and cyclic bending moment of Group-Down and Group-Up in Case 2

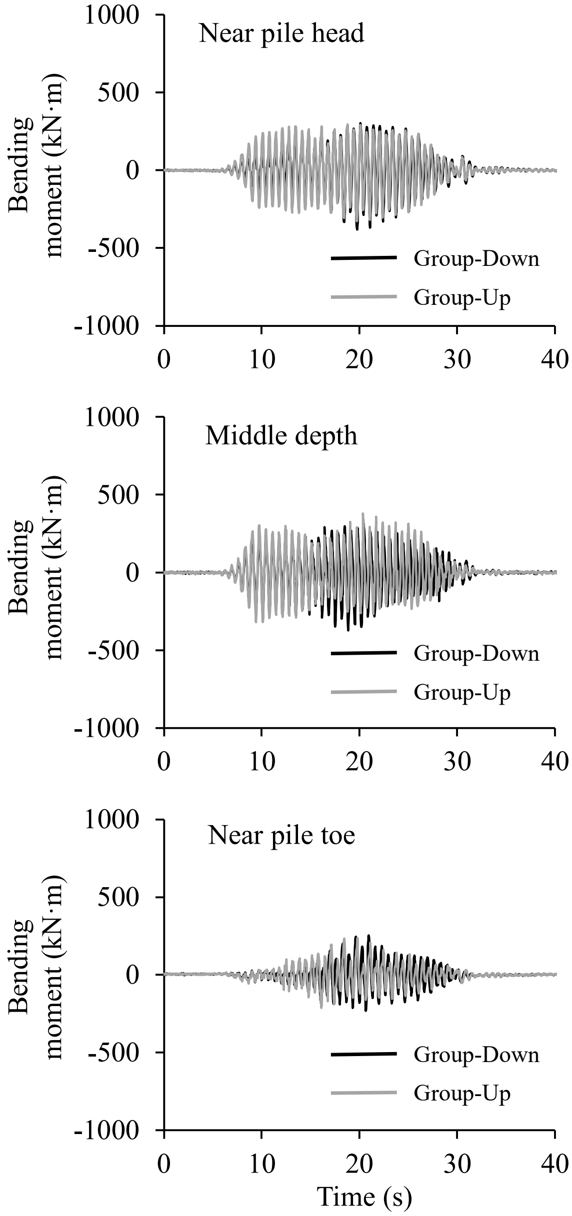

(b) Cyclic bending moment

Figure 4-(continued) Time histories of monotonic and cyclic bending moment of Group-Down and Group-Up in Case 2

4.3 Variation in axial load distribution

4.3.1 Evaluation of negative skin friction and drag load

The negative skin friction is caused by the relative settlement of the adjacent soil pulling the pile downward. Fellenius (2017) stated that the ultimate skin friction between the ground and the pile is independent of the direction. Thus, the negative skin friction can be calculated based on the interface shear strength between the ground and the pile as follows:

$$f_s = K\sigma_v' \tan\delta \qquad (4\text{-}1)$$

$$f_s = \beta\sigma_v' \qquad (4\text{-}2)$$

where, f_s is the ultimate skin friction (=negative skin friction), K is the coefficient of lateral earth pressure, σ_v' is the effective overburden stress, δ is the mobilized soil–pile interface friction angle, and β is the combined skin friction coefficient.

δ can be considered as the soil friction angle ϕ for the piles with rough surfaces (Frost & DeJong, 2005). Fleming et al. (2008) suggested that the values of K for the static bored pile in sand and silt were 0.9 and 0.6, respectively, which were larger than the coefficient of lateral earth pressure at rest. In particular, Sinha et al. (2022) proposed $K = 1$ and $\delta = \phi$ in the analysis of liquefaction-induced downdrag. However, K is difficult to be determined because it depends on various factors such as the friction angle and the stress increment caused by superstructure (Kulhawy, 1991; Meyerhof & Adams, 1968).

Instead of using K and δ, the skin friction can be expressed proportionally to the effective overburden stress using a coefficient β by Eq. (4-2). The β-coefficient varies with factors such as soil type, friction angle, relative density, pile surface roughness, and effective overburden stress (Fellenius, 2017; Fioravante, 2002; Loukidis & Salgado, 2008). The β-coefficient for the cohesionless soil was proposed based on the various case histories (Clausen et al., 2005; Fellenius, 2017; Rollins et al., 2005). Based on these works, CFEM (2006) suggested the β-coefficient of drilled piles with soil type for a practical design purpose, as shown in Table 4-1.

Table 4-1 β-coefficient of bored piles from CFEM (2006)

Soil type	β
Silt	0.2-0.3
Loose sand	0.2-0.4
Medium sand	0.3-0.5
Dense sand	0.4-0.5
Gravel	0.4-0.7

The drag load is calculated by accumulating negative skin friction along the pile length as follows.

$$Q_d = \int A_s f_s = \int \pi D \beta \sigma_v' \, dz = 0.5 \pi D \beta \gamma_{sub} z^2 \qquad (4\text{-}3)$$

where, Q_d is the accumulated drag load, A_S is the circumference of the pile, D is the pile diameter, γ_{sub} is the submerged unit weight of soil, and z is the considered depth. The determination of the drag load in Eq. (4-3) is applicable to the end-bearing pile embedded in a submerged and uniform ground.

4.3.2 Drag load before shaking

Loose model ground settled down as centrifugal acceleration (g-level) increased by centrifuge spinning. Figure 4-9 shows the g-level increment and the settlement behind the slope crest during centrifuge spinning. The g-level was back-calculated based on hydrostatic pressure, and settlement and dynamic time were expressed in a model scale considering the g-level change. Centrifuge spinning caused ground confinement on the pile shaft and ground settlement, which are the ingredients for skin friction. After the centrifugal acceleration reached the target g-level, the ground settled approximately 1.5 cm on the prototype scale, which was enough to induce ultimate skin friction (Han et al., 2017; Wada, 2004).

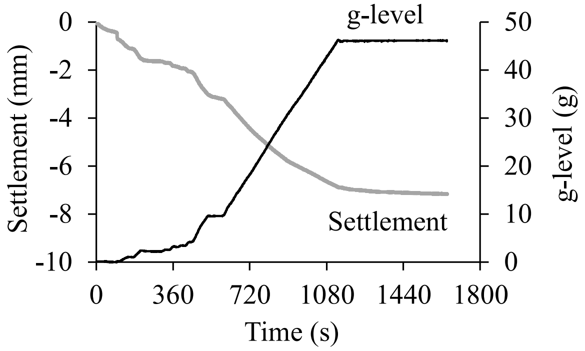

Figure 4-9 Crest settlement and g-level increment during centrifuge spin (in model scale)

Such settlement caused negative skin friction on the pile shaft provided that the elastic compression of the end-bearing pile in this study was ignorable. Figure 4-10a shows the pile axial load distribution before shaking. The axial load above the ground was a pile head load caused by the mass block 370 kN. Two grey lines showed the lower and upper boundaries of accumulated drag load based on the CFEM β-coefficient for loose sand. The spin-induced negative skin friction was in the range of the upper and lower bounds of CFEM recommendation. This agreement implied that the negative skin friction can be estimated by the CFEM β-method originally suggested for positive skin friction. A similar observation can be found in the study of the effect of liquefaction-induced downdrag on piles in the multi-layered ground by Sinha et al. (2022), as shown in Figure 4-10b.

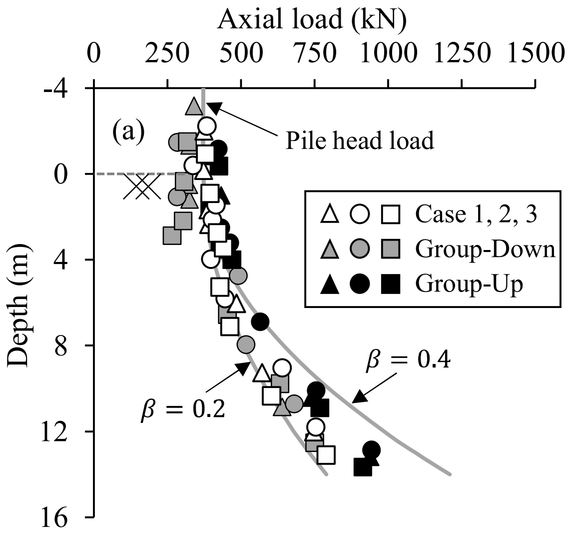

Figure 4-10 Spin-induced drag load within the range of CFEM β-coefficient for loose sand: (a) this study, (b) Sinha et al. (2022)

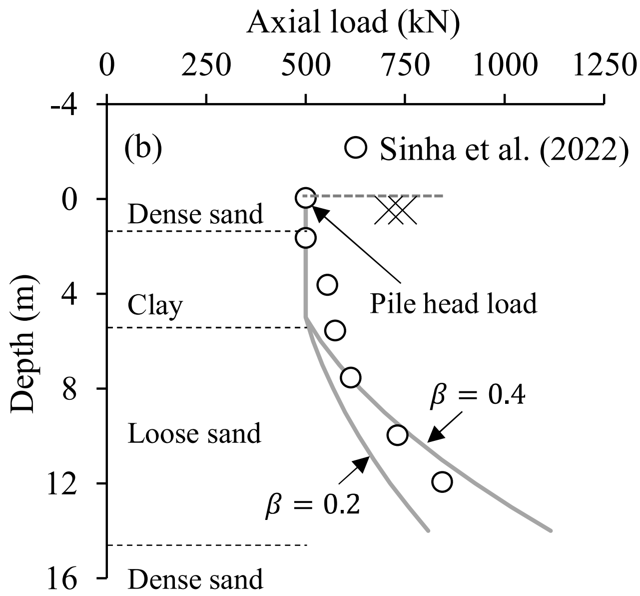

Figure 4-(continued) Spin-induced drag load within the range of CFEM β-coefficient for loose sand: (a) this study, (b) Sinha et al. (2022)

4.3.3 Loss of skin friction during shaking

Shaft resistance and drag load were based on interface shear strength between the pile shaft and adjacent soil (Lashkari, 2013; Loukidis & Salgado, 2008). Excess pore pressure loosened contact pressure between them. Thus, skin friction can be reduced by liquefaction. Figure 4-11a and Figure 4-11b show the axial load time history at various depths in a single pile and group piles, respectively, with r_u increment in Case 2. The accumulated drag load was sharply diminished as the r_u increased during shaking. During liquefaction, the axial load at all depths and in piles Group-Up and Group-Down converged on the pile head load.

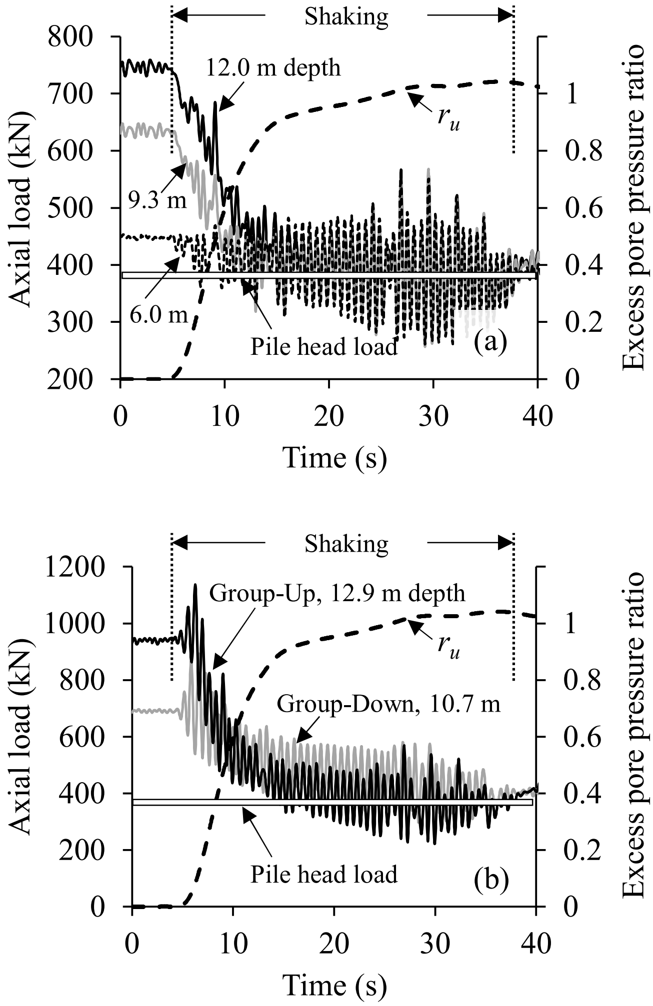

Figure 4-11 Loss of drag load during shaking in Case 2, (a) single pile and (b) group piles

Figure 4-12 shows the decrease of spin-induced drag load following excess pore pressure development. Y-axis was defined as the ratio of the current drag load to the spin-induced drag load. The drag load was linearly decreased with the increase of excess pore pressure ratio in all cases, implying that a certain level of shaft resistance could be reduced during shaking even if the ground was not completely liquefied.

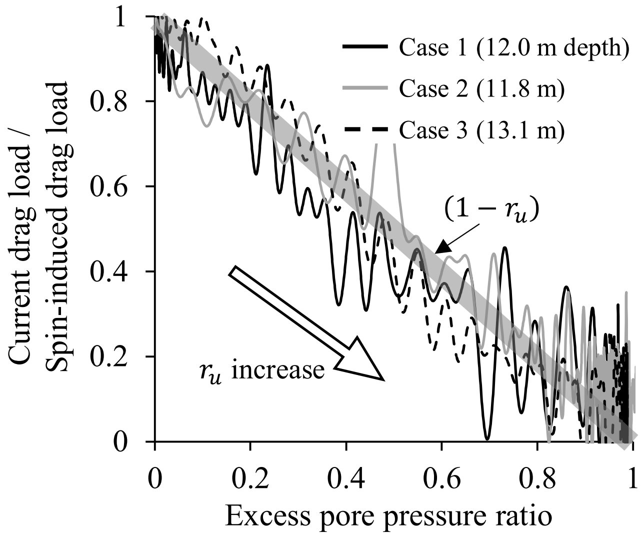

Figure 4-12 Reduction in drag load following excess pore pressure development

4.3.4 Drag load after shaking

The excess pore pressure dissipation began when the shaking ceased. Reconsolidation settlement and subsequent densification occur in liquefied soils (Thevanayagam et al., 2001). At the same time, negative skin friction was rebuilt while the ground restored confinement to the pile shaft.

The reconsolidation settlements measured behind the crest were approximately 11 cm and 18 cm in Cases 1 and 3, respectively. The settlement was enough to mobilize ultimate skin friction. The reconsolidation was in progress in Cases 1 and 3. Data measurements were stopped up to the r_u of

0.38 and 0.35 in Cases 1 and 3, respectively, because of the data capacity limit. In Case 2, where the dissipation progressed to a r_u of less than 0.1, the reconsolidation settlement failed to be measured because of the liquefied slope failure during shaking. The markers contacting to LVDTs tip escaped away from the original position.

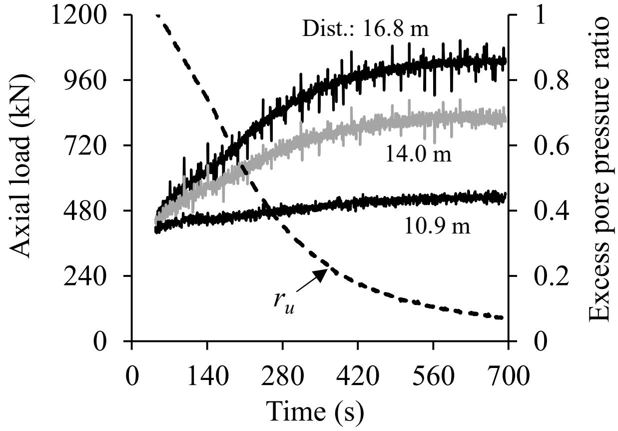

Figure 4-13 Reconsolidation-induced drag load on single pile in Case 2. "Dist." denotes the distance from the pile head to the measurement location.

Figure 4-13 shows the axial load time history with excess pore pressure dissipation in Case 2, single pile. Measurement location was indicated by the distance from the pile head, not the depth; a large change in the initial ground surface level was expected because of liquefied slope failure. The axial load, which was converged to the pile head load at all depths, increased again by the drag load with the excess pore pressure dissipation. The reconsolidation-induced drag load increased more rapidly in the deeper depth because it was proportional to the confining pressure. The r_u dropped to less than 0.1 approximately 10 minutes after the shaking ceased. The axial loads at each depth were almost close to the maximum.

Figure 4-14a and Figure 4-14b present the axial load time histories of Group-Up and Group-Down with excess pore pressure dissipation in Cases 2 and 3, respectively. The axial load time histories of Group-Up and Group-Down in Case 2 were identical. However, in Case 3, the Group-Up's axial load increment was faster than Group-Down's axial load at each depth, implying that the liquefied slope collapsed and flattened in Case 2, but the inclination survived after the shaking in Cases 1 and 3. This difference was due to the shaking duration after the ground was liquefied. In Case 2, the liquefied ground had been shaken for approximately 25 s, whereas those in Cases 1 and 3 had been shaken only for approximately 5 s.

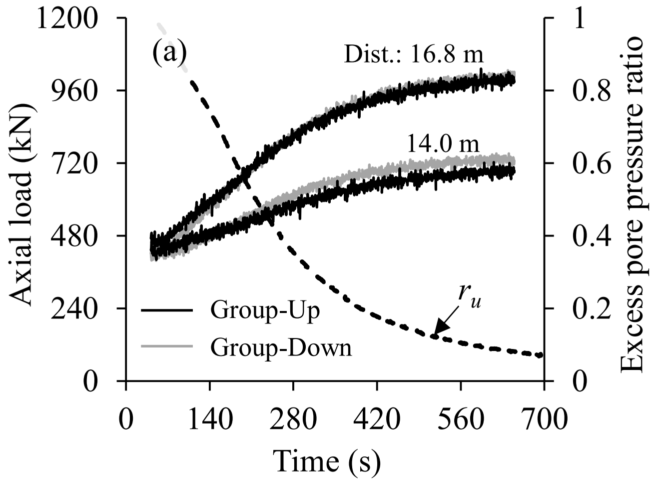

Figure 4-14 Reconsolidation-induced drag load on group piles: (a) in Case 2 and (b) in Case 3

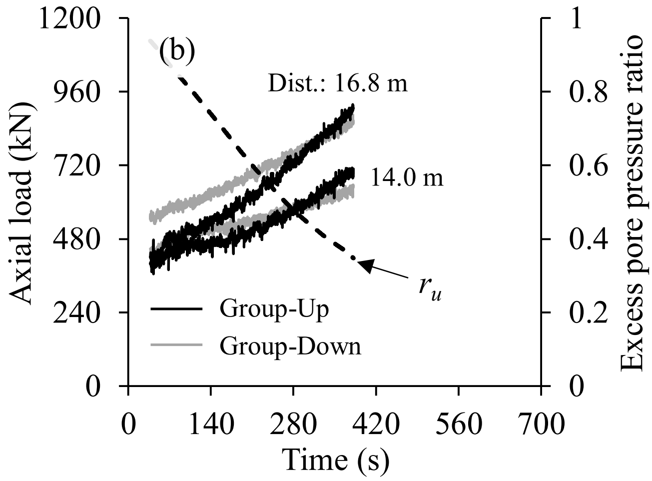

Figure 4-(continued) Reconsolidation-induced drag load on group piles: (a) in Case 2 and (b) in Case 3

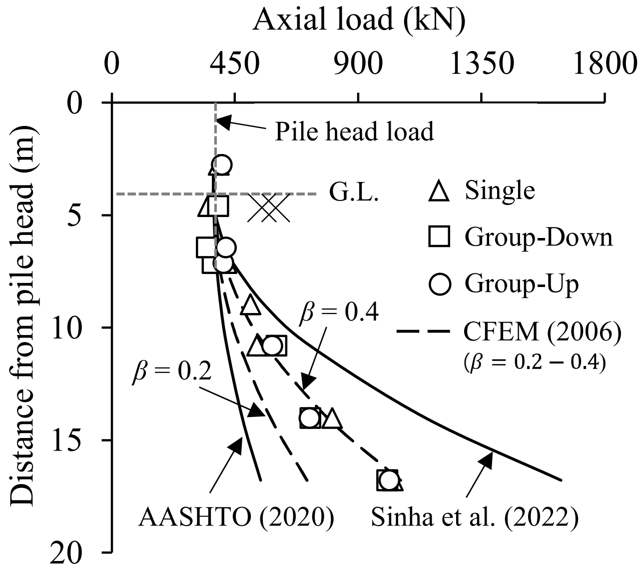

Figure 4-15 Comparison of estimated and measured axial load distribution in Case 2

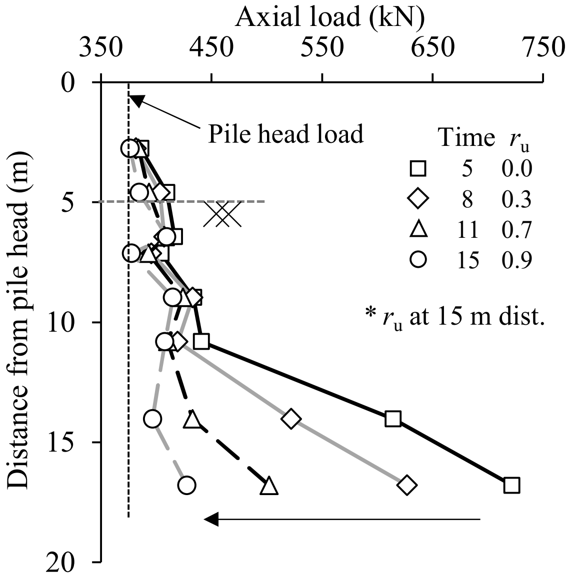

Figure 4-16 Load transfer curves during shaking

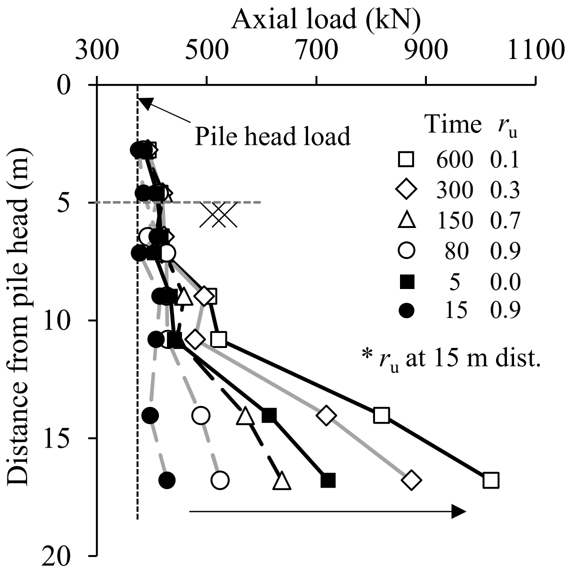

Figure 4-17 Load transfer curves after shaking

Figure 4-15 shows the axial load distribution after the excess pore pressure dissipation in Case 2. The axial load distributions included the pile head load above the flattened ground level and the reconsolidation-induced drag load below the ground surface. The axial load distributions were compared with those estimated based on the recommendations. The measured data were consistent with the distribution based on the CFEM β-method. The drag load induced by the reconsolidation was close to the upper boundary ($\beta = 0.4$), whereas it was smaller as near as the lower boundary ($\beta = 0.2$) during spinning. This difference was due to the densification of the model ground after the dissipation.

Sinha et al. (2022) suggested the maximum negative skin friction because of the reconsolidation is the drained interface shear strength. The model ground was excited for six successive base motions, resulting in a significantly higher densification. The axial load distribution estimated following Sinha et al. (2022) was greatly larger than the measurement in this study. AASHTO (2020) recommended adopting residual shear strength as negative skin friction of the liquefied layer. Idriss and Boulanger (2015) suggested that the residual shear strength is smaller than 10% of the effective overburden stress for loose sand with a relative density of less than 50%. The axial load distribution calculated by AASHTO (2020) underestimated measured data because the effect of dissipation was not accounted for.

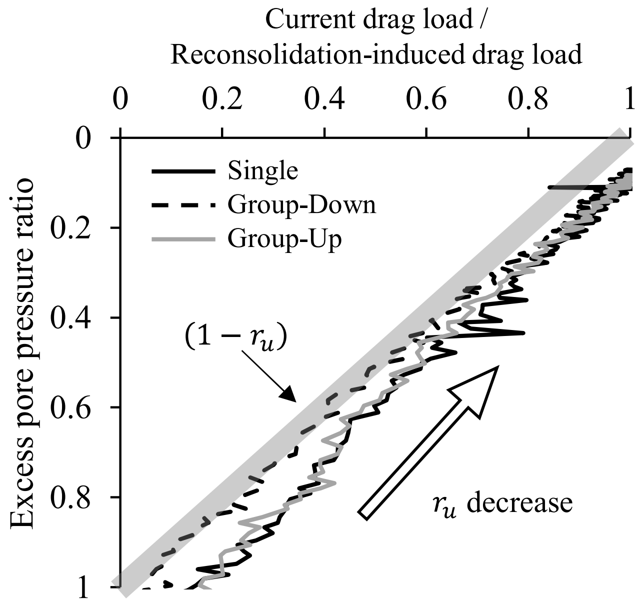

Figure 4-18 Increase of drag load following excess pore pressure dissipation in Case 2

Figure 4-18 shows an increase in drag load following the dissipation of excess pore pressure. The negative correlation between these variables during dissipation is similar to that at the liquefaction occurrence and is consistent with the suggestion of Boulanger and Brandenberg (2004).

4.4 Summary

In this chapter, analysis on seismic behavior of centrifuge model was conducted. Based on the lateral deck displacement and pile bending moment, lateral response of pile-deck system was described. Variation in axial load distribution before, during, and after seismic loading were analyzed. It was found that liquefaction of the foundation soil considerably affected on time-dependent axial pile behavior.

The main conclusions can be summarized as follows.

(1) The liquefied slope pushed the deck in the downslope direction while shaking. The deck displacement in the viscous fluid kept increasing until the end of shaking. This monotonic accumulation of deck displacement could be responsible for the delayed girder failures observed in the field. After the end of shaking, the displacement had been maintained with the dissipation of excess pore pressure. This implies that the piles were pushed by liquefied lateral force during shaking and held by ground confinement in post-liquefaction.

(2) Lateral displacement of liquefied ground pushed the pile to the downslope resulting in a large bending moment below the ground surface. The mass inertia and the liquefied soil force were dominant at the pile head and the pile toe, respectively. However, the magnitude of the monotonic bending moment was significantly larger than the cyclic bending moment. Therefore, the stability of a pile foundation on a finite slope susceptible to liquefaction is considerably affected by the liquefied soil force rather than

an inertia force.

(3) Negative skin friction along the pile length was caused by the ground settlement during the centrifuge spinning. The spin-induced drag loads were within the range of the values calculated with the CFEM β-method for loose sand. Since the obtained and calculated drag loads are in close agreement, it can be deduced that the negative skin friction can be estimated by the CFEM β-method, which was originally suggested for positive skin friction.

(4) The spin-induced drag load was diminished with the increase in the developed excess pore pressure during shaking. After liquefaction, the axial load of single and group piles below the ground surface converged to the pile head load that corresponds to the deck mass. Furthermore, the drag load linearly decreased with the increase in the excess pore pressure ratio, implying that partial liquefaction can induce significant decrease in the shaft resistance.

(5) The reconsolidation settlement generated negative skin friction after the shaking has ceased. The negative skin friction was found to be larger than the liquefied residual strength recommended in the AASHTO LRFD bridge design specifications. Therefore, it is seen that the consideration of the strength reduction is not necessary for the calculation of negative skin friction induced by reconsolidation, since the liquefied ground regains skin friction after the dissipation.

Chapter 5. Numerical studies of piles in liquefied slope

5.1 Introduction

This chapter aims to utilize the computational platform to perform various numerical studies based on the data obtained from the experiments described in Chapters 3 and 4, in order to obtain and validate additional information.

In section 2, a liquefaction-induced lateral force model suitable for finite slopes is proposed by using experimental data obtained from single piles subjected to liquefaction at different locations within slope. The applicability of the conventional linear and uniform distribution of liquefied soil pressure is examined by conducting numerical analyses of laterally loaded piles. The improved empirical factors are used to assess the applicability of the proposed liquefied soil force model to a group of piles and the group effect.

In section 3, a numerical modeling of the liquefiable finite slope is performed to analyze the ground motion which is not directly observed in the experiment. The accuracy of the numerical analysis results is improved by detailed simulation using the liquefiable soil model, beam elements for a separation of rigid container and liquefied soil, and the quiet boundary to prevent energy reflection. The results of the numerical analysis are validated by comparing with the measured experimental data which are ground acceleration, excess pore pressure, and crest settlement.

In section 4, soil–pile interface modeling with consideration of liquefaction is proposed. Based on the interface modeling, a series of numerical modeling of the piles in liquefiable finite slope are carried out to simulate the conducted centrifuge model tests in Chapters 3 and 4. The effect of transforming the 3D experimental model into 2D plane-strain numerical model is discussed. The results of the numerical analysis are validated by comparing with the measured experimental data which are pile bending moment and deck acceleration.

In section 5, based on the validated model in section 4, parametric studies are conducted to assess the effects of slope inclinations and amplitude of input motions.

5.2 Liquefaction-induced lateral force

5.2.1 Computational platform

In this study, LPILE and GROUP v2019 were used to perform the analysis of single and group piles under horizontal static load. LPILE and GROUP are software that analyzes the behavior of a pile-column with non-linear support by solving the differential equations.

These platforms have the advantage of being able to analyze the behavior of piles subjected by liquefied soil easily without introducing complex soil models by converting liquefied soil load into non-linear springs or distributed loads. The reliability of the analysis has already been verified under horizontal loading and liquefaction conditions by previous studies (Dobry et al., 2003; Mostafa, 2022; Reese & Wang, 2006; Souri et al., 2019; Yang & Zhang, 2017).

While LPILE is a software for relatively simple 1D conditions of single piles, GROUP can analyze the behavior of 2D or 3D conditions of group piles. In this study, GROUP analysis was performed by applying different lateral force profiles to the piles in upslope and downslope.

In this study, the optimal liquefaction-induced lateral force distribution was determined by comparing the calculated bending moment profile from the software with the measured bending moment from the experiment.

5.2.2 Single piles

The distribution of lateral soil pressure on the pile can be calculated by the double derivative of the bending moment profile. Analyzing the derived soil pressure profile was difficult owing to its irregular shape. Therefore, previously recommended profiles of linear and uniform soil pressure, each of which was determined by fitting the bending moment measured at the end of shaking, were adopted in this study.

The bending moment of single piles at the end of shaking was estimated using the conventional liquefied soil pressure. The analysis was conducted using LPILE v2019, which is a computing software for the analysis of deep foundation under lateral loading. The end-bearing pile in centrifuge experiment was modelled by beam element embedded in strong rock layer with prototype dimensions and mechanical properties. The pile was subjected to lateral force calculated with liquefied soil pressure.

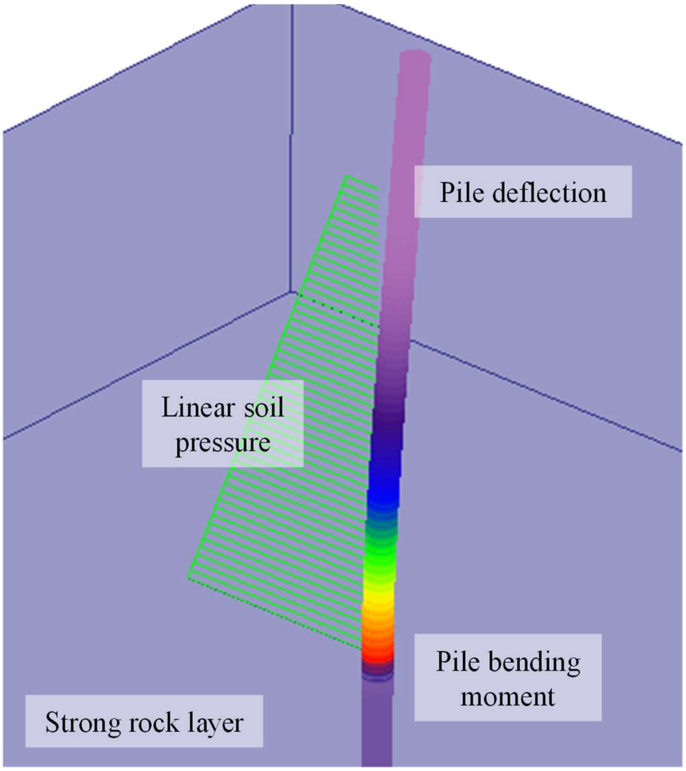

Figure 5-1 Modeling of single pile subjected to liquefied soil pressure

The bending moment profile estimated using the uniform soil pressure profile agreed well with the recorded data on Pile Single-Down, whereas the profile based on the linear pressure worked well with that on Pile Single-Up. The uniform soil pressure profile was likely to underestimate the bending moment at the pile toe. However, the linear pressure can consider the overburden stress of the liquefied layer and thus give a conservative estimate of the bending moment at the pile toe. Therefore, the method of applying the linear soil pressure profile was selected for further analyses of single and group piles.

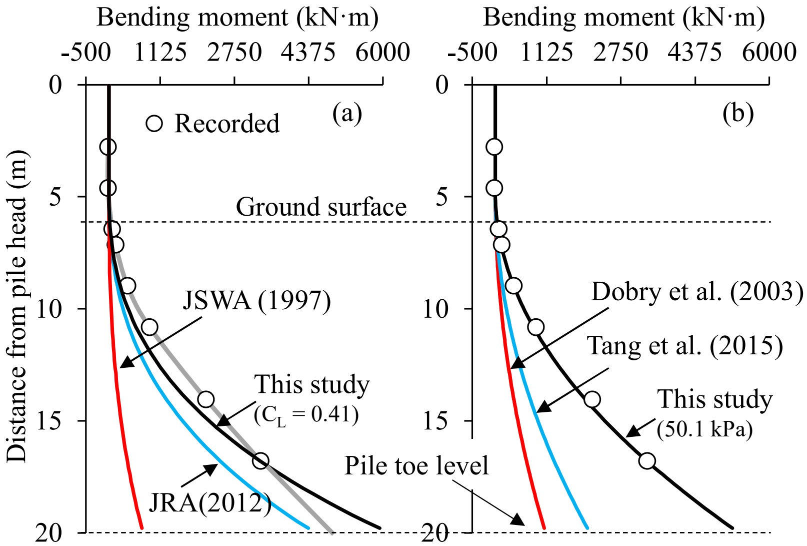

Figure 5-2 Comparison of bending moment profiles estimated using (a) linear soil pressure distribution and (b) uniform soil pressure distribution for Single-Down in Case 2

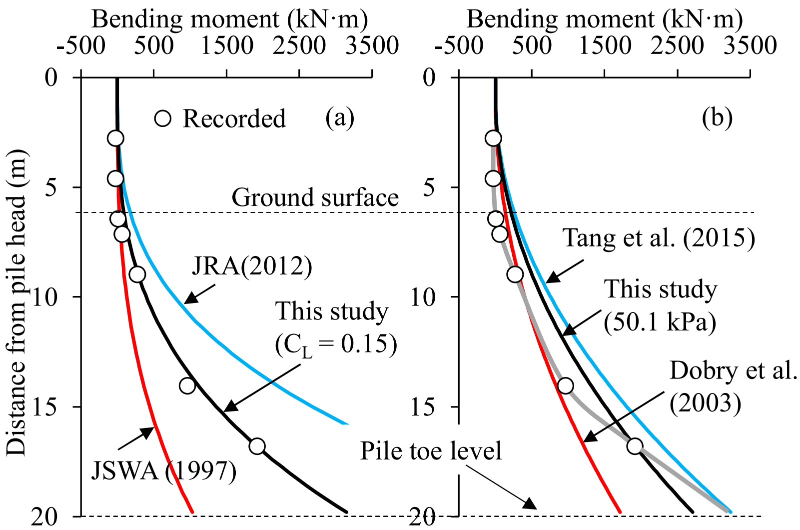

Figure 5-3 Comparison of bending moment profiles estimated using (a) linear soil pressure distribution and (b) uniform soil pressure distribution for Single-Up in Case 2

Figure 5-2 and Figure 5-3 present the estimated profile of the bending moment of Piles Single-Down and Single-Up in Case 2 according to the different distribution of lateral soil pressure. To achieve the best fit, the empirical factor for the linear soil pressure profile of Piles Single-Down and Single-Up in Case 2 were 0.41 and 0.15, and α of them were 50.1 and 16.3 kPa, respectively. Pile Single-Up in Case 2, which may be subjected to a small mass of sliding soil block due to slope failure, revealed a considerably small empirical factor for the linear soil pressure profile as well as the magnitude of uniform soil pressure compared with Pile Single-Down.

Different conditions (relative pile location within slope, type of seismic loading, and slope inclination) investigated in this study are not considered in the conventional liquefied soil pressure method. However, the empirical factors and uniform soil pressure showed large differences according to the conditions.

Figure 5-4 presents the empirical gradient factors estimated for single piles according to the test conditions. A relative pile location was defined as a distance ratio between the distance from slope toe to pile and the total length of the slope. The empirical factor for the single pile due to the liquefied slope was considered as large as close to the slope toe based on the comparison of piles Single-Down and Single-Up. The factors for Single-Up did not show a significant difference depending on the Cases. However, the factors for Single-Down varied with test conditions.

Table 5-1 Calibrated empirical factor and uniform pressure

Case No.	Pile location	Empirical factor	Uniform pressure (kPa)
1	-	0.22	22
2	Downslope	0.41	50
	Upslope	0.15	16
3	Downslope	0.3	36
	Upslope	0.15	16
4	Downslope	0.24	26
	Upslope	0.11	12

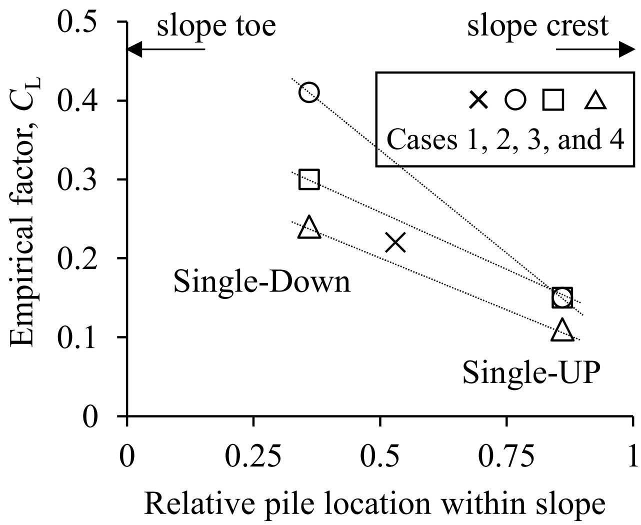

Figure 5-4 Empirical gradient factor depending on several test conditions

The empirical factor of 0.22 for the single pile in Case 1 (water pore fluid) was in the range of those for piles Single-Down and Single-Up in Case 2 (viscous pore fluid). It was seen that the factor in Case 1 was smaller than the linearly correlated factor of 0.32 considering relative pile location. This effect of pore fluid viscosity was consistent with the observation by González et al. (2009). The liquefied soil pressure estimated using the centrifuge test with low viscosity pore fluid (water) can be underestimated.

The empirical factors were affected by other conditions (type of seismic loading and the inclination of liquefied slope). The change in the ground response may affect the interaction between the soil and the pile, and thus should be included in determining lateral soil pressure. The input motion can alter the response of the liquefiable ground (Dashti & Karimi, 2017; Ishihara, 1977). The slope inclination also affects the sliding failure mechanism (Feng et al., 2021).

The factors of 0.3 and 0.24 for Single-Down in Cases 3 (long and weak motion) and 4 (15° slope) were smaller than that in Case 1, respectively. However, the factors of 0.15 and 0.11 for Single-Up in Cases 3 and 4 were similar to that of 0.15 in Case 1. For piles Single-Down, the variation of empirical factor was relatively large compared to that for piles Single-Up. This implies that the lateral soil pressure was affected by sliding block due to the liquefied slope failure.

5.2.3 Group piles

The bending moment of group piles at the end of shaking induced by the lateral soil pressure distribution was estimated by performing a 3D modeling of the group pile–deck system through GROUP 2019 (Reese et al., 2019). The pile and the deck were modelled using beam element and rigid body, respectively. The connection between the pile and the deck was set as a rigid type to reflect the experimental condition. The pile toe was embedded in a very strong layer. The prototype dimensions and mechanical properties presented in Chapter 3 were applied to the structural elements. Finally, the bending moment response of the group pile was obtained by applying the lateral soil force profile to individual piles.

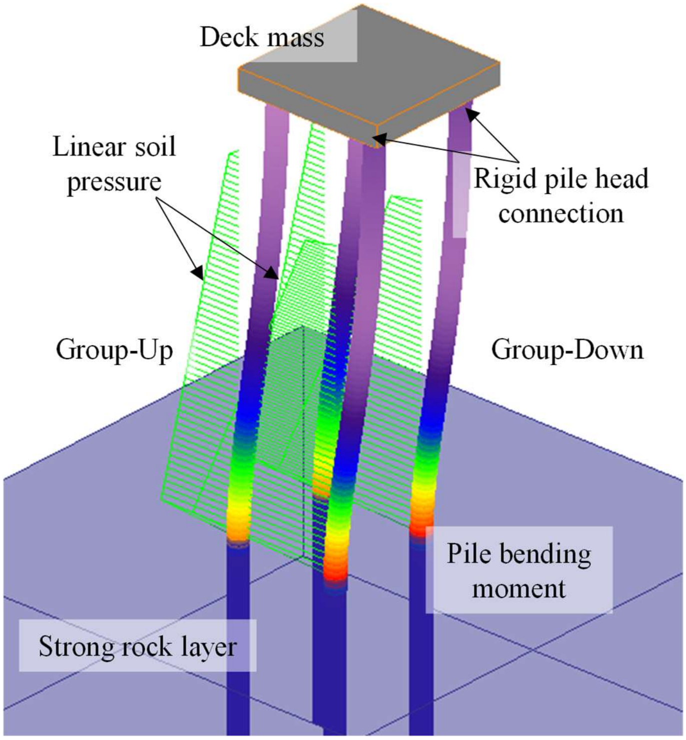

Figure 5-5 Modeling of deck supported by pile group subjected to liquefied soil pressure

Linear lateral force profiles recommended by JRA (2012) and JSWA (1997) were adopted in the GROUP analysis. JSWA (1997) considered the pile in group independently respond to the lateral pressure induced by the soil movement. The empirical factor of the selected linear profile was determined based on calibrated values for each pile in the group according to their locations along the slope. Values of empirical factor for piles Group-Down and Group-Up were summarized in Table 5-2. The analyses using JRA (2012) and JSWA (1997) in combination with empirical factor evaluated by this study were denoted as This study-JRA and This study-JSWA, respectively.

Table 5-2 Calibrated empirical factors for group piles

Case No.	Pile location	Relative pile location within slope	Calibrated empirical factor
2	Downslope	0.22	0.48
	Upslope	0.51	0.33
3	Downslope	0.22	0.34
	Upslope	0.51	0.25
4	Downslope	0.22	0.38
	Upslope	0.51	0.20

In Cases 2 and 3, the bending moment profile of Pile Group-Up estimated by This study-JRA and This study-JSWA methods agreed well with the measured data as shown in Figure 5-6. Meanwhile, the JRA and JSWA methods greatly underestimated or overestimated the maximum bending moment near the pile toe because the effect of the pile location along the slope was not taken into account.

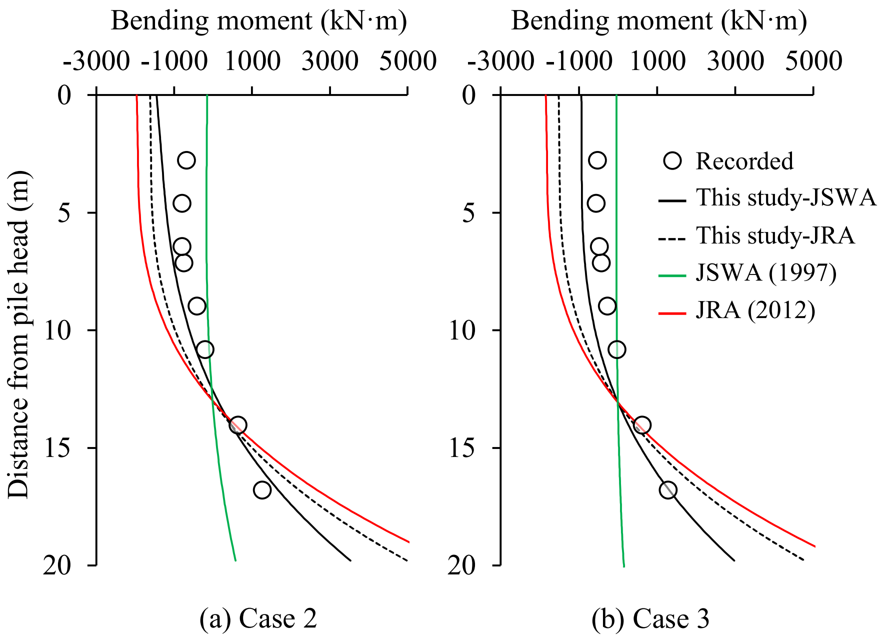

Figure 5-6 Comparison of bending moment profiles estimated by different methods for Group-Up in (a) Case 2 and (b) Case 3

This study-JRA method significantly overestimated 60–80% the bending moment profile of Pile Group-Up. This overestimation was due to an assumption that the pile group and the trapped soil resisted the liquefied soil movement together. The relatively low error in estimating the maximum bending moment by This-JSWA method was roughly 33% and 2% for Cases 2 and 3, respectively. This difference implied that the actual lateral force applied to the group pile was reduced due to the soil–pile interaction, which became more pronounced with the strong base motion.

5.3 Numerical simulation of liquefied slope

5.3.1 Computational platform

In this study, numerical simulation of model structure and ground under seismic loading was performed using Fast Lagrangian Analysis of Continua in 2 Dimensions (FLAC2D). This software has an advantage on dealing with the analysis of dynamic and large deformation problems because it uses explicit, finite difference, and Lagrangian analysis methods to solve the differential equations of a continuum.

When the constitutive model and initial and boundary conditions of the continua are given, FLAC2D calculates the velocity and displacement that satisfy the equations of motion at each node using finite difference method. Then, the stress and loads satisfying the constitutive model are determined based on the calculated velocity and displacement at each node for that timestep using explicit method. The computation is applied based on Lagrangian analysis that updates the coordinate system at each step, leading to numerical stability by considering the deformation as a small variation at each timestep.

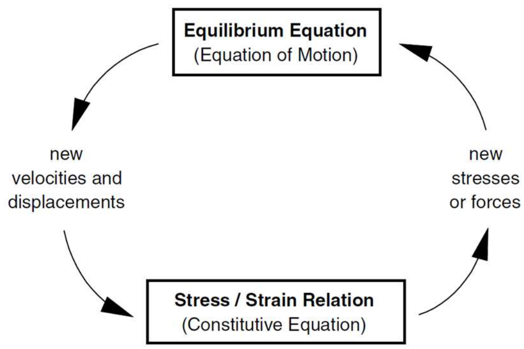

Figure 5-7 Basic explicit calculation cycle (Itasca, 2019)

5.3.2 Numerical modeling and simulation

Figure 5-8 shows a numerical model simulating the centrifuge model test without pile foundation. The thickness of the rigid container was set to 5 m for the stability of the analysis. The model has an interface that allow for separation between the container and soil.

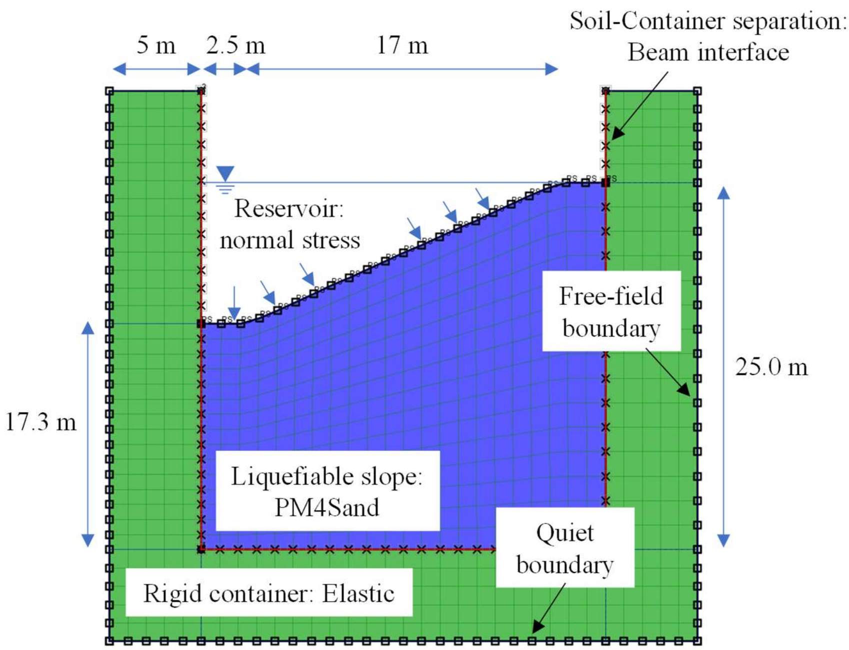

Figure 5-8 2D numerical model for simulation of liquefied slope in rigid container

- Soil model

PM4Sand model is adopted as a liquefiable soil model. This model is a plasticity soil model that determines soil behavior based on stress ratio. PM4Sand model is developed specifically for simulating the liquefaction behavior of sand soil in dynamic analysis conditions (Boulanger & Ziotopoulou, 2015).

The primary input parameters of PM4Sand model are relative density, shear modulus coefficient, and contraction rate parameter. The relative density was directly applied with the value obtained from experiments (26%). The shear modulus coefficient was determined based on the Eqs. (5-1) ~ (5-4) by Tran (2021) for silica sand. The secondary input parameters of permeability, maximum and minimum void ratio, and critical friction angle were determined based on the lab test of Kim et al. (2016) for silica sand. The values of input parameters for PM4Sand are summarized in Table 5-3.

$$G_o = \rho \times V_s^2 \tag{5-1}$$

$$V_s = \alpha_1 \left(\frac{\sigma_m}{\sigma_a}\right)^{\alpha_2} \tag{5-2}$$

$$\alpha_1 = 0.961 \times D_r + 159.280 \tag{5-3}$$

$$\alpha_2 = 0.22 \tag{5-4}$$

where, G_o: shear modulus coefficient, ρ: density of soil, V_s: shear wave velocity of soil, σ_m: confining pressure, σ_a: reference pressure (1 atm), D_r: relative density.

- Elastic model for rigid container

The rigid soil container was modeled as elastic materials with high stiffness (Table 5-4).

Table 5-3 Input parameters of PM4Sand model

Parameters	Values
Relative density, %	26
Shear wave velocity, m/s	184
Contraction rate	0.4
Min. void ratio	0.6
Max. void ratio	1.1
Permeability, m/s	6.e-5
Critical friction angle, °	36.6
Cohesion, Pa	1e4

Table 5-4 Input properties of rigid container

Properties	Container
Density, kg/m^3	2,400
Bulk modulus, Pa	7.50e10
Shear modulus, Pa	2.50e10

- Interface between container and soil

The beam interface was inserted between the container and soil to simulate the separation due to the liquefaction. Considering the role of the beam, an unrealistic but economical property was input for the calculation efficiency. The spring between the beam and the container was set as an elastic spring with a sufficient modulus to prevent the soil from penetrating into the container. On the other hand, the spring between the beam and the soil was given a friction angle to allow for separation between the soil and the container (Kamai & Boulanger, 2013).

Table 5-5 Input properties of beam between container and soil

Properties	Values
Density, kg/m^3	10
Young's modulus, Pa	6.0e2
Area, m^2	1.0e3
Moment of inertia, m^4	1.0

Table 5-6 Input properties of interface spring between container and soil

Properties	Beam–container	Beam–soil
normal spring coefficient, N/m/m	1.0e9	1.0e9
shear spring coefficient, N/m/m	1.0e9	1.0e9
friction angle of normal and shear spring, °	-	20

- Boundary conditions

The boundary conditions of the model consist of the ground surface, the horizontal boundary of the container, and the bottom boundary of the container. Normal stress was applied to the ground surface to simulate the hydrostatic pressure caused by the reservoir. In order to prevent reflection of seismic waves, the horizontal and bottom boundaries of the container were set as a free field boundary and a quiet boundary, respectively.

- Considerations in simulation

In order to increase the accuracy and stability of the analysis, a few numerical techniques are applied. The model should establish static equilibrium under dry and saturated conditions prior to dynamic analysis. PM4Sand model was applied after construction of static equilibrium with Mohr-Coulomb model.

The dynamic shear modulus, one of the key properties of dynamic analysis, was determined according to the effective confining stress. To prevent mesh distortion near the ground surface, which has weak strength due to a low confining stress, 1 kPa of cohesion was applied. Initial pore pressure level and the saturation status of ground surface was fixed so that the dissipation of the excess pore pressure was not disturbed.

In this analysis, quiet boundary was set to control the reflection of the input wave at the bottom boundary, so the base motion was input through the form of shear stress instead of acceleration. Also, Rayleigh damping was set on the foundation and soil to control the high-frequency noise.

5.3.3 Simulated results and analyses

- Validation of simulation results

The accelerations simulated in numerical analysis showed good agreement up to approximately 10-15 s before the full liquefaction of the model ground. Note that the location of the accelerometers cannot be assured after liquefaction.

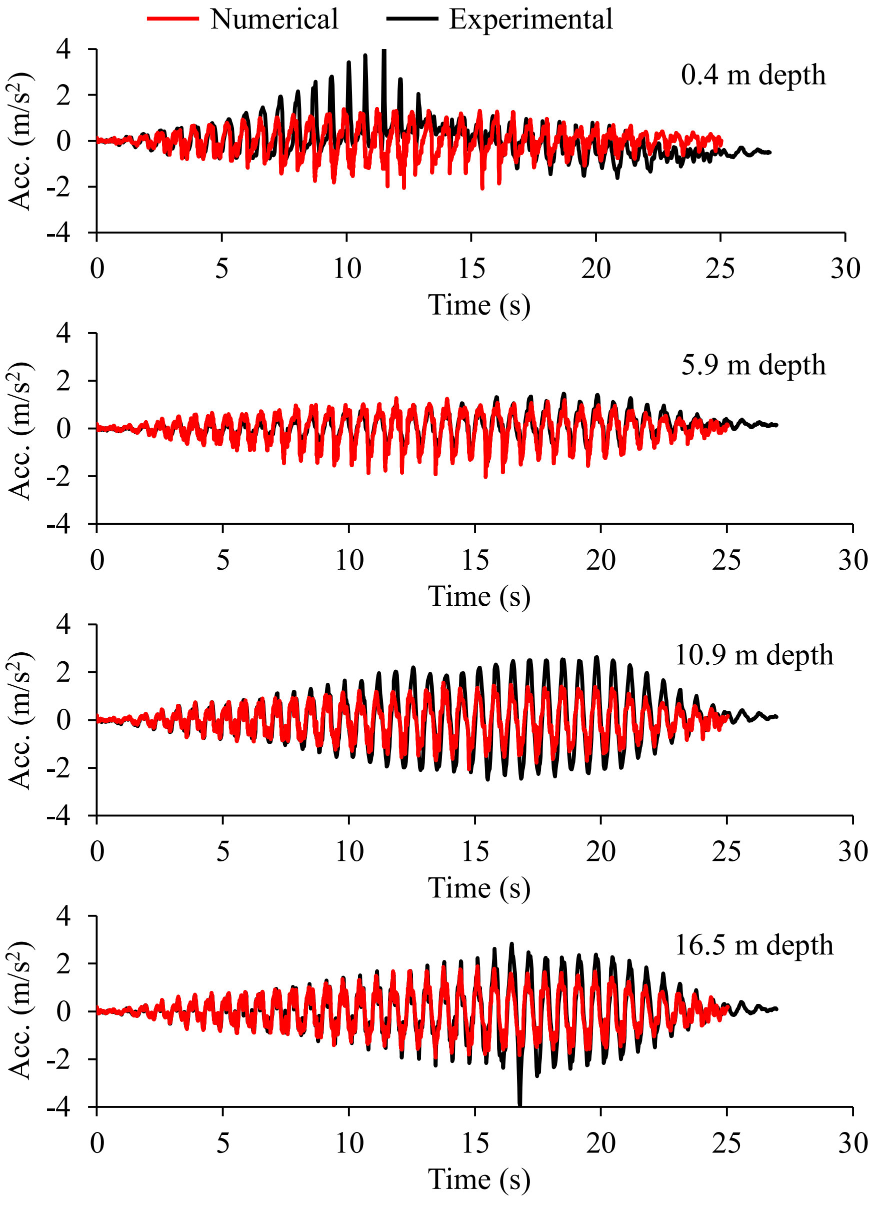

Figure 5-9 Comparison of numerical and experimental results in ground acceleration in Case 2

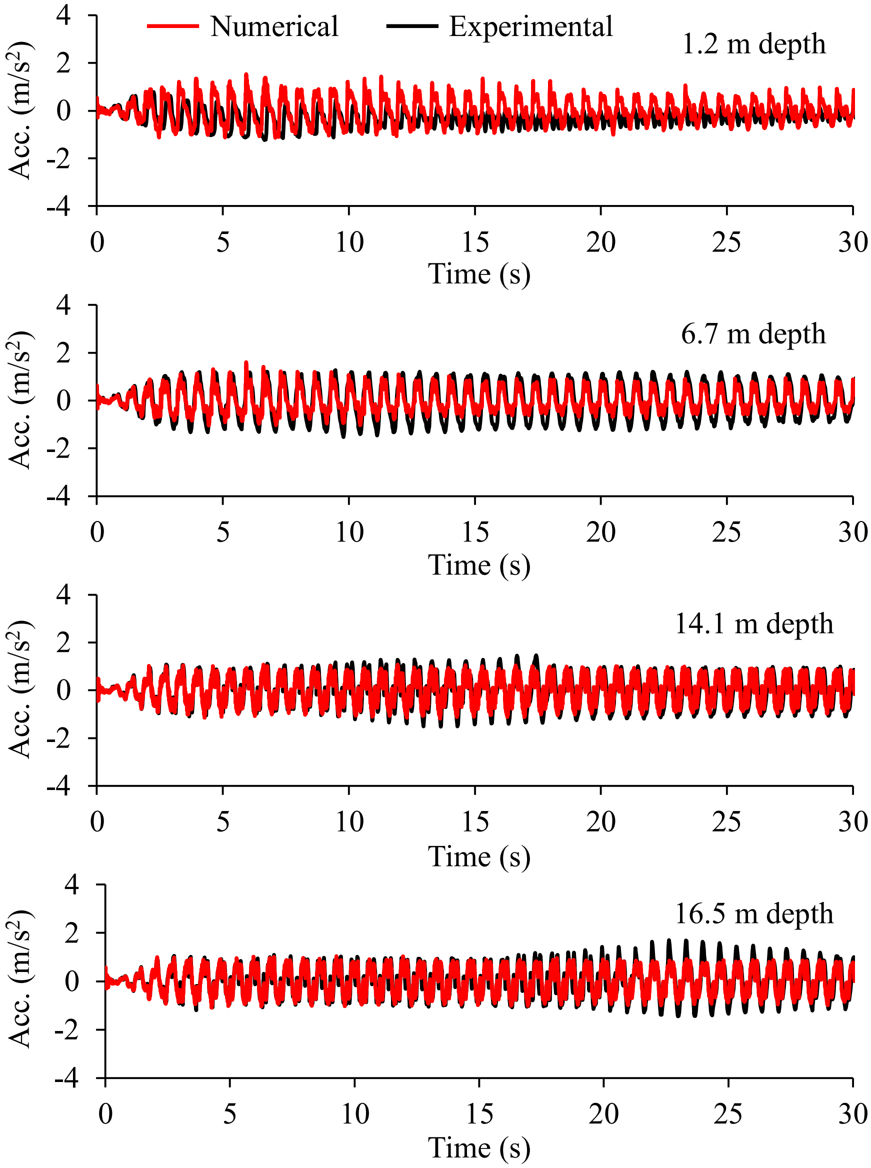

Figure 5-10 Comparison of numerical and experimental results in ground acceleration in Case 3

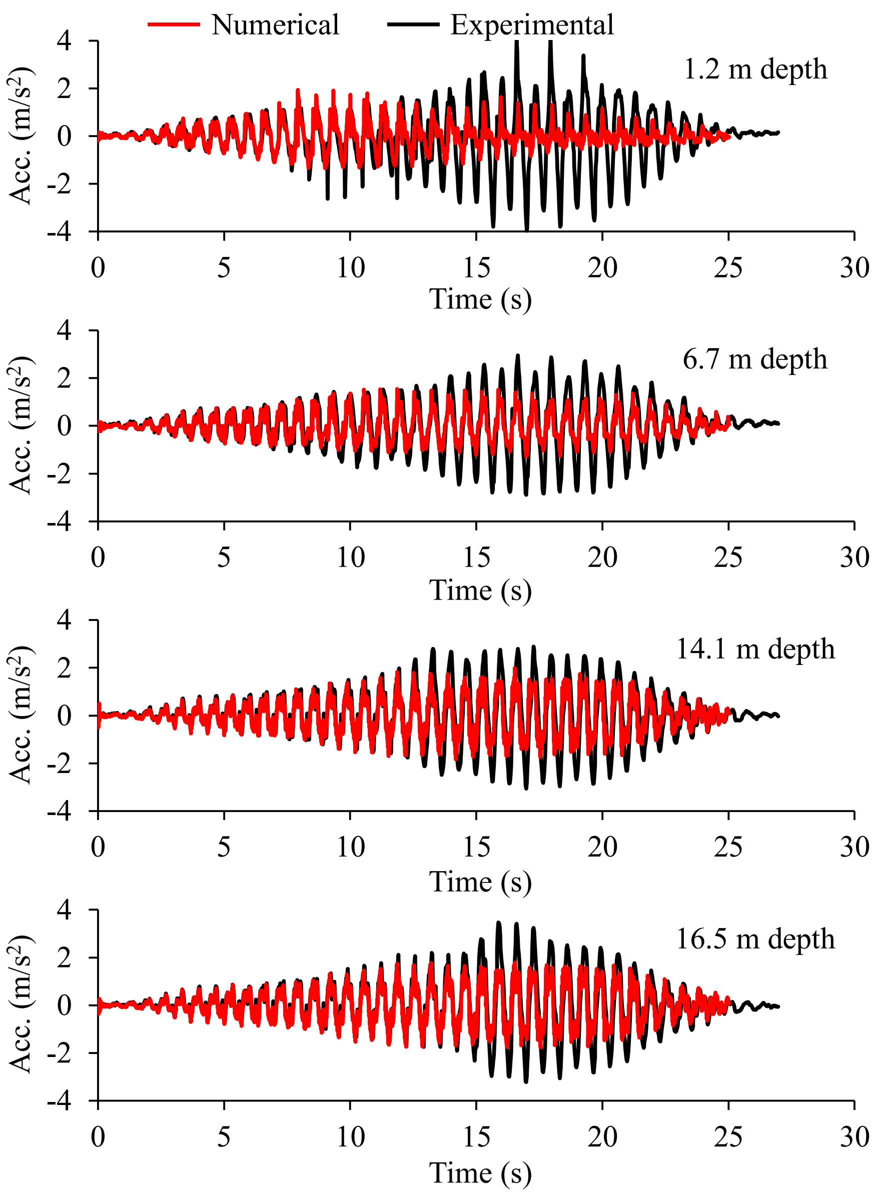

Figure 5-11 Comparison of numerical and experimental results in ground acceleration in Case 4

The simulation results of the excess pore pressure showed good overall agreement. In numerical analysis, the excess pore pressure of the soil close to the bottom of the container was not increased properly due to the deformation confinement by the rigid container. However, the experimental result showed that the smooth development of excess pore pressure because the cork allowed deformation of the soil close to the bottom of the container.

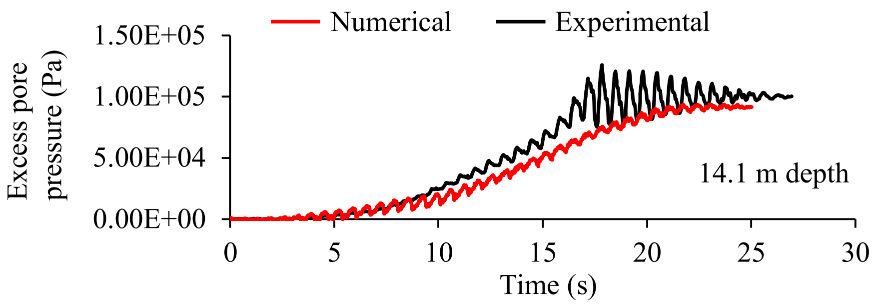

Figure 5-12 Comparison of numerical and experimental results in excess pore pressure in Case 2

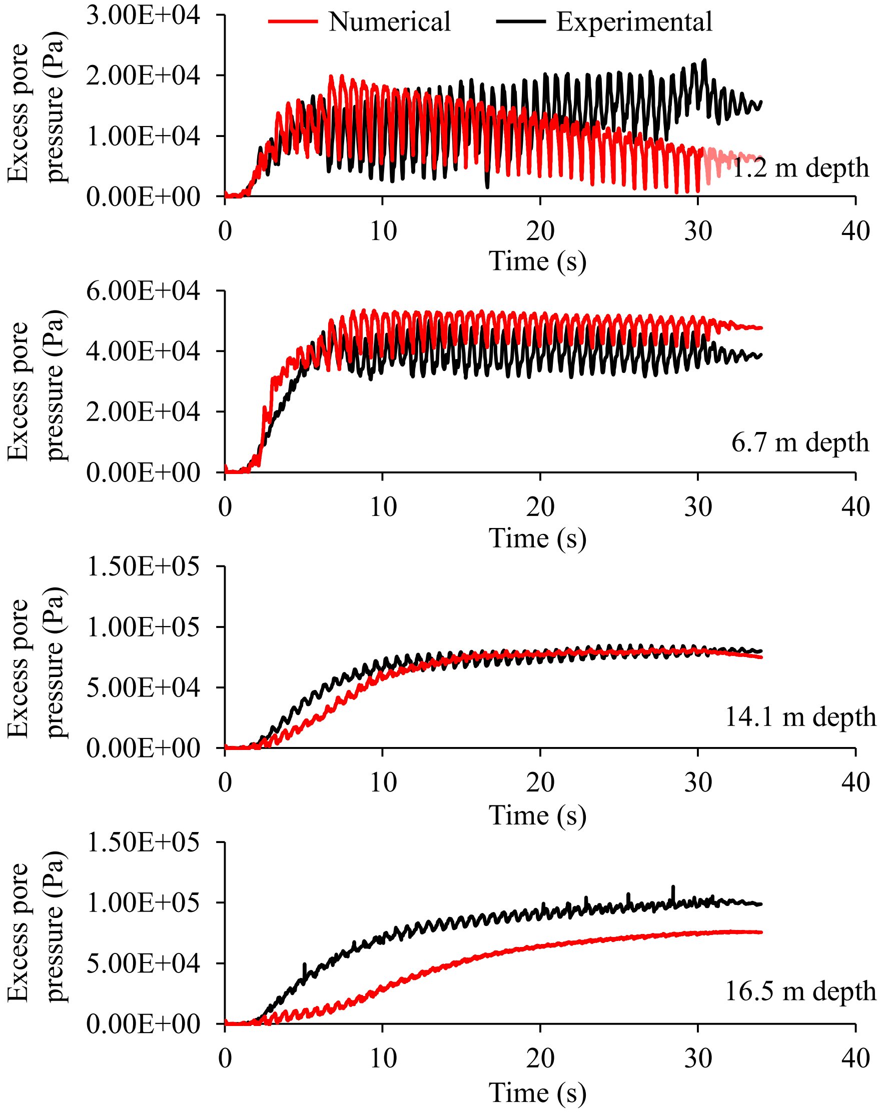

Figure 5-13 Comparison of numerical and experimental results in excess pore pressure in Case 3

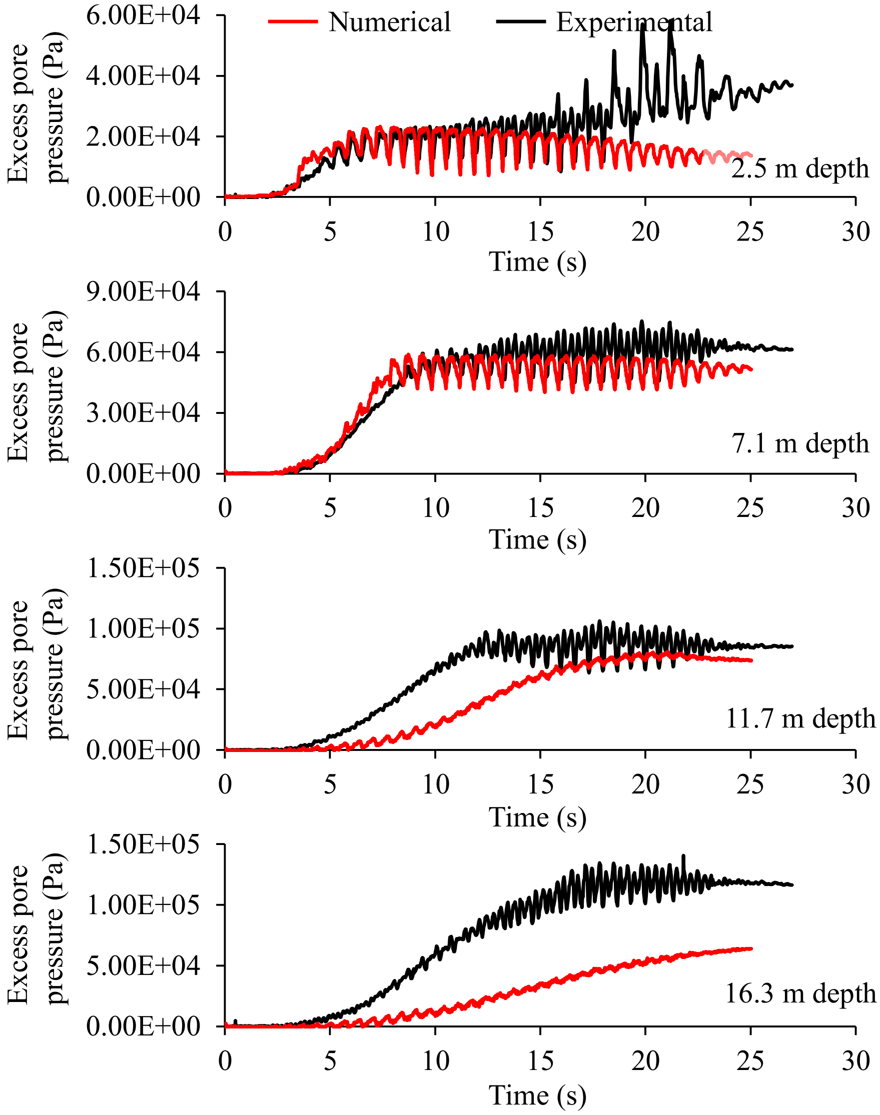

Figure 5-14 Comparison of numerical and experimental results in excess pore pressure in Case 4

The results of the numerical analysis showed good agreement between the experimental data of slope crest settlement.

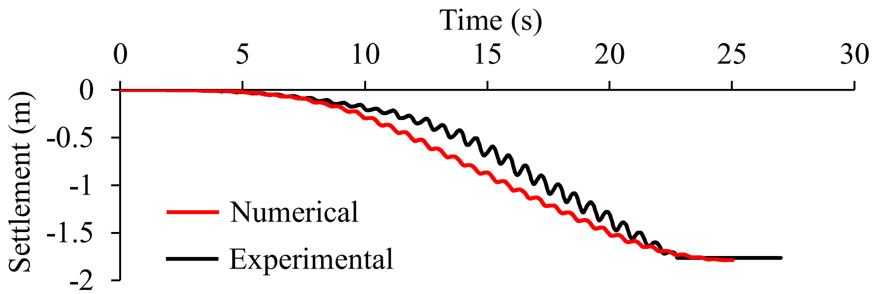

Figure 5-15 Comparison of numerical and experimental results in slope crest settlement in Case 2

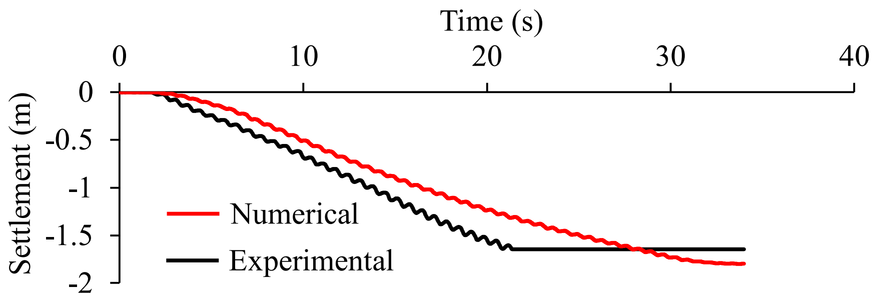

Figure 5-16 Comparison of numerical and experimental results in slope crest settlement in Case 3

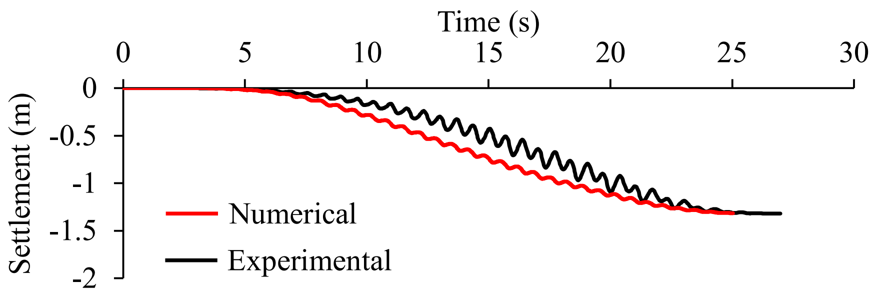

Figure 5-17 Comparison of numerical and experimental results in slope crest settlement in Case 4

- Failure mode of liquefied slope

Figure 5-18 shows the contours of the XY displacement of the ground grid. The sliding surface is represented by connecting the ground grids of the boundary where the displacement equals zero.

The model ground showed the circular failure mode as the liquefaction progresses by gradually expanding the sliding surface. As the slope failure progresses, the model slope gradually became flat, and as a result, the height of the ends of the sliding surface located on the lower and upper sides of the slope gradually approached each other.

Figure 5-19 shows the sliding surface on the contours of the excess pore pressure ratio at each time. The blue band, representing complete liquefaction, spread from the slope toe to the entire model ground. On the other hand, the ground near the slope crest showed negative pore pressure because the PM4Sand model simulates positive and negative excessive pore pressures according to the compression and expansion of the ground.

The liquefaction of the ground led to the expansion of the sliding surface. As seen in the numerical model at 7 s, the liquefied soil stayed in parts of the slope toe, so the displacement and area of the sliding mass was relatively small. However, as the liquefaction spread from the slope toe to the entire model, the displacement and area of the sliding mass greatly increased.

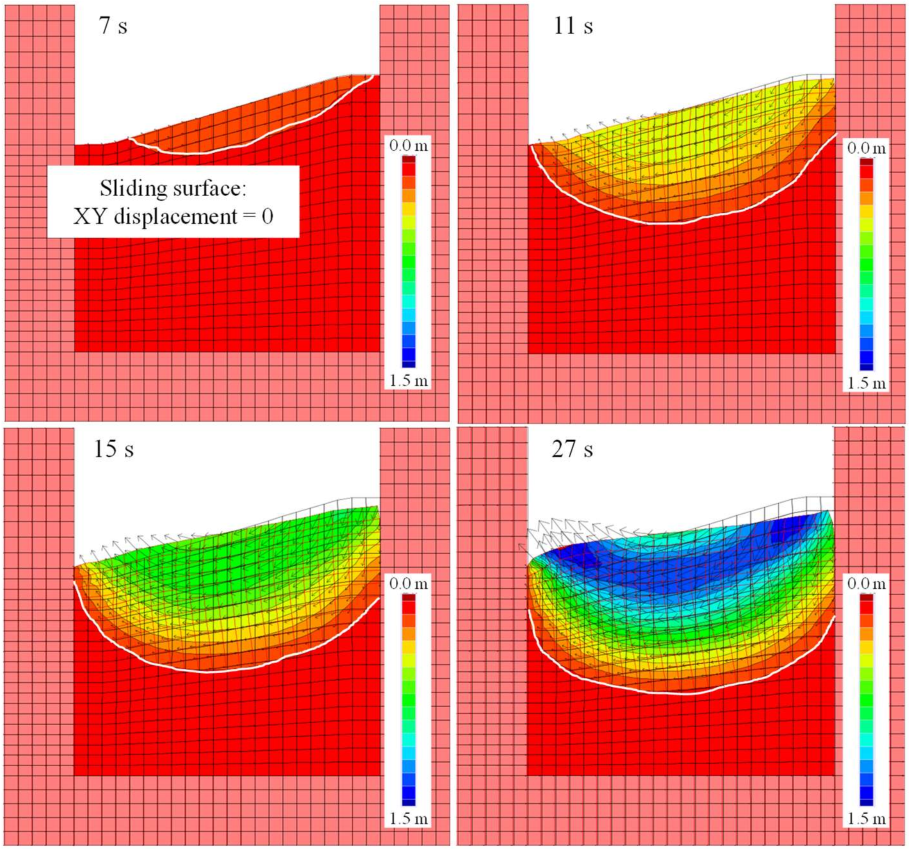

Figure 5-18 XY-displacement contour

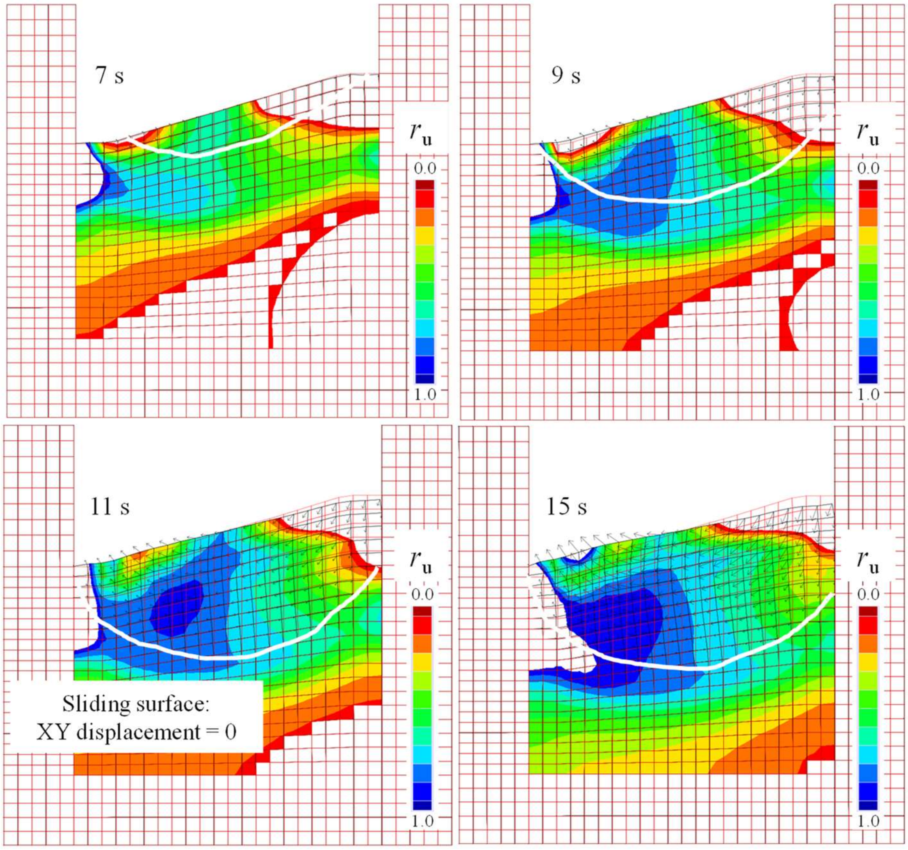

Figure 5-19 Excess pore pressure ratio contour with sliding surface

5.4 Numerical simulation of piles in liquefied slope

5.4.1 Structure modeling with consideration of dimension effect

Figure 5-20 show a numerical model simulating piles in liquefied slope. The dimensions of the performed centrifuge model tests were directly applied to model liquefiable slope, deck, and group piles. The model has two types of interface that allow for separation between materials. One is the beam interface inserted between the container and soil, and the other is the interface spring between the pile and soil.

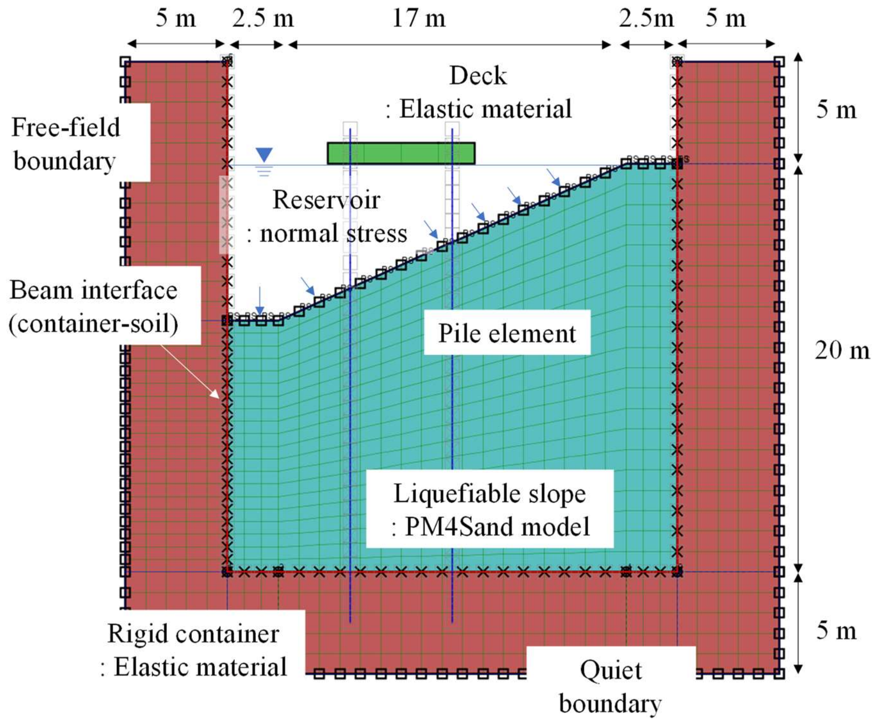

Figure 5-20 2D numerical model for simulation of the centrifuge tests

The deck was modeled as elastic materials with high stiffness, as it has significantly higher strength compared to piles. The spacing of the piles and density of the deck were adjusted to consider the effects that arise from converting the 3D experimental model to a 2D numerical model.

Figure 5-21 illustrates the effects of transforming from 3D experimental model to 2D numerical model. The experimental model was created by cutting a portion of a long wharf supported by many rows of piles. In order to convert the experimental model back to plane-strain conditions, which is the numerical model, deck mass supported by a row of piles was selected as an equivalent section. A half length of the deck was determined as a spacing for piles in numerical model. Considering the unit length of the numerical model, the density of the deck was increased by 3.6 times.

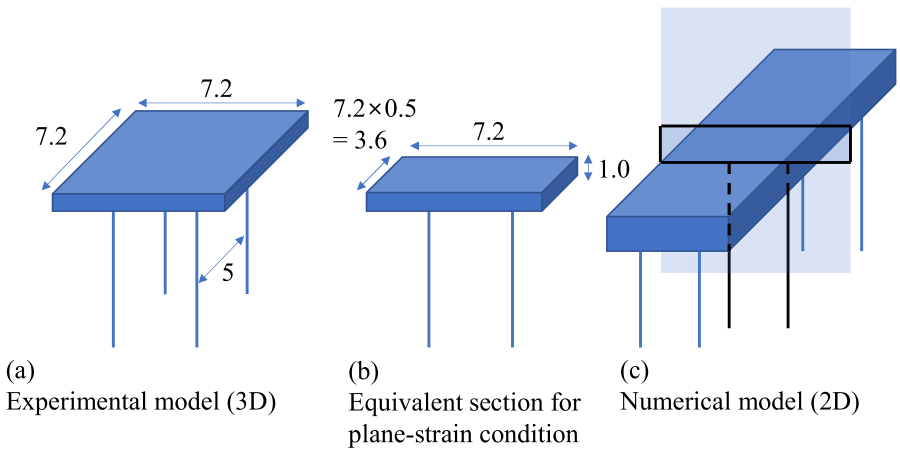

Figure 5-21 Transformation effect of from experimental 3D to numerical 2D

Table 5-7 Input properties of elastic materials

Properties	Deck
Density, kg/m^3	9,684
Bulk modulus, Pa	6.21e10
Shear modulus, Pa	2.38e10

Table 5-8 Input properties of pile beam element

Properties	Values
Density, kg/m^3	2,690
Young's modulus, Pa	6.33e10
Area, m^2	1.24e-1
Moment of inertia, m^4	1.19e-2
Perimeter, m	2.89
Spacing, m	3.6

5.4.2 Soil–pile interface modeling with consideration of liquefaction

The group pile was modeled using beam elements with interface springs to simulate the flexural behavior of the pile and the interaction with the soil. The interface springs represent the relationship between a pile node and a soil grid containing the node. Note that the interface spring is a different concept from the commonly used p-y curve, which represents the adjacent soil to the pile.

The modeling of the interaction between liquefied soil and pile requires simulation of push and pull between the two, which depends on the interface normal spring. However, no proposal has been made yet for the properties of the normal spring used to simulate the interaction between the liquefied soil and pile.

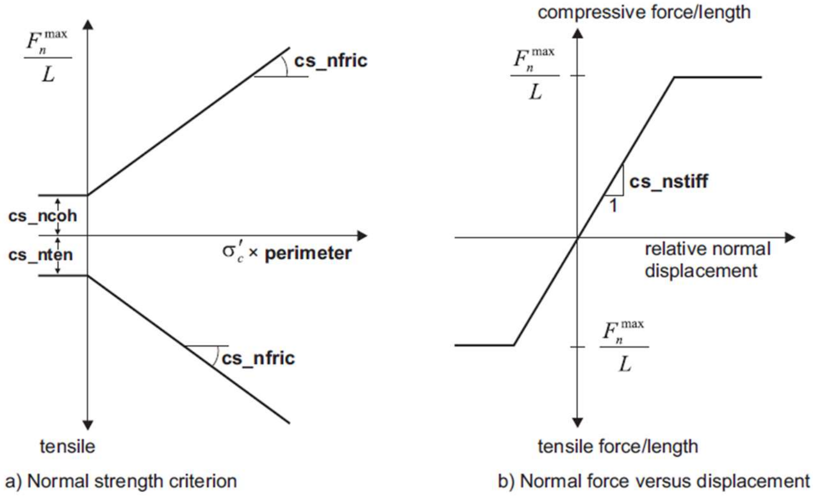

Figure 5-22 Material behavior of normal coupling spring for soil–pile interface (Itasca, 2019)

The friction angle of the normal spring for piles embedded in drained condition has been proposed to be no less than 80 °or not allowing separation, regardless of soil type (Fayyazi et al., 2016; McCullough, 2004). Itasca (2019) has suggested a static simulation of pushing a section of pile under single stress condition to determine the friction angle of normal spring. In this study, following the recommendation of Itasca (2019), the friction angle of the normal spring was determined to be 60° and 7.8° for the soil modeled using Mohr-Coulomb model and PM4Sand model, respectively.

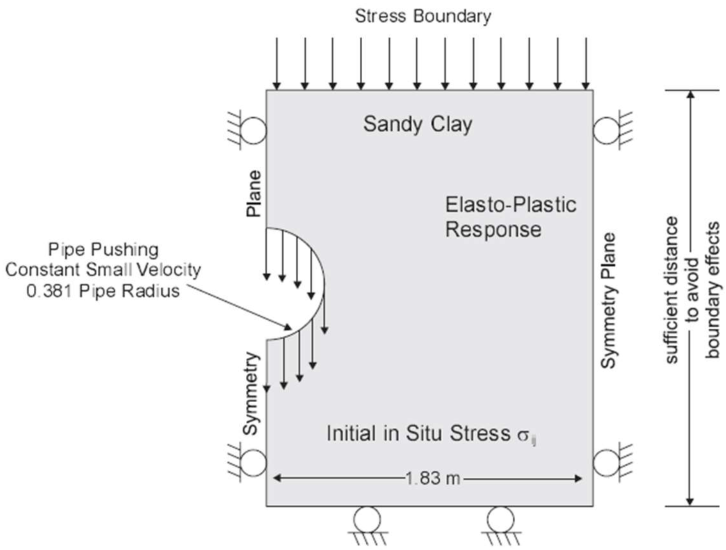

Figure 5-23 Conceptual model to estimate normal coupling spring properties (Itasca, 2019)

Table 5-9 Input properties of the static simulation for interface spring

Properties	Mohr-Coulomb	PM4Sand
Cohesion, Pa	1.0e3	-
Friction angle, °	37.7	-
Relative density, %	-	26
Shear wave velocity, m/s	-	184
Contraction rate	-	0.4

The friction angle of the interface normal spring can decrease due to the liquefaction of the ground. Tran et al. (2022) proposed that the friction angle of the interface normal spring decreases as the embedment depth decreases. Therefore, in this study, a linear decrease in the tangential friction angle to 5%

of initial value with an increase in the excess pore pressure ratio was applied.

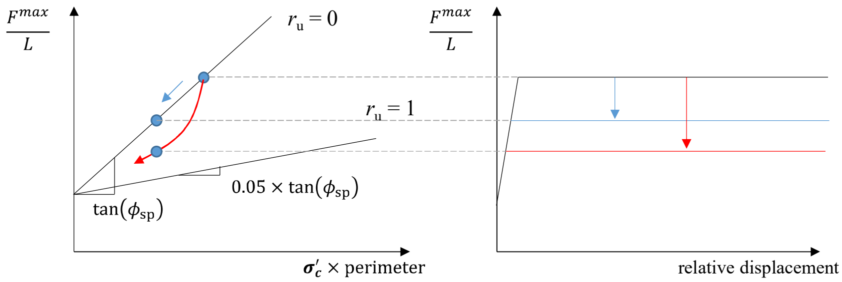

Figure 5-24 Mechanism of interface normal spring subjected to development of excess pore pressure

Figure 5-24 shows the mechanism of the interface normal spring operating between the pile node and the soil grid including the node. The normal spring with sufficiently large coefficient generates maximum normal force when it is subjected to the relative displacement between pile and soil.

The normal spring proposed for dry soil does not consider the change in friction angle due to changes in excess pore pressure ratios. As a result, the increase of excess pore pressure ratio in the soil grid including the pile node decreases the normal force through the decrease of effective confining stress. On the other hand, the proposed method considers the decrease in tangential friction angle due to the increase in excessive pore pressure ratios, leading to a faster decrease in the maximum normal force.

Table 5-10 Friction angle of normal spring

Models	Friction angle of normal spring, °
Mohr-Coulomb model (MC)	60
PM4Sand model (PM)	7.8
Proposed model	Initial: 60, Min: 5

In order to simulate rigid connections between deck–pile and container–pile, sufficient cohesion (1.0e10 Pa) was applied to the interfaces.

5.4.3 Simulated results and analyses

Figure 5-25 shows the effect of the friction angle of the interface normal spring on the bending moment of the group piles. Compared to the MC and PM models with a constant friction angle, the proposed model that decreases the friction angle according to the excess pore pressure ratio showed better agreement with experimental results.

The MC model overestimated the bending moments from approximately 15 s, when was the excess pore pressure ratio of the deep layer started to increase. The lack of reduction in friction angle led to an overestimation of the lateral soil load caused by the liquefaction-induced slope failure.

The PM model predicted that the bending moment would decrease after approximately 20s as the deep layer became fully liquefied. On the other hand, the proposed model predicted that the bending moment would be maintained with the quick recovery of the normal force in shallow layer due to the negative pore pressure.

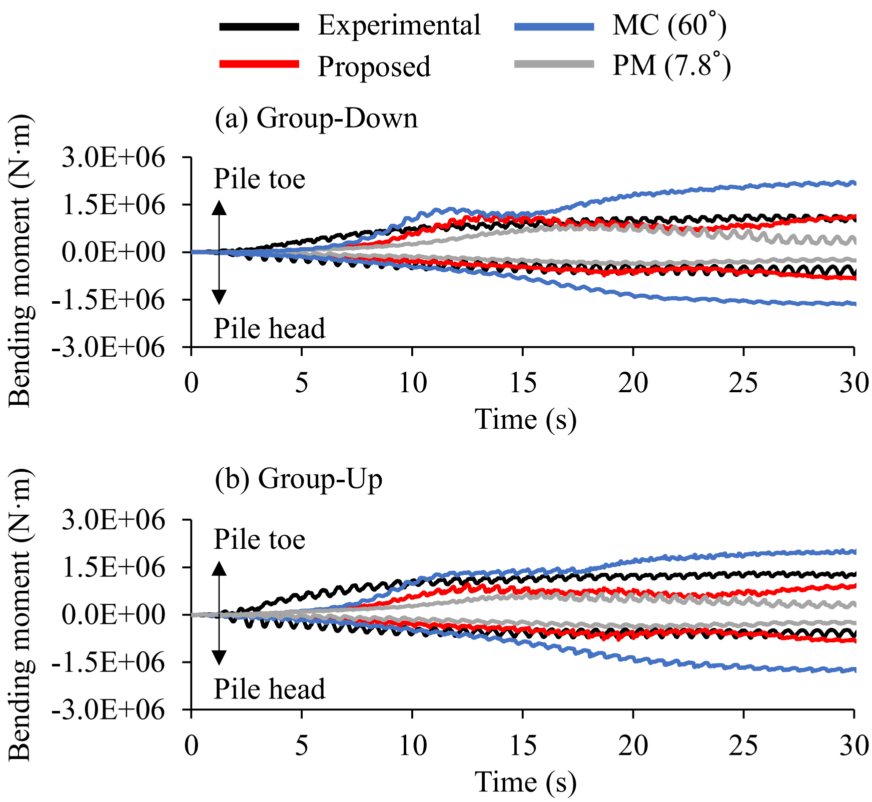

Figure 5-25 Effect of friction angle of interface normal spring in Case 4

- Validation of simulation results

The simulation results of the pile bending moment at the pile toe and pile head showed good agreement with experimental results.

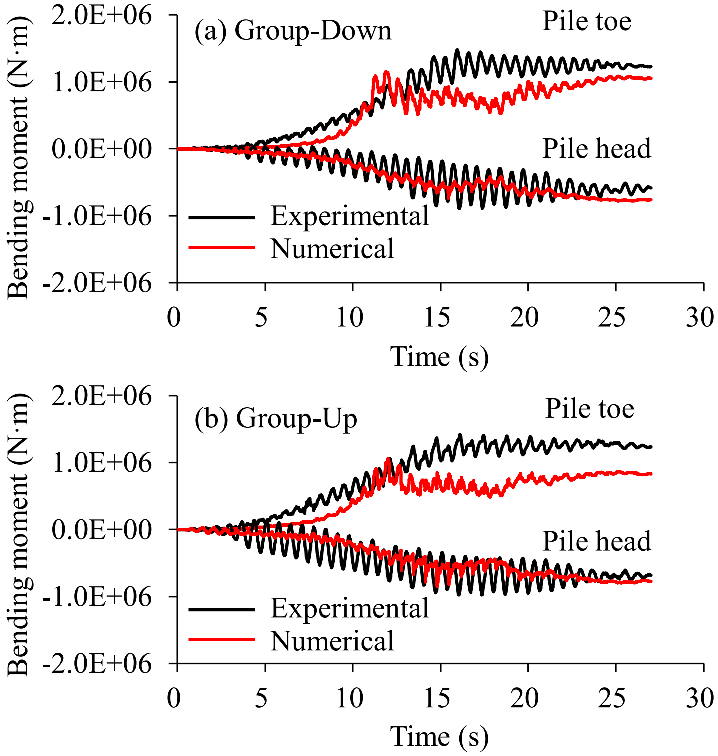

Figure 5-26 Comparison of numerical and experimental results in pile bending moment at pile toe and pile head in Case 2

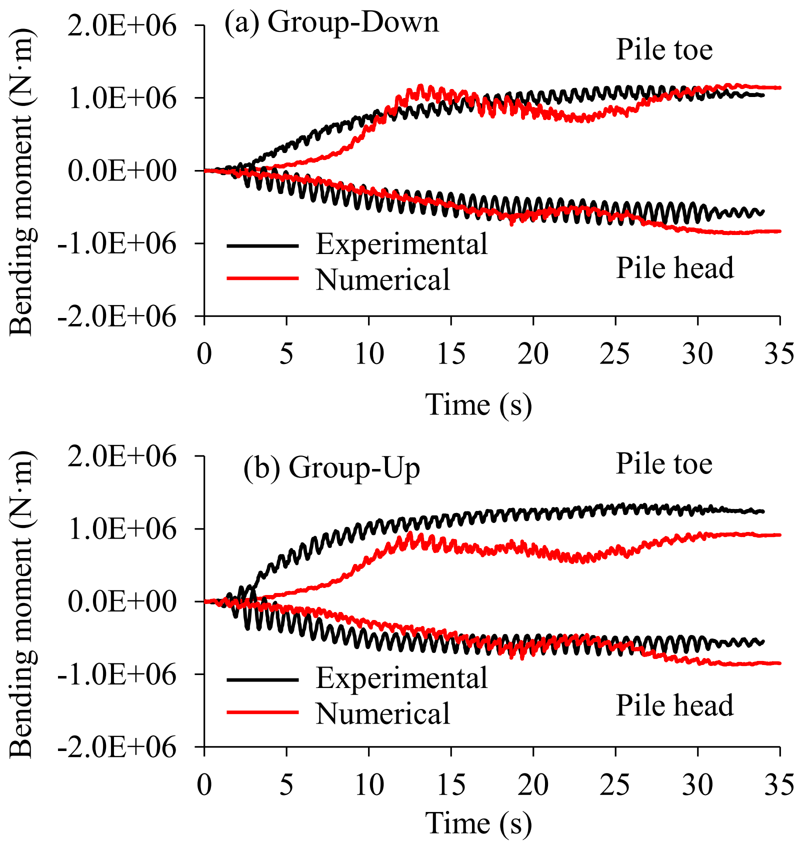

Figure 5-27 Comparison of numerical and experimental results in pile bending moment at pile toe and pile head in Case 3

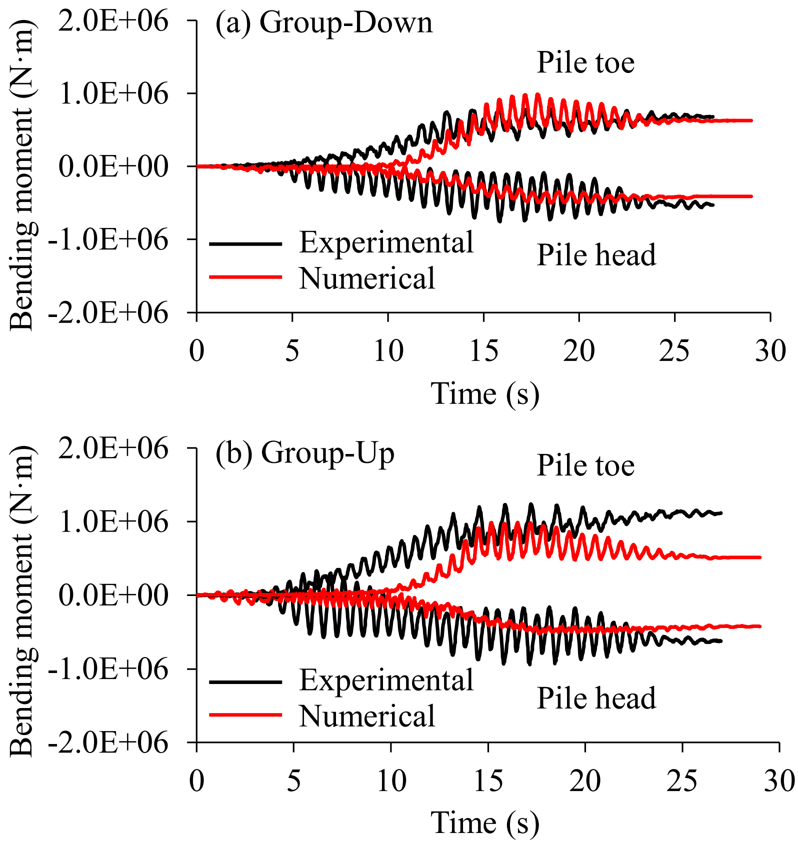

Figure 5-28 Comparison of numerical and experimental results in pile bending moment at pile toe and pile head in Case 4

The simulation results for deck acceleration showed good agreement with the experimental results in terms of the initial amplification trend and the reduction trend due to liquefaction. However, the simulation results for Cases 2 and 4 underestimated the experimental results due to the change in the natural frequency of the structure caused by converting the 3D experimental model into a 2D plane-strain condition.

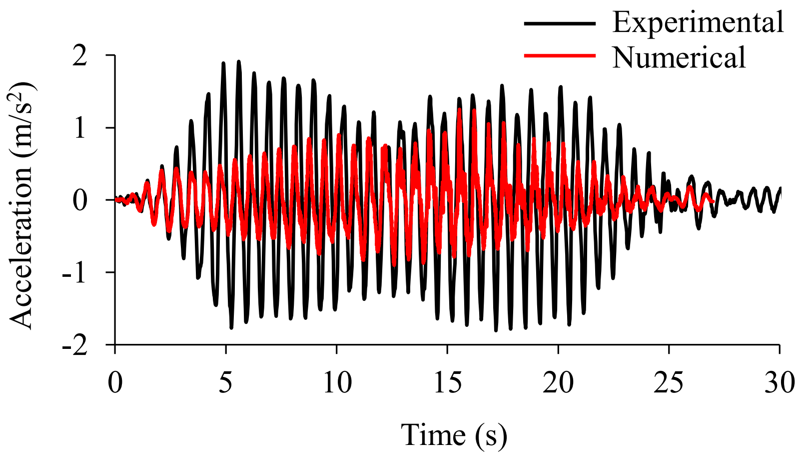

Figure 5-29 Comparison of numerical and experimental results in deck acceleration in Case 2

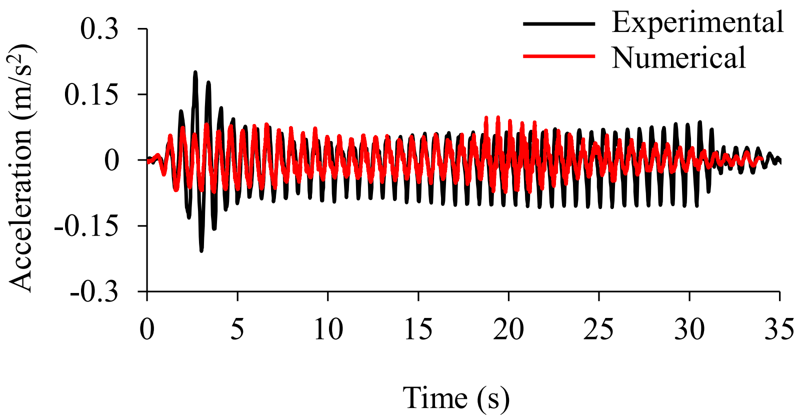

Figure 5-30 Comparison of numerical and experimental results in deck acceleration in Case 3

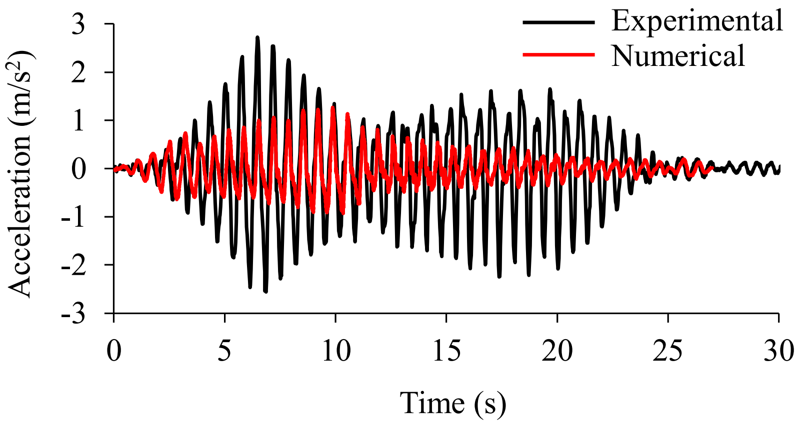

Figure 5-31 Comparison of numerical and experimental results in deck acceleration in Case 4

5.5 Parametric studies

5.5.1 Effect of slope inclinations

The results of the experiments and numerical analysis shown in Chapters 4 and 5 indicate that the pile is subjected to horizontal loads due to liquefied slope failure. The displacement and sliding mass of liquefied slope is influenced by the slope inclination. Therefore, various slope inclinations ranging from 12.5° to 33.7°were examined to analyze the effect of slope inclination. The slope inclination was adjusted by the location of the slope toe with fixed slope crest.

The profile of residual lateral displacement of soil at slope toe was a sharply increasing shape, reaching its maximum at ground surface, while those at slope center and crest showed maximum values at a depth of approximately 5D with a bulging shape due to the failure of liquefied slope (Figure 5-32). The increase in slope inclination led to an increase in lateral displacement of soil regardless of the location. Further, the increase in slope inclination resulted in a larger increase in lateral displacement of the soil closer to the ground surface than deeper soil.

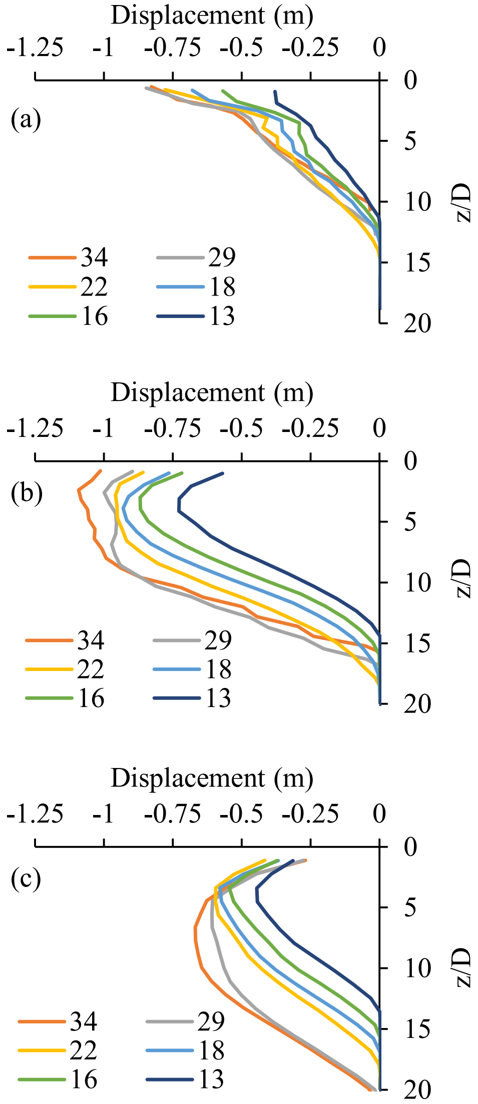

Figure 5-32 Profiles of residual lateral displacement of soil at (a) slope toe, (b) center, and (c) crest

Figure 5-34 shows the profiles of residual bending moment of Group-Up and Group-Down. The neutral point where the bending moment becomes zero was observed at a 12 m distance from the pile head, regardless of the slope inclination and pile location. As the slope inclination increases, the moment both above and below the neutral point showed a tendency to increase.

Figure 5-33 shows the residual bending moment at pile head and toe according to the slope inclinations. When the slope inclination is less than 20°, the moment at pile head and toe were almost symmetric, and there was no significant difference between those of Group-Up and Group-Down. However, when the slope inclination was larger than 20°, the residual moment at the pile toe was much larger than that at the pile head.

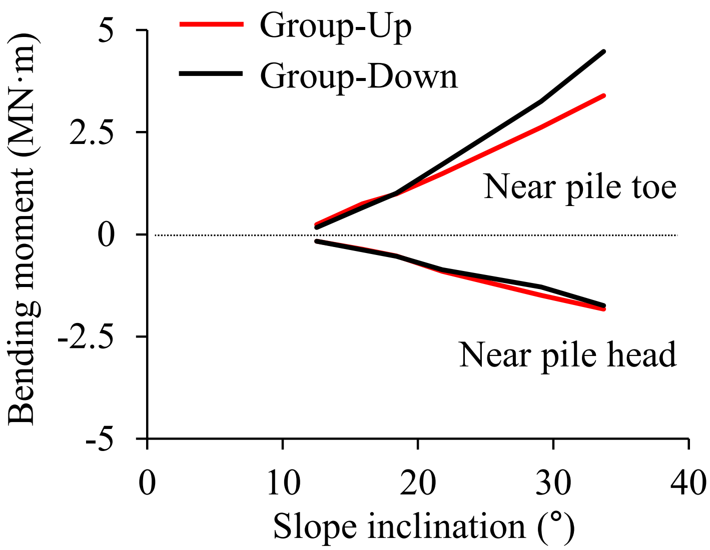

Figure 5-33 Residual bending moment according to the slope inclination

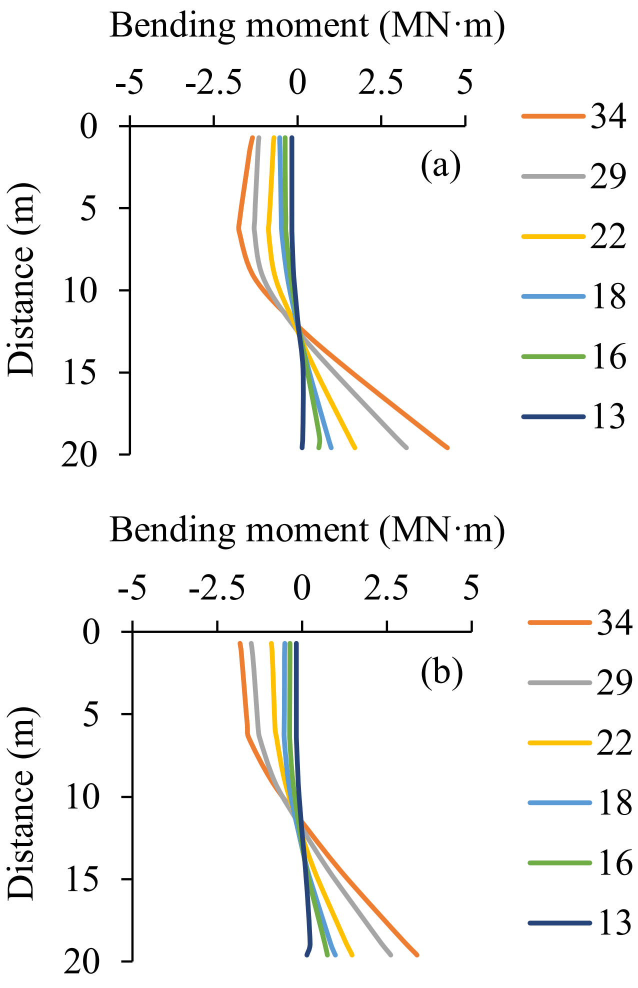

Figure 5-34 Residual bending moment profiles at (a) Group-Down and (b) Group-Up

5.5.2 Effect of amplitude of input motion

The excess pore pressure of the ground is induced by cyclic shear load from a seismic motion. In this study, the effect of the amplitude of input motion is analyzed by varying the maximum acceleration from 0.05g to 0.25g. The input motions were prepared by adjusting the motion used in the experiment.

Figure 5-35 shows the excess pore pressure profile after the end of shaking according to the input amplitude. The increase in the excess pore pressure of the ground is shown to occur for a certain level of input amplitude. As shown in Chapter 3.3.2, the input motion with a maximum acceleration of 0.05 g did not induce the excess pore pressure of the ground. On the other hand, input motion with a maximum acceleration larger than 0.15 g caused full liquefaction of the ground. The intermediate level of maximum acceleration, 0.1 g, did not induce liquefaction in the ground at depths greater than 10m.

Figure 5-36 shows the lateral displacement profile of the ground after the end of shaking according to the input amplitude. The profile caused by the motions with maximum acceleration less than 0.15 g showed linear shape regardless of the slope location. However, input motions with maximum acceleration greater than 0.2 g made the shape of profile change according to the slope location. These motions particularly caused the sliding of the soil block which was from the ground surface to a depth of 10D in the center of the slope.

The lateral displacement of the ground due to input motion induced residual bending moment in piles. Figure 5-37 shows the residual bending moment profile of group piles according to the input amplitude. Input motions weaker than 0.1 g failed to cause liquefaction of the ground at deep depths, resulting in the maximum bending moment occurred not at the pile toe but within the ground.

Despite the input motions stronger than 0.15 g induced full liquefaction of the ground, a smaller residual bending moment appeared for 0.15 g input amplitude compared to others. This suggests that in addition to the complete liquefaction of the soil, the input amplitude also affected the failure of liquefied slope. Furthermore, the residual bending moment induced by the 0.2 g and 0.25 g input motions was approximately identical, indicating that beyond a certain level of input amplitude, there is no longer an increase in the bending moment of the piles.

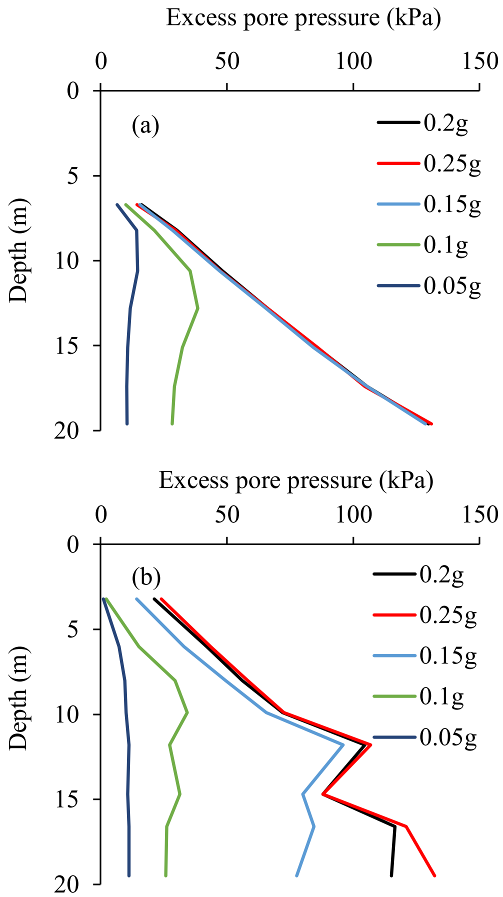

Figure 5-35 Excess pore pressure profile after end of shaking at (a) slope center and (b) crest

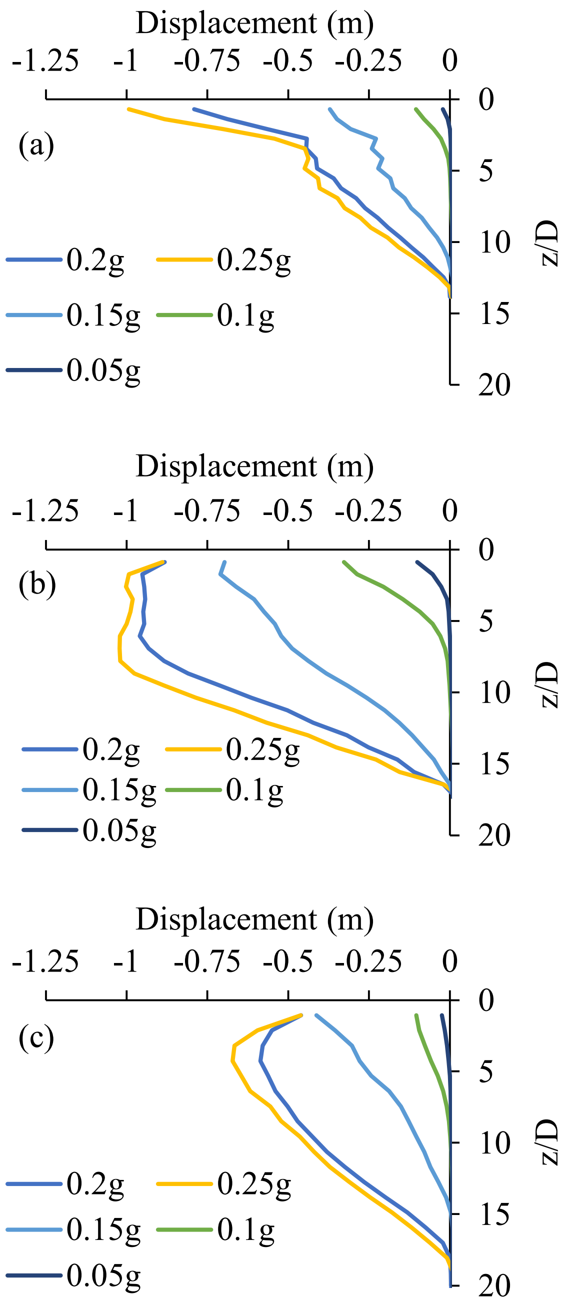

Figure 5-36 Profiles of residual lateral displacement of soil at (a) slope toe, (b) center, and (c) crest

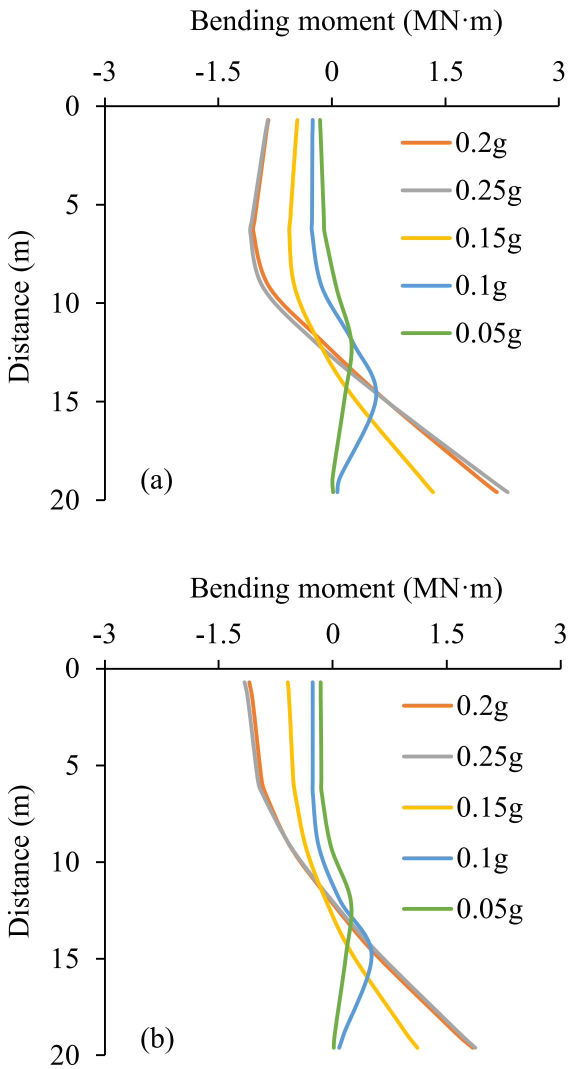

Figure 5-37 Residual bending moment profiles at (a) Group-Down and (b) Group-Up

5.6 Summary

In this chapter, numerical studies on liquefied lateral soil pressure, behavior of liquefied slope, and the seismic behavior of piles in liquefied slope was conducted.

The main conclusions can be summarized as follows.

(1) Linear and uniform lateral soil pressure profiles, which have been recommended for pile analysis in liquefied ground, were examined on the basis of the maximum bending moment measured in this study. The linear soil pressure profile produced a reasonable bending moment profile compared to the results of the uniform profile. Therefore, the linear soil pressure profile is recommended for the practical design of piles in finite slope susceptible to liquefaction.

(2) For single piles, the empirical factor C_L, defined as the proportional coefficient of the linear soil pressure, was found to be large near the slope toe and when the piles were subjected to strong motion. The relation of C_L with pile location and input motion evaluated from the centrifuge test results was implemented in the pile group analysis. The maximum bending moment profiles predicted in accordance with JRA (2012) and JSWA (1997) differed significantly from the current measurement. By applying the factor C_L of this study to these recommendations, the bending moment prediction was considerably enhanced.

(3) The seismic behavior of finite slopes in a rigid container was simulated through numerical modeling. The accuracy of the model was improved by

adopting the PM4Sand model as a liquefiable soil, beam elements for a separation of liquefied soil and container, and quiet boundary for a dissipation of the motion. The validated simulation results, compared to the results of experimental data, showed the circular failure mode of liquefied finite slopes. The liquefaction of the soil, starting from the slope toe and spreading throughout the entire model, gradually expanded the failure surface and finally flattened the initial slopes.

(4) A soil-pile interface model that considers the liquefaction effects was proposed. The proposed model modified the conventional model by reducing the friction angle of the normal spring by up to 5% of the initial value as the excess pore pressure increases. The simulation results based on the conventional models considerably overestimated or underestimated the experimental residual bending moment, while the proposed model showed good agreement with the experimental results throughout the entire time history, not just the residual value.

(5) Based on the validated numerical model, parametric studies on the effects of slope inclinations and amplitude of input motions were conducted. As the slope inclination increased, the area of the sliding soil increased, causing a larger bending moment in the piles. The lateral displacement of the soils and the bending moment of the piles occurred with sufficient input amplitude to induce full liquefaction of the model ground. Furthermore, beyond input amplitude, which is sufficient to induce failure of liquefied slope, no further increase in the bending moment was observed.

Chapter 6. Conclusions and Recommendations

6.1 Conclusions

Liquefaction of the ground has induced damage of pile foundation. It is common that pile foundations of waterfront structure are installed in finite slopes. However, previous studies on pile foundation subjected to liquefaction of the ground have been mainly conducted on the level ground or infinite slopes. Therefore, seismic behavior of piles in liquefied slope was investigated through experimental and numerical approaches.

In the experimental approach, a carefully designed centrifuge model experiments were performed. Loose sandy slopes were prepared with a viscous fluid to simulate liquefied slopes with consideration of centrifuge scale law. The experimental pile and deck were manufactured to simulate a prototype pile-supported wharf in the consideration of flexural stiffness and weight, respectively. The model slope fully liquefied and caused deformation of the model structure.

In numerical approach, several modeling methods for the simulation of soil–pile interaction were investigated. A method of substituting liquefied soil to distributed lateral force on pile foundation was examined. A rigorous numerical reconstruction of the centrifuge experiment was conducted. The simulation results were validated with the experimental data.

The main conclusions are summarized below.

Effect of pore fluid viscosity on ground liquefaction in centrifuge test

- The development of excess pore pressure was observed in model ground regardless of the pore fluid viscosity. In the experiment with viscous pore fluid, the delayed consolidation due to the decrease in permeability of model ground provided a complete undrained loading condition. Consequently, the model ground was liquefied from shallow to deep. However, in the experiment with water pore fluid, the development of excess pore pressure at the shallower depth was restrained due to the fast drainage condition. The suppressed increment of excess pore pressure implied that the model ground with water pore fluid in the dynamic centrifuge test was failed to simulate undrained condition of seismic loading in the field.

Lateral behavior of pile-deck system subjected to liquefied slope

- The liquefied slope failure pushed the deck in the downslope direction while shaking. The deck displacement kept increasing until the end of shaking. This monotonic accumulation of deck displacement could be responsible for the delayed girder failures observed in the field. After the end of shaking, the displacement had been maintained with the dissipation of excess pore pressure. This implies that the piles were pushed by liquefied lateral force during shaking and held by ground confinement in post-liquefaction.

- The pile-deck system in liquefiable slope was subjected to the mass inertia and the liquefied soil force resulting in a bending moment along the pile length. The monotonic bending moment induced by liquefied soil force was the significantly larger than the cyclic bending moment due to the inertia. Therefore, the stability of a pile foundation on the slope susceptible to liquefaction is considerably affected by the liquefied soil force rather than an inertia force.
- The seismic behavior of finite slopes in a rigid container was simulated through numerical modeling. The accuracy of the model was improved by adopting the PM4Sand model as a liquefiable soil, beam elements for a separation of liquefied soil and container, and quiet boundary for a dissipation of the motion. The validated simulation results, compared to the results of experimental data, showed the circular failure mode of liquefied finite slopes. The liquefaction of the soil, starting from the slope toe and spreading throughout the entire model, gradually expanded the failure surface and finally flattened the initial slopes.
- A soil-pile interface model that considers the liquefaction effects was proposed. The proposed model modified the conventional model by reducing the friction angle of the normal spring by up to 5% of the initial value as the excess pore pressure increases. The simulation results based on the conventional models considerably overestimated or underestimated the experimental residual bending moment, while the proposed model showed good agreement with the experimental results throughout the entire time history, not just the residual value.

- Based on the validated numerical model, parametric studies on the effects of slope inclinations and amplitude of input motions were conducted. As the slope inclination increased, the area of the sliding soil increased, causing a larger bending moment in the piles. The lateral displacement of the soils and the bending moment of the piles occurred with sufficient input amplitude to induce full liquefaction of the model ground. Furthermore, beyond input amplitude, which is sufficient to induce failure of liquefied slope, no further increase in the bending moment was observed.

Axial pile performance during and after the seismic loading

- Negative skin friction along the pile length was caused by the ground settlement during the centrifuge spinning. The spin-induced drag loads were within the range of the values calculated with the CFEM β-method for loose sand. Since the obtained and calculated drag loads are in close agreement, it can be deduced that the negative skin friction can be estimated by the CFEM β-method, which was originally suggested for positive skin friction.
- The spin-induced drag load was diminished with the increase in the developed excess pore pressure during shaking. After liquefaction, the axial load of single and group piles below the ground surface converged to the pile head load that corresponds to the deck mass. Furthermore, the drag load linearly decreased with the increase in the excess pore pressure ratio, implying that partial liquefaction can induce significant decrease in the

shaft resistance.

- The reconsolidation settlement generated negative skin friction after the shaking has ceased. The negative skin friction was found to be larger than the liquefied residual strength recommended in the AASHTO LRFD bridge design specifications. Therefore, it is seen that the consideration of the strength reduction is not necessary for the calculation of negative skin friction induced by reconsolidation, since the liquefied ground regains skin friction after the dissipation.

6.2 Recommendations for further research

Experimental and numerical studies presented in this dissertation have contributed to the understanding of the seismic behavior of piles in liquefied slope. Further research on the following topics can be conducted on the potential topics as follows.

- Considerable soil displacement in vertical and horizontal direction is accompanied by liquefaction of slope. In this study, the settlement measured at the slope crest was used to validate the numerical simulation results for the liquefied slope. However, more advanced research could be performed if it was possible to measure lateral displacement within the ground instead of at the ground surface. These requirements may be achieved by applying a high-speed camera technique or particle image velocimetry (PIV) method.
- In order to focus on the interaction between pile shaft and adjacent

liquefied soil, homogeneous model ground overlying rigid container base was prepared. For a further experimental study, the need for considering multi-layered soil conditions including gravel cover layer, hydraulic fill overlying base layer and stiffness of the base layer.

- Variation of skin friction of end-bearing piles with changes in excess pore pressure was analyzed under relatively simple conditions where settlement of the piles was negligible. However, in the case of floating piles which has weak bearing capacity, different behavior may be expected due to the relative displacement between the soil and piles.
- Finally, the practice design codes are conservative in involving advanced research works on geotechnical structures under the liquefaction of foundation soil. Appropriate liquefaction assessment in probabilistic approach may introduce the economic necessity of the advanced design, which allows liquefaction occurrence for a certain level of earthquake.

List of References

AASHTO. (2020). *LRFD bridge design specifications*. American Association of State Highway and Transportation Officials.

Abdoun, T., & Dobry, R. (2002). Evaluation of pile foundation response to lateral spreading. *Soil Dynamics and Earthquake Engineering*, *22*(9-12), 1051-1058. https://doi.org/10.1016/S0267-7261(02)00130-6

Adamidis, O., & Madabhushi, G. (2016). Post-liquefaction reconsolidation of sand. *Proceedings of the Royal Society A: Mathematical, Physical and Engineering Sciences*, *472*(2186), 20150745. https://doi.org/https://doi.org/10.1098/rspa.2015.0745

Adamidis, O., & Madabhushi, G. S. P. (2015). Use of viscous pore fluids in dynamic centrifuge modelling. *International Journal of Physical Modelling in Geotechnics*, *15*(3), 141-149.

AIJ. (2001). Recommendations for design of building foundations. In: Architectural Institute of Japan.

ASCE. (2014). Seismic design of piers and wharves.

Basu, D., Montgomery, J., & Stuedlein, A. W. (2022). Observations and challenges in simulating post-liquefaction settlements from centrifuge and shake table tests. *Soil Dynamics and Earthquake Engineering*, *153*, 107089. https://doi.org/https://doi.org/10.1016/j.soildyn.2021.107089

Berrill, J., Christensen, S., Keenan, R., Okada, W., & Pettinga, J. (2001). Case study of lateral spreading forces on a piled foundation. *Géotechnique*, *51*(6), 501-517. https://doi.org/10.1680/geot.2001.51.6.501

Bhattacharya, S., & Madabhushi, S. (2008). A critical review of methods for pile design in seismically liquefiable soils. *Bulletin of Earthquake Engineering*, *6*(3), 407-446.

Boulanger, R., & Ziotopoulou, K. (2015). PM4Sand (Version 3): A sand plasticity model for earthquake engineering applications. *Center for Geotechnical Modeling Report No. UCD/CGM-15/01, Department of*

Civil and Environmental Engineering, University of California, Davis, Calif.

Boulanger, R. W., & Brandenberg, S. J. (2004). Neutral plane solution for liquefaction-induced down-drag on vertical piles. https://doi.org/https://doi.org/10.1061/40744(154)32

Boulanger, R. W., & Idriss, I. (2015). Magnitude scaling factors in liquefaction triggering procedures. *Soil Dynamics and Earthquake Engineering*, *79*, 296-303. https://doi.org/https://doi.org/10.1016/j.soildyn.2015.01.004

Boulanger, R. W., Kutter, B. L., Brandenberg, S. J., Singh, P., Chang, D., & University of California, D. C. f. G. M. (2003). *Pile foundations in liquefied and laterally spreading ground during earthquakes: centrifuge experiments & analyses*.

Bradshaw, A., & Baxter, C. (2007). Sample preparation of silts for liquefaction testing. *Geotechnical Testing Journal*, *30*(4), 324-332.

Brandenberg, S. J., Boulanger, R. W., Kutter, B. L., & Chang, D. (2005). Behavior of pile foundations in laterally spreading ground during centrifuge tests. *Journal of Geotechnical and Geoenvironmental Engineering*, *131*(11), 1378-1391. https://doi.org/https://doi.org/10.1061/(ASCE)1090-0241(2005)131:11(1378)

Brandenberg, S. J., Boulanger, R. W., Kutter, B. L., & Chang, D. (2007). Static pushover analyses of pile groups in liquefied and laterally spreading ground in centrifuge tests. *Journal of Geotechnical and Geoenvironmental Engineering*, *133*(9), 1055-1066. https://doi.org/10.1061/(ASCE)1090-0241(2007)/133:9(1055)

CFEM. (2006). *Canadian Foundation Engineering Manual* (4th ed. ed.). Richmond, BC : Canadian Geotechnical Society.

Chian, S., & Madabhushi, S. (2010). Influence of fluid viscosity on the response of buried structures in earthquakes. 7th international conference of physical modelling in geotechnics, Clausen, C., Aas, P., & Karlsrud, K. (2005). Bearing capacity of driven piles in sand, the NGI approach. Proceedings of Proceedings of International Symposium. on Frontiers in Offshore Geotechnics, Perth,

Dash, S., Rouholamin, M., Lombardi, D., & Bhattacharya, S. (2017). A practical method for construction of py curves for liquefiable soils. *Soil Dynamics and Earthquake Engineering*, *97*, 478-481. https://doi.org/10.1016/j.soildyn.2017.03.002

Dashti, S., & Karimi, Z. (2017). Ground motion intensity measures to evaluate I: the liquefaction hazard in the vicinity of shallow-founded structures. *Earthquake spectra*, *33*(1), 241-276. https://doi.org/10.1193/1.2194970

Dewoolkar, M. M., Ko, H.-Y., Stadler, A. T., & Astaneh, S. (1999). A substitute pore fluid for seismic centrifuge modeling. *Geotechnical Testing Journal*, *22*(3), 196-210.

Dobry, R., Abdoun, T., O'Rourke, T. D., & Goh, S. (2003). Single piles in lateral spreads: Field bending moment evaluation. *Journal of Geotechnical and Geoenvironmental Engineering*, *129*(10), 879-889. https://doi.org/https://doi.org/10.1061/(ASCE)1090-0241(2003)129:10(879)

Elvis, I. (2018). Liquefaction-induced dragload and/or downdrag on deep foundations within the New Madrid seismic zone. https://doi.org/https://scholarworks.uark.edu/etd/2766

Fayyazi, M. S., Taiebat, M., & Ji, J. (2016). Soil-pile separation and sliding in 3D simulation of pile groups under lateral loading. Proceedings of the 69th Canadian Geotechnical Conference,

Fellenius, B. (2017). *Basics of foundation design*. Lulu. com.

Fellenius, B. H., Abbasi, B., & Muhunthan, B. (2020). Liquefaction induced downdrag for the Juan Pablo II Bridge at the 2010 Maule Earthquake in Chile. *Geotech. Eng. J*, *51*(2), 1-8.

Feng, K., Wang, G., Huang, D., & Jin, F. (2021). Material point method for large-deformation modeling of coseismic landslide and liquefaction-induced dam failure. *Soil Dynamics and Earthquake Engineering*, *150*, 106907.

Fioravante, V. (2002). On the shaft friction modelling of non-displacement piles in sand. *Soils and Foundations*, *42*(2), 23-33. https://doi.org/https://doi.org/10.3208/sandf.42.2_23

Fleming, K., Weltman, A., Randolph, M., & Elson, K. (2008). *Piling engineering*. CRC press.

Frost, J. D., & DeJong, J. T. (2005). In situ assessment of role of surface roughness on interface response. *Journal of Geotechnical and Geoenvironmental Engineering*, *131*(4), 498-511. https://doi.org/https://doi.org/10.1061/(ASCE)1090-0241(2005)131:4(498)

Gibson, L., Easterling, K., & Ashby, M. F. (1981). The structure and mechanics of cork. *Proceedings of the Royal Society of London. A. Mathematical and Physical Sciences*, *377*(1769), 99-117. https://doi.org/https://doi.org/10.1098/rspa.1981.0117

González, L., Abdoun, T., & Dobry, R. (2009). Effect of soil permeability on centrifuge modeling of pile response to lateral spreading. *Journal of Geotechnical and Geoenvironmental Engineering*, *135*(1), 62-73. https://doi.org/10.1061/(ASCE)1090-0241(2009)135:1(62)

Guan, Z., Wang, Y., & Stuedlein, A. W. (2022). Efficient three-dimensional soil liquefaction potential and reconsolidation settlement assessment from limited CPTs considering spatial variability. *Soil Dynamics and Earthquake Engineering*, *163*, 107518. https://doi.org/https://doi.org/10.1016/j.soildyn.2022.107518

Ha, I.-S., Olson, S. M., Seo, M.-W., & Kim, M.-M. (2011). Evaluation of reliquefaction resistance using shaking table tests. *Soil Dynamics and Earthquake Engineering*, *31*(4), 682-691. https://doi.org/https://doi.org/10.1016/j.soildyn.2010.12.008

Hamada, M., & O'Rourke, T. (1992). *'Case studies of liquefaction and lifeline performance during past earthquakes. Volume 1, Japanese Case Studies* (Technical Rep. NCEER-92, Issue.

Han, F., Salgado, R., Prezzi, M., & Lim, J. (2017). Shaft and base resistance of non-displacement piles in sand. *Computers and Geotechnics*, *83*, 184-197. https://doi.org/https://doi.org/10.1016/j.compgeo.2016.11.006

He, L., Elgamal, A., Abdoun, T., Abe, A., Dobry, R., Hamada, M., Menses, J., Sato, M., Shantz, T., & Tokimatsu, K. (2009). Liquefaction-Induced Lateral Load on Pile in a Medium DrSand Layer. *Journal of Earthquake Engineering*, *13*(7), 916-938. https://doi.org/10.1080/13632460903038607

Huang, Y., Wen, Z., Wang, L., & Zhu, C. (2019). Centrifuge testing of liquefaction mitigation effectiveness on sand foundations treated with nanoparticles. *Engineering Geology*, *249*, 249-256.

Hussein, A. F., & El Naggar, M. H. (2021). Seismic axial behaviour of pile groups in non-liquefiable and liquefiable soils. *Soil Dynamics and Earthquake Engineering*, *149*, 106853. https://doi.org/https://doi.org/10.1016/j.soildyn.2021.106853

Idriss, I., & Boulanger, R. W. (2015). 2nd Ishihara Lecture: SPT-and CPT-based relationships for the residual shear strength of liquefied soils. *Soil Dynamics and Earthquake Engineering*, *68*, 57-68. https://doi.org/https://doi.org/10.1016/j.soildyn.2014.09.010

Ishibashi, I., Sherif, M., & Tsuchiya, C. (1977). Pore-pressure rise mechanism and soil liquefaction. *Soils and Foundations*, *17*(2), 17-27.

Ishihara, K. (1977). Simple method of analysis for liquefaction of sand deposits during earthquakes. *Soils and Foundations*, *17*(3), 1-17. https://doi.org/10.3208/sandf1972.17.3_1

Ishimwe, E., Coffman, R. A., & Rollins, K. M. (2018). Analysis of post-liquefaction axial capacities of driven pile and drilled shaft foundations. In *IFCEE 2018* (pp. 272-283).

https://doi.org/https://doi.org/10.1061/9780784481578.028

JRA. (2012). Specifications for highway bridges, Part V. In *Earthquake resistant design* (Vol. 228): Japan Road Association.

JSWA. (1997). Seismic countermeasure guidelines for sewage facilities. In: Japan Sewage Works Association.

Kamai, R., & Boulanger, R. W. (2013). Simulations of a centrifuge test with lateral spreading and void redistribution effects. *Journal of Geotechnical and Geoenvironmental Engineering*, *139*(8), 1250-1261.

Kawamura, S., Nishizawa, T., & Wada, H. (1985). Damage to piles due to liquefaction found by excavation twenty years after earthquake. *Nikkei Architecture*, *27*, 130-134.

Kevan, L. I. (2017). *Full-scale testing of blast-induced liquefaction downdrag on driven piles in sand*. Brigham Young University. https://doi.org/http://hdl.lib.byu.edu/1877/etd9510

Kim, H.-S., Kim, M., Baise, L. G., & Kim, B. (2021). Local and regional evaluation of liquefaction potential index and liquefaction severity number for liquefaction-induced sand boils in Pohang, South Korea. *Soil Dynamics and Earthquake Engineering*, *141*, 106459.

Kim, J. H., Choo, Y. W., Kim, D. J., & Kim, D. S. (2016). Miniature Cone Tip Resistance on Sand in a Centrifuge. *Journal of Geotechnical and Geoenvironmental Engineering*, *142*(3). https://doi.org/https://doi.org/10.1061/(ASCE)GT.1943-5606.0001425

Knappett, J., & Madabhushi, S. (2008). Liquefaction-induced settlement of pile groups in liquefiable and laterally spreading soils. *Journal of Geotechnical and Geoenvironmental Engineering*, *134*(11), 1609-1618. https://doi.org/https://doi.org/10.1061/(ASCE)1090-0241(2008)134:11(1609)

Konkol, J. (2014). Derivation of the scaling laws used in geotechnical centrifuge modelling-application of dimensional analysis and Buckingham Π theorem. *Technical Sciences/University of Warmia and*

Mazury in Olsztyn(17 (1), 31-44.

Kramer, S. L. (1996). *Geotechnical earthquake engineering*. Pearson Education India.

Kuerbis, R., & Vaid, Y. (1988). Sand sample preparation-the slurry deposition method. *Soils and Foundations*, *28*(4), 107-118.

Kulhawy, F. H. (1991). Drilled shaft foundations. In *Foundation engineering handbook* (pp. 537-552). Springer. https://doi.org/DOI: 10.1007/978-1-4757-5271-7_14

Lashkari, A. (2013). Prediction of the shaft resistance of nondisplacement piles in sand. *International Journal for numerical and analytical methods in geomechanics*, *37*(8), 904-931. https://doi.org/https://doi.org/10.1002/nag.1129

Li, X., Tang, L., Man, X., Qiu, M., Ling, X., Cong, S., & Elgamal, A. (2021). Liquefaction-induced lateral load on pile group of wharf system in a sloping stratum: A centrifuge shake-table investigation. *Ocean Engineering*, *242*, 110119. https://doi.org/https://doi.org/10.1016/j.oceaneng.2021.110119

Lim, H., & Jeong, S. (2018). Simplified py curves under dynamic loading in dry sand. *Soil Dynamics and Earthquake Engineering*, *113*, 101-111.

Liu, L., & Dobry, R. (1995). Effect of liquefaction on lateral response of piles by centrifuge model tests.

Liu, L., & Dobry, R. (1997). Seismic response of shallow foundation on liquefiable sand. *Journal of Geotechnical and Geoenvironmental Engineering*, *123*(6), 557-567.

Loukidis, D., & Salgado, R. (2008). Analysis of the shaft resistance of non-displacement piles in sand. *Géotechnique*, *58*(4), 283-296. https://doi.org/https://doi.org/10.1680/geot.2008.58.4.283

Lusvardi, C. M. (2020). *Blast-induced liquefaction and downdrag development on a micropile foundation* Brigham Young University].

Madabhushi, G. (2017). *Centrifuge modelling for civil engineers*. CRC press.

https://doi.org/10.1201/9781315272863

McCullough, N. J. (2004). *The seismic geotechnical modeling, performance, and analysis of pile-supported wharves*. Oregon State University.

Meyerhof, G., & Adams, J. (1968). The ultimate uplift capacity of foundations. *Canadian geotechnical journal*, *5*(4), 225-244. https://doi.org/https://doi.org/10.1139/t68-024

Mostafa, H. H. (2022). Lateral response evaluation of single piles based on pressuremeter test results (using Foxta) versus standard penetration test results (using Lpile). *Innovative Infrastructure Solutions*, *7*(4), 271.

Muhunthan, B., Vijayathasan, N. V., & Abbasi, B. (2017). *Liquefaction-induced downdrag on drilled shafts*.

PIANC. (2001a). Seismic Design Guidelines for Port Structures. In *Working Group*: Permanent International Navigation Association.

PIANC. (2001b). Seismic Design Guidelines for Port Structures. In: Working Group No. 34 of the Maritime Navigation Commision, International Navigation Association.

Reese, L. C., & Wang, S.-T. (2006). Verification of computer program LPile as a valid tool for design of a single pile under lateral loading. *Retrieved March*, *25*, 1-27.

Reese, L. C., Wang, S.-T., & Vasquez, L. (2019). A Program for the Analysis of a Group of Piles Subjected to Vertical and Lateral Loading (Technical Manual), for ENSOFT. In: INC.

Rollins, K., & Hollenbaugh, J. (2015). Liquefaction induced negative skin friction from blast-induced liquefaction tests with auger-cast piles. Procs., 6th Intl. Conf. on Earthquake Geotechnical Engineering, Christchurch, New Zealand, New Zealand Geotechnical Society,

Rollins, K. M., Clayton, R. J., Mikesell, R. C., & Blaise, B. C. (2005). Drilled shaft side friction in gravelly soils. *Journal of Geotechnical and Geoenvironmental Engineering*, *131*(8), 987-1003. https://doi.org/DOI: 10.1061/(ASCE)1090-0241(2005)131:8(987)

Rollins, K. M., Strand, S. R., & Hollenbaugh, J. E. (2018). Liquefaction induced downdrag and dragload from full-scale tests. In *Developments in Earthquake Geotechnics* (pp. 89-109). Springer. https://doi.org/DOI: 10.1007/978-3-319-62069-5_5

Saha, P., Horikoshi, K., & Takahashi, A. (2020). Performance of sheet pile to mitigate liquefaction-induced lateral spreading of loose soil layer under the embankment. *Soil Dynamics and Earthquake Engineering*, *139*, 106410.

Sawamura, Y., Inagami, K., Nishihara, T., Kosaka, T., Hattori, M., & Kimura, M. (2021). Seismic performance of group pile foundation with ground improvement during liquefaction. *Soils and Foundations*, *61*(4), 944-959.

Sinha, S. K., Ziotopoulou, K., & Kutter, B. L. (2022). Centrifuge Model Tests of Liquefaction-Induced Downdrag on Piles in Uniform Liquefiable Deposits. *Journal of Geotechnical and Geoenvironmental Engineering*, *148*(7), 04022048. https://doi.org/DOI:10.1061/(ASCE)GT.1943-5606.0002817.

Souri, M., Khosravifar, A., Schlechter, S., McCullough, N., & Dickenson, S. (2019). Experimental PY curves from centrifuge tests on pile foundations subjected to liquefaction and lateral spreading. 2019 44th Annual Conference on Deep Foundations,

Stringer, M., & Madabhushi, S. (2013). Axial load transfer in liquefiable soils for free-standing piles. *Géotechnique*, *63*(5), 400-409. https://doi.org/https://doi.org/10.1680/geot.11.P.078

Su, L., Tang, L., Ling, X., Liu, C., & Zhang, X. (2016). Pile response to liquefaction-induced lateral spreading: a shake-table investigation. *Soil Dynamics and Earthquake Engineering*, *82*, 196-204. https://doi.org/10.1016/j.soildyn.2015.12.013

Sumer, B. M., Ansal, A., Cetin, K. O., Damgaard, J., Gunbak, A. R., Hansen, N.-E. O., Sawicki, A., Synolakis, C. E., Yalciner, A. C., & Yuksel, Y.

(2007). Earthquake-induced liquefaction around marine structures. *Journal of waterway, port, coastal, and ocean engineering*, *133*(1), 55-82.

Tang, L., Ling, X., Zhang, X., Su, L., Liu, C., & Li, H. (2015). Response of a RC pile behind quay wall to liquefaction-induced lateral spreading: a shake-table investigation. *Soil Dynamics and Earthquake Engineering*, *76*, 69-79. https://doi.org/10.1016/j.soildyn.2014.12.015

Thevanayagam, S., Martin, G., Shenthan, T., & Liang, J. (2001). Post-liquefaction pore pressure dissipation and densification in silty soils.

Tokimatsu, K., & Asaka, Y. (1998). Effects of liquefaction-induced ground displacements on pile performance in the 1995 Hyogoken-Nambu earthquake. *Soils and Foundations*, *38*, 163-177. https://doi.org/10.3208/sandf.38.Special_163

Tran, N. X. (2021). *Experimental and Numerical Study on Seismic Behavior of Piles in Sloping Ground* 서울대학교 대학원].

Tran, N. X., Gu, K.-Y., Yoo, M., & Kim, S.-R. (2022). Numerical evaluation of slope effect on soil–pile interaction in seismic analysis. *Applied Ocean Research*, *126*, 103291.

Vaid, Y., & Negussey, D. (1988). Preparation of reconstituted sand specimens. *Advanced triaxial testing of soil and rock, ASTM STP*, *977*, 405-417.

Vaid, Y. P., & Negussey, D. (1984). Relative density of pluviated sand samples. *Soils and Foundations*, *24*(2), 101-105. https://doi.org/https://doi.org/10.3208/sandf1972.24.2_101

Varghese, R. M., & Madhavi Latha, G. (2014). Shaking table tests to investigate the influence of various factors on the liquefaction resistance of sands. *Natural hazards*, *73*(3), 1337-1351.

Verdugo, R., & Peters, G. (2010). Informe Geotécnico Fase Anteproyecto Infraestructura Puente. *Mecano Eje Chacabuco*.

Wada, A. (2004). Skin Friction and Pile Design.

Wilson, D. W. (1998). *Soil-pile-superstructure interaction in liquefying sand*

and soft clay [Ph.D. Thesis, University of California, Davis].

Xu, L.-Y., Song, C.-X., Chen, W.-Y., Cai, F., Li, Y.-Y., & Chen, G.-X. (2021). Liquefaction-induced settlement of the pile group under vertical and horizontal ground motions. *Soil Dynamics and Earthquake Engineering*, *144*, 106709. https://doi.org/https://doi.org/10.1016/j.soildyn.2021.106709

Yang, Z., & Zhang, X. (2017). Impact of ground freezing on seismic performance of bridge pile foundations subject to liquefaction-induced lateral spread. *Transportation Research Record*, *2656*(1), 71-80.

Yen, W. P., Chen, G., Buckle, I., Allen, T., Alzamora, D., Ger, J., & Arias, J. G. (2011). *Post-earthquake reconnaissance report on transportation infrastructure: impact of the February 27, 2010, Offshore Maule earthquake in Chile*.

Yoshida, N. (1990). Damage to foundation piles and deformation pattern of ground due to liquefaction-induced permanent ground deformations. Proc. 3rd Japan-US Workshop on Earthquake Resistant design of lifeline facilities and countermeasures for soil liquefaction,

Youd, T. L. (1993). Liquefaction-induced damage to bridges. *Transportation Research Record*, *1411*, 35-41.

Youd, T. L. (2018). Application of MLR procedure for prediction of liquefaction-induced lateral spread displacement. *Journal of Geotechnical and Geoenvironmental Engineering*, *144*(6), 04018033. https://doi.org/10.1061/(ASCE)GT.1943-5606.0001860

Zeghal, M., Elgamal, A.-W., Zeng, X., & Arulmoli, K. (1999). Mechanism of liquefaction response in sand–silt dynamic centrifuge tests. *Soil Dynamics and Earthquake Engineering*, *18*(1), 71-85. https://doi.org/https://doi.org/10.1016/S0267-7261(98)00029-3

초 록

지진 하중에 의한 지반의 액상화는 말뚝 기초의 수평 및 연직 안정성에 심각한 손상을 입힐 수 있다. 액상화로 인해 유발된 지반의 수평 변위는 말뚝에 측방 하중으로 작용하여 말뚝의 휨 파괴를 유발할 수 있다. 또한, 지반 진동에 의해 나타나는 말뚝 기초지반 내 과잉간극수압의 발생과 소산은 각각 말뚝의 좌굴 파괴와 부마찰력으로 인한 침하를 유발할 수 있다. 그러므로, 합리적인 내진설계를 위해서는 기초 지반의 액상화로 인한 말뚝 기초의 거동을 면밀히 파악해야 한다.

지반 액상화 현상과 관련된 말뚝 기초 연구는 주로 수평 지반 또는 경사도가 작은 무한 사면에 대해 수행되었다. 하지만, 잔교식 안벽과 같이 강가 또는 해안에 인접한 시설은 상대적으로 경사도가 큰 유한 사면에 말뚝 기초를 두고 있다. 액상화로 인한 유한 사면의 활동은 무한 사면과 달리 사면의 길이, 폭, 각도와 같은 다양한 영향 요소를 갖는다. 또한, 유한 사면에 근입된 말뚝 기초는 사하중, 관성하중, 액상화 측방유동력, 그리고 액상화 후 침하로 인한 부마찰력 등 복합적인 하중을 받는다. 따라서, 경사도가 큰 유한사면에 근입된 말뚝의 액상화 거동에 대한 연구가 필요하다.

본 연구에서는 유한 사면의 액상화가 말뚝 기초에 미치는 영향을 분석하기위해 포항 신항의 잔교식 안벽을 모사하는 원심모형실험을 수행하였다. 실험 모델은 단일말뚝과 2×2 무리말뚝에 의해 지지되는 질량체로 구성하였고, 말뚝 기초는 27°, 15°경사의 느슨한 포

화 모래 지층을 통과하는 선단지지 말뚝을 모사하였다. 가진 모델은 1.5 Hz의 최대가속도 0.2 g의 점진증가형 강진과 가속도가 0.1 g로 유지되는 유지형 약진으로 구성하여 토조 바닥에서부터 실험 모델을 진동하였다.

포화 지반을 모사하는 원심모형실험에서는 압밀 시간에 대한 상사 문제로 인해 간극액의 점성을 높여주어야 한다. Hydroxypropyl methyl cellulose (HPMC) 용액을 이용하여 간극액의 점성을 조정하였다. 간극액의 점성은 지반의 과잉간극수압 발생과 소산, 그리고 모델 구조의 동적 거동에도 큰 영향을 미쳤다. 증류수를 이용한 실험에서는 경사하부 방향으로 휘어졌던 구조물이 진동이 끝나기 전에 변형을 회복한 반면, 점성유체를 이용한 실험에서는 진동이 끝난 뒤에도 변형이 회복되지 않고 잔류하였다.

원심모형실험 중 말뚝의 연직축력분포를 진동 전, 중, 그리고 후에 따라 계측하였다. 원심가속도 증가에 따른 모형 지반의 침하는 말뚝에 부마찰력을 유발하였다. 부마찰력의 크기는 유효상재하중에 비례하는 beta법으로 결정한 주면마찰력과 같게 나타났다. 원심가속도에 의해 발생한 지반의 부마찰력은 과잉간극수압 증가에 따라 감소하였다. 진동 종료 후, 과잉간극수압 소산에 따라 지반 침하가 발생하였고, 이로 인해 지반의 부마찰력이 재형성되었다. 현행 기준은 액상화 유발 부마찰력을 액상화 지반의 잔류강도를 이용하도록 하고 있다. 그러나, 실험 말뚝에서 발생한 부마찰력은 액상화 중 강도 약화의 영향을 받지 않는 것으로 나타났다.

본 연구에서는 다양한 수치적 방법을 통해 액상화 지반을 모델링하여 원심모형실험 결과를 모사하였다. 먼저, 액상화 유한사면에

근입된 말뚝의 휨모멘트 평가를 위해 액상화 지반의 영향을 정적인 선형의 분포하중으로 치환하는 방법을 시험하였다. 원심모형실험 결과를 바탕으로 전응력에 비례하는 선형토압의 경험계수를 각 실험 조건에 따라 보정하고, 보정된 경험계수를 통해 사면 내 말뚝의 위치, 가진 모델, 그리고 사면 경사가 액상화 사면의 토압에 미치는 영향을 평가하였다. 무리말뚝 해석을 수행하여 기존 선형토압법과 보정된 선형토압법의 휨모멘트 예측 결과를 비교하였다.

액상화 유한 사면에 근입된 말뚝의 지진거동을 평가하기 위해 지반, 말뚝, 토조 등 원심모형실험의 구성 요소를 직접 모델링한 수치모델을 구성하였다. 정확한 수치 모델을 구성하기 위해 지반의 액상화를 고려한 지반–말뚝 인터페이스를 제안하였다. 구성된 수치모델에 대한 해석 결과는 원심모형실험 결과와 비교하여 신뢰도를 검증하였다. 해석 결과를 바탕으로 유한 사면의 액상화 거동과 그에 따른 말뚝의 지진 거동을 분석하였다. 검증된 수치모델을 바탕으로 변수연구를 수행하여 사면 기울기, 최대가속도 크기가 말뚝과 유한 사면의 지진거동에 미치는 영향을 분석하였다.

주요어: 말뚝기초, 사면, 액상화, 동적 거동, 원심모형실험, 동적수치해석, 측방유동토압, 부마찰력
학 번: 2018-37864

감사의 글

힘겨운 재수 생활을 끝내고 더 이상 공부는 없다며 서울대학교에 들어온 지 햇수로 14년이 되었습니다. 부족한 머리로 공부하려니 따라가는 것만으로도 벅차고 어려운 나날들이 있었습니다. 하지만, 이끌어주시는 교수님들, 가르쳐주시는 선배님들, 함께 해주는 친구들, 밀어주는 후배들이 있었기에 드디어 관악산에서 하산할 수 있을 것 같습니다.

산만하고 나태해서 제 자리에 멈추기 좋아하는 저를 계속 앞으로 나아갈 수 있도록 채찍질해주시고 이끌어주신 김성렬 교수님께 감사드립니다. 철없고 놀기만 좋아하던 저를 어엿한 한 명의 인간으로 만들어 주시고 따뜻하게 안아주신 정충기 교수님께 감사드립니다. 유머와 위트로 언제나 밝은 표정으로 가르쳐주신 박준범 교수님께 감사드립니다.

혼자서는 절대 못했을 학위를 받기까지 너무나 많은 선배들의 도움을 받았습니다. 지금까지 모든 순간 그리고 앞으로도 항상 저의 최고의 멘토가 되어주실 곽태영 형님, 덩치만큼 큰 마음으로 부족한 부사수 이끌어주신 이승환 형님, 언제나 최고의 능력으로 앞장서서 보여주신 백성하 형님, 곽이백이 없었다면 지금의 저는 없었을 겁니다. 그리고 그들을 길러내신 유민택, 권선용, 김석중, 김준영, 김한샘, 박가현 형/누나께 감사드립니다.

동고동락한 친구와 후배들이 없었다면 힘들 때마다 마음이 꺾여 포기하고 말았을지도 모릅니다. 경태야, 민호야 청수사의 눈발을

잊을 수가 없다. 규범아 이제 우리도 술 적당히 먹자. 범희형, 쑥스러워서 말은 못했지만 항상 부드러운 카리스마로 함께 해줘서 정말 고마웠어요. 교영이형, 까칠한 동생 4년 넘게 성질 받아주느라 고생 많았습니다. Tran, 말로 다할 수 없을 만큼 고마워, 어디에서 지내든 내가 항상 연락하고 보러 갈게.

인현아, 피부 관리 잘하고 하던 대로만 계속하면 좋은 결과 있을 거야, 화이팅. 택규야, 석사때도 박사 중에도 언제나 응원의 말로 기분 좋게 해줘서 정말 고마웠다. 재규야, 나랑 같이 운동하느라 힘들었지? 다 너 좋으라고 한 거니까 오해마라. 성호야, 못난 형이 맨날 심술부리고 짜증내는 거 받아주느라 정말 고생 많았다. 이왕 이렇게 된 거 앞으로도 쭉 잘 부탁한다. 병윤아, 태훈아, 이 논문은 우리의 피, 땀, 눈물로 쌓은 작은 첫 결실이다. 너무 감사하고 앞으로도 쭉 함께하자. 실험하고 연구하느라 바쁘다고 또 코로나 핑계로 많이 챙겨주지 못한 우리 연구실 후배님들, 경선이, 재인이, 석준이, 정우, 정현이, 민호 연구실 생활에 문제없이 오직 연구에만 집중할 수 있게 도와줘서 정말 고맙습니다.

멀리서 소리 없이 무한한 사랑으로 기도해주시고 응원해주시는 부모님, 부족한 아들이라 남들보다 오래 키우셨습니다. 그 보답으로 아들이 오래오래 모실 수 있도록 항상 건강하시고 행복하세요. 마지막으로, 힘들 때고 좋을 때고 언제나 모든 것을 함께하고 싶은 고마운 아내에게 이 논문을 바칩니다.